Modelling and testing of thermoplastic composite components using Building Block approach integrating process simulation.

By

Nithin Amirth Jayasree

******

Supervisor:
Prof. Massimiliana Carello

Doctoral Examination Committee:
Prof. Alessandro Fasana, Co-examiner, Politecnico di Torino
Prof. David Hughes, Referee, Teesside University
Prof. Roger Serra, Referee, INSA
Prof. Simonetta Boria, Co-examiner, Università di Camerino
Prof. Stefano Mauro, Co-examiner, Politecnico di Torino

Politecnico di Torino
May 23, 2018

I hereby declare that, the contents and organisation of this dissertation constitute my own original work and does not compromise in any way the rights of third parties, including those relating to the security of personal data.

....
Nithin Amirth Jayasree
Turin, June 23, 2018

Summary

Currently, the automotive sector is exploring the feasibility of replacing metals with composite materials for structural and non-structural applications. This is mainly driven by the demand for lighter and increasingly complex components, which will be extremely difficult to fabricate with the traditional metal forming approaches. This prompted the need for exploring textile reinforced composite materials, where they stand out about their ability to allow complex designs with high specific strength and stiffness. Which further helps to reduce mass and increase fuel efficiency. However, a disadvantage right now is the use of composites is limited by an inability to accurately analyse and predict these composite structures for its mechanical performance. This thesis presents methodology employing finite element techniques for predictive modelling of textile reinforced composite materials by considering the process simulations. The Building Block approach is introduced and implemented as a guideline, to efficiently substantiate the durability and performance of the component design sequentially.

FEA simulation of a composite component was done using two composite failure criterions for comparison, Crasurv (modified Tsai-Wu) and Hashin; after completing a detailed material characterisation and card fitting for creating FE material. The results of the structural simulations are compared against experimental results, which is kept as a benchmark for future comparisons and review.

The next step was to conduct process simulations to analyse the composite forming process to investigate the locally varying microstructure to account for the anisotropic behaviour in the composite part during its production that can alter the structural integrity of the component. An additive split between isotropic, elasto-plastic matrix and anisotropic hyper-elastic fibers material card is used in LS-Dyna explicit solver for conducting process simulations. A detailed material characterisation was done on the textile reinforced fabric and the composite laminate at forming temperature to study its tensile, shear, frictional and bending properties. The process simulation helps to obtain reliable structural simulation models by mapping.

This thesis aims to establish an accurate predictive model on a rational basis, by creating an innovative methodology for the structural analysis of thermoplastic composite components integrating process simulation. The final scope of the research is to simplify the product development phase for general lightweight automotive parts made with thermoplastic composite materials.

Acknowledgment

I would like to dedicate this thesis to my Achan, Amma and Sreekutti.

Contents

List of Tables

List of Figure

Chapter 1

Thesis Outline

The research attempts to create an accurate FE model for a thermoplastic composite component for structural analysis integrating process simulation results. The process flow of the research done is displayed in Fig.1, detailing the four main phases of the research.

The current chapter, Chapter 1 outlines the entire research done detailing the work done in each chapter. Chapter 2 gives a detailed introduction on the present state of the thermoplastic composites specifically in the automotive sector, the prospects of thermoplastic composite forming and how the current research fits in.

Chapter 3 reviews the literature and the core concepts, and then it serves as the foundation of this research. The existing 'state of the art', primarily for characterising the composite laminate/fabric at the process temperature is reviewed.

Chapter 4 focusses on the characterisation methods explicitly adopted tensile, compression and shear for creating the material FE cards for the composite part. The appropriate composite failure criterions such as Crasurv and Hashin are explained, and its feasibility is demonstrated in this section. The chapter also includes a notable section on the card fitting describing how the experimental values are transformed into FE material card with the appropriate failure criterion. Finally, the structural simulations of the chosen composite component are done by comparing the different failure criterions, and the associated material card developed.
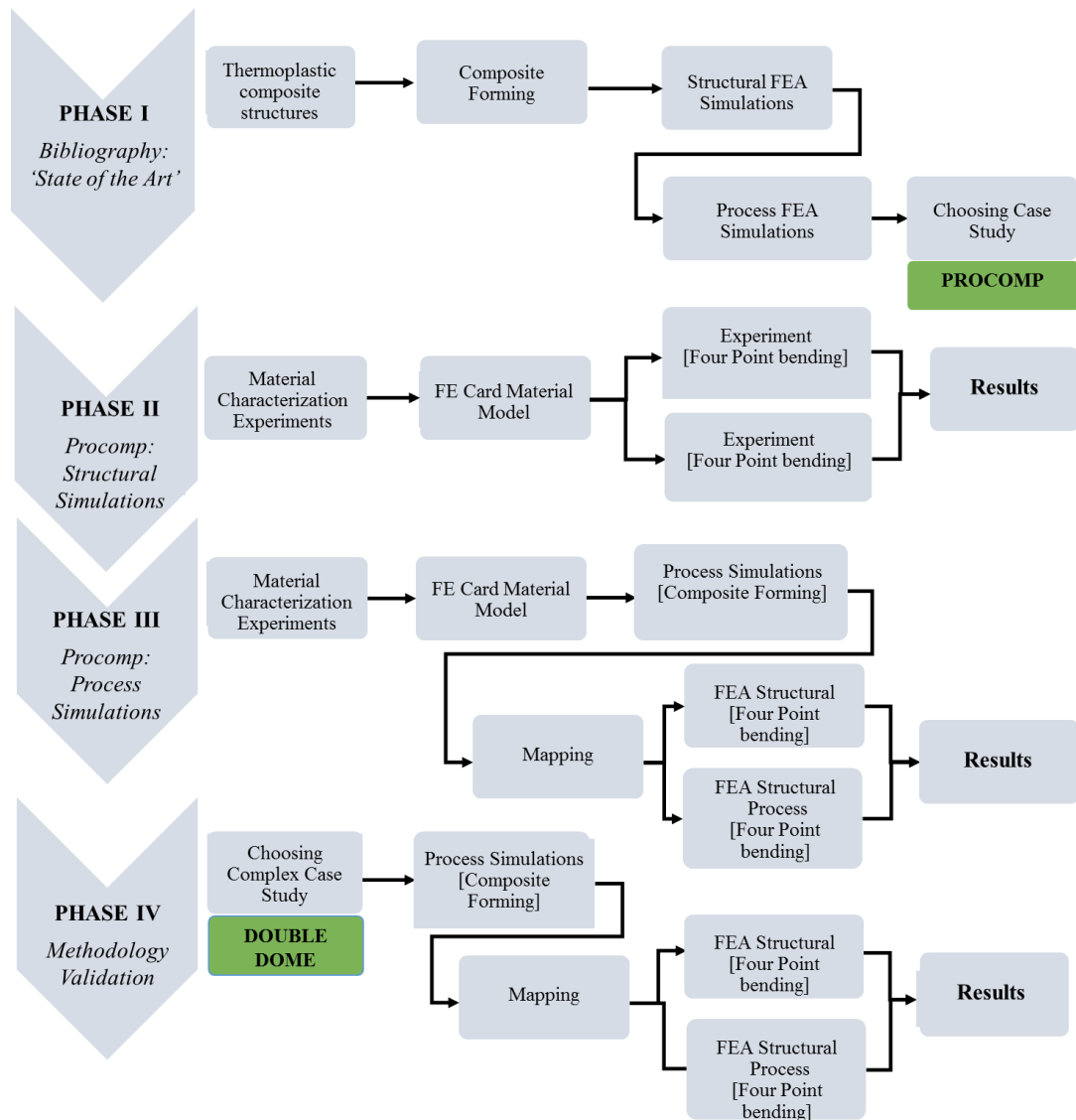
Figure 1 Outline for the PhD research

Chapter 5 introduces process simulation by detailing the necessary characterisation tests required by adding state of the art test and modelling methodologies to determine the material properties specific to this research efficiently. Emphasis was kept on creating an accurate FE material card for the material at its forming state. Two separate shear tests are done, the trellis frame and bias extension test, to self-validate the results. Frictional and bending tests are done to determine the frictional coefficients and the bending modulus to increase the accuracy of process simulations further. An accurate process simulation allows to

capture the forming operation of the composite laminate. "Mapping" is introduced and explained in detail where the process simulation data is transferred to the structural FE model. The chapter concludes by re-doing the FE structural simulation and is compared with the old result obtained in Chapter 4.
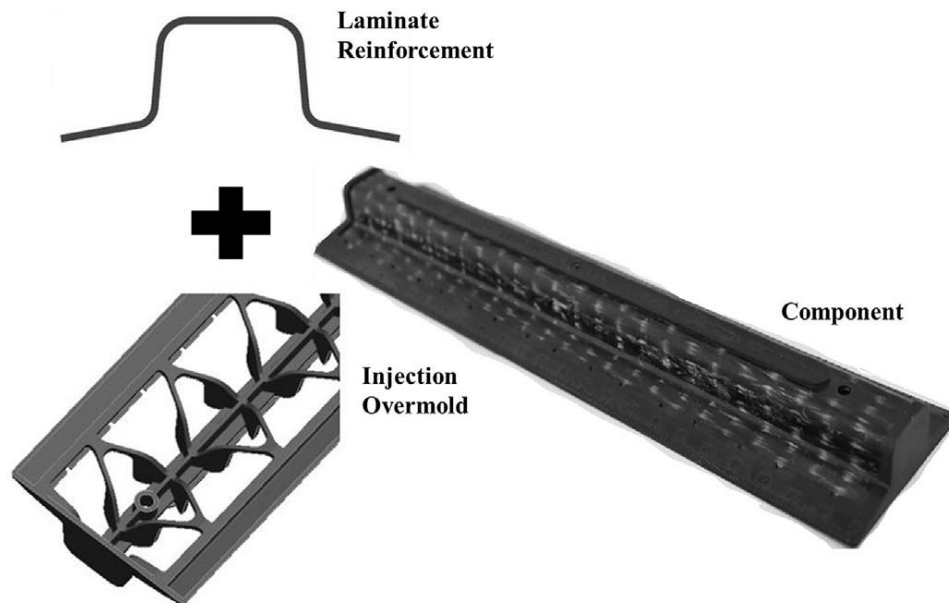
Figure 2 Procomp overmolded component considered for the research [1]

Fig 2 shows the overmolded Component (Procomp) considered for the study [2] as shown on the process flow diagram shown at the end of 'phase I' in Fig 1. The hybrid moulding process employed for this research constitutes a continuous glass fiber reinforcement, consolidated with a polymer layer as a substrate. The laminate reinforcement was focussed for the process simulations done in Chapter 5.

Chapter 6 illustrates the summary of the whole research, highlighting the methodologies implemented and the significant results obtained. The section reiterates the entire research explaining the significance of the research done and some conclusive remarks for future developments.

Lastly, Chapter 7 validates the entire process with another composite component discussing the sophistication and the capability of the methodology adopted.

Chapter 2

Introduction

As per the online statistics company Statista Inc., the automotive composite material market globally is anticipated to peak 15 Billion USD in 2018 and 30 Billion USD by 2026 (Fig 3 [3]). Although it looks expensive, it only represents less than 2% of the entire lightweight automotive production in 2018. The primary reason why manufacturers are reluctant to use composite materials even after its unique advantages is because of its complicated design phase compared to the quicker and cost effective design process for aluminium or steel parts. [4].
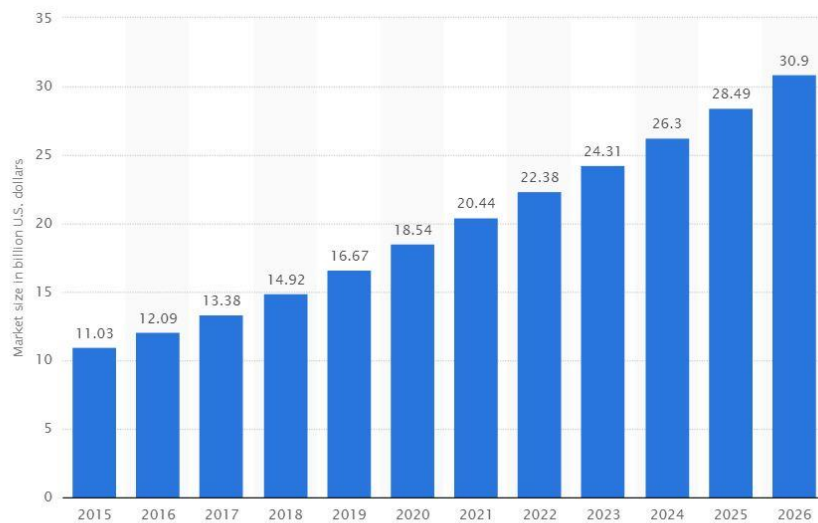
© Statista 2017

Figure 3 Global automotive composites material market size from 2015 to 2026 (in billion U.S. dollars) [3]

The unique ability of composite materials is to allow intricate designs to be tailor-made for its design flexibility to meet high specific strength and stiffness. They consist of a compliant polymeric matrix material acting as a reinforcement with low density to give structural volume with additional reinforcing composite fabric embedded inside it giving the required strength and rigidity. The combination

provides exceptional stiffness and durability with a very low density making it an ideal candidate for a variety of applications including automotive structures like the leaf Spring Fig 3 and B-pillar Fig 4. The most widely used reinforcement fabric are carbon, glass and aramid fibres, which come in short, long and continuous fibres depending on the application. [5]

Material selection is an essential criterion for early design state of a composite, where the engineer chooses the material based on the properties, which are most relevant. The commonly used combinations are PolyEther Ether Ketone (PEEK), PolyPhenylene Sulphide (PPS) or PolyEther Ketone Ketone (PEKK) with a glass or carbon reinforcement [6].
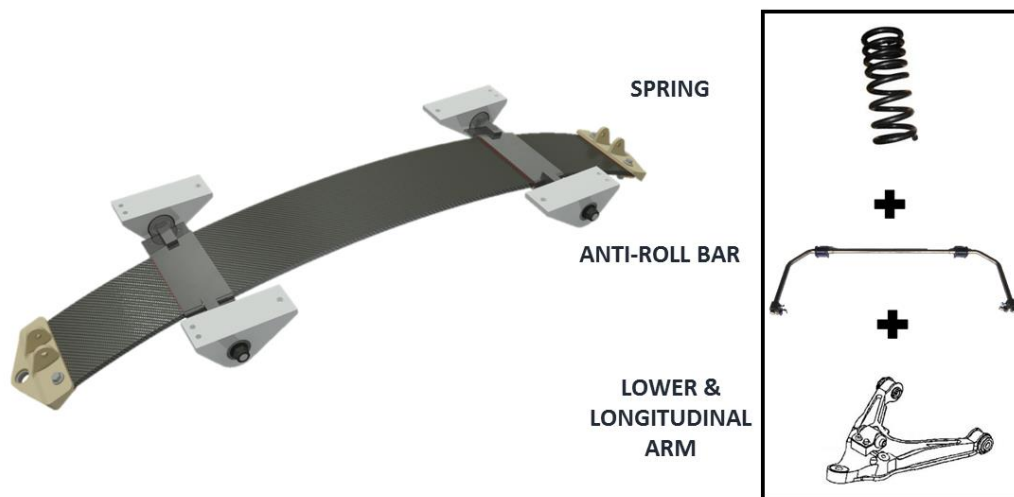
Figure 4 Functionally integrated CFRP leaf spring developed by the IEHV research group, Politecnico di Torino [7]

2.1. Thermoplastic composite materials

Thermoplastic composite material usage has been growing steadily in the lightweight automotive sector where a high specific strength, low density and corrosion resistance is crucial [8, 9-11]. Although composite materials have been widely considered in the automotive field [12, 13], they are still not widely implemented due to uncertainty and complexity involved in the prediction of durability in the design phase. Contrary to the aerospace industry [14] where the final efficiency and robustness of the component is given more priority with more product development cycle time. Another limiting factor is, as the design complexity increases, the modelling gets more complicated and requires sophisticated Finite Element Analysis FEA techniques and dependable standards [15].

Up until recently, the composites industry did not consider much about manufacturing waste and end of life parts resulting in much of composite material manufacture based on thermoset materials. [16] However, the limitations of thermoset materials such as the inability to re-melt, shorter shelf life, higher storage costs and longer curing times are gradually opening opportunities for thermoplastic composite materials. Another main reason being the new directive from the European Unions end of life (ELV) dictates that 85% of the total mass of an automobile should be recyclable [17]. This directive marks the ability of thermoplastic to re-melt with minimal loss of its material properties making it the primary candidate when recyclability is considered. One of the most recent innovation being virtually unchanged material properties of the thermoplastic composites even after recycling as in the PArCF30 thermoplastic composites as demonstrated in the Tokyo Motor show, 2016 (Fig 5 [18]).

For FE analysis of composite components; on a theoretical level, various analytical and semi-analytic approaches are proposed [19, 20] but creating a prediction model on a commercial level is still uncertain. The main issue is the lack of a conventional standard methodology or knowledge sharing of methods for material characterisation, FEA (Finite element Analysis) and validation.

To develop a functional thermoplastic component to sustain the required non-crash load conditions such as normal loading, fatigue life cycle, durability, vibrations etc. in different conditions such as frontal perpendicular, angular side collisions require a complete characterisation of the component. This involves an extensive characterisation of the composite material, and the process characterisation, which influences the final strength of the component. The process in this context is the manufacturing method in which the composite laminate is moulded to the 3D component (e.g. thermoforming, compression moulding, resin

transfer moulding. etc) and the characterisation of the composite laminate at it forming temperature is called as process characterisation. The influence of process on the structural integrity of the component depends directly on its geometry, i.e. the effect is higher for complex geometry and vice versa.
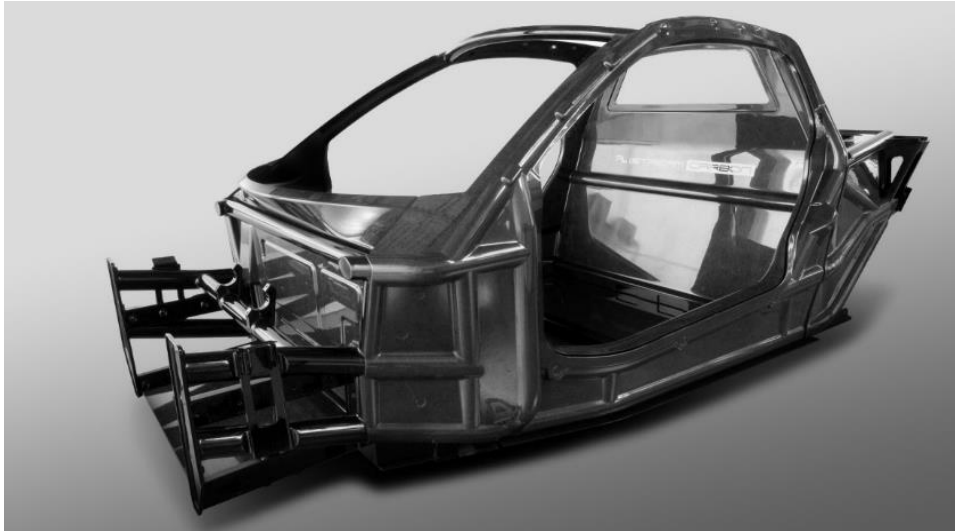
Figure 5 Recycled carbon fiber used in Gordon Murray Design's CFRP intensive iStream Carbon chassis [18]

2.2 Thermoforming of thermoplastic composite materials

Thermoforming of composite materials can be defined as a high deformation rate process in which composite materials are deformed by heating above its glass transition temperature. The typical steps involve pre-consolidation which consists of stacking of uniform or variable textile reinforced plies, heating, forming and solidification. A hot blank is pressed between the male and female molds tool after preheating (Fig 6) forming the blank with the required consolidation pressure. A subsequent trimming process is done to discharge excess materials.
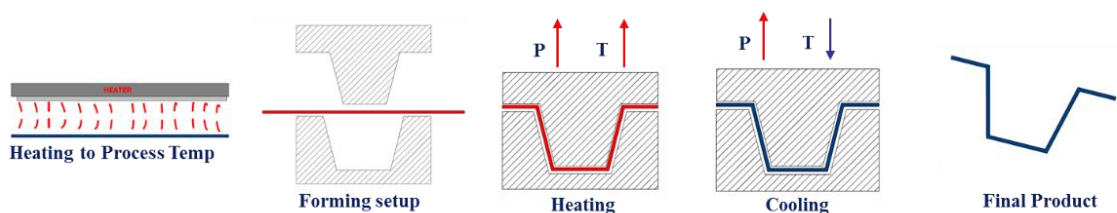
Figure 6 The thermoforming process

Focusing on the thermoplastic polymers at its forming state, it consists of polymer chains with a high molecular weight interacting with each other via physical bonds namely entanglements and van der Waals forces. These physical bonds are overcome by addition of thermal energy. Thermoplastic composites can be shaped in its viscous state (drop in stiffness), at its glass transition temperature (Tg) or its melting temperature (Tm) depending on being amorphous or semi-crystalline thermoplastic (Fig 7). [21]
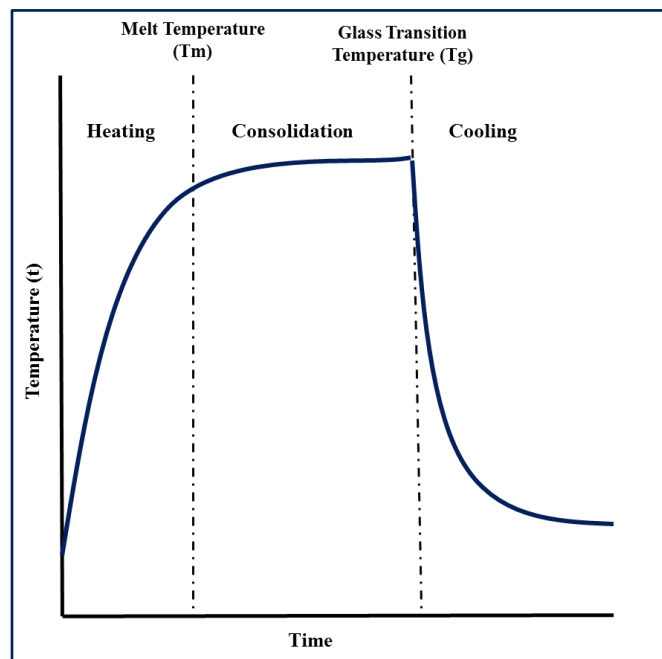
Figure 7 Typical thermoplastic composite process cycle [adapted from 21]

To process thermoplastic composites requires working at high temperature & pressure with robust & complex tooling and additional energy for their processing. Some thermoplastics commonly used are reported in Table 1, giving an understanding of the glass transition, melting and processing temperatures.

Table 1 Process temperatures of thermoplastic composite materials [adapted from 21]

Matrix	Tg(ºC)	Tm(ºC)	T Process(ºC)
PEKK	156	306	340
PPS	89	307	327
PEI	217	--	330
PEEK	143	343	390
PP	-20	176	190
PA-12	52	176	224
PA-6	48	219	245
PBT	56	223	250

2.3 The Building Block Approach

A building block approach has been set as a guideline and implemented for this research, developed by NASA for their Advanced Composite Technology (ACT) and High-Speed Research Program [22] to efficiently substantiate the durability and performance of the component design sequentially as illustrated in Fig 8 [23].

Both cost and performance objectives are met with the building block approach by characterising the material by testing on some less expensive specimen as a first step; evaluating technology risk early and progressively building a knowledge database at various structural complexity levels of the specimen [24].

The building block approach involves:

- Level 1 characterising the material experimentally and validating by FEA;
- Level 2 progressing on to component validation experimentally and by FEA;
- Level 3 moving on to component optimisation to examine the change in the component behaviour during the manufacturing process;
- Level 4 integrating the model into complicated full-scale components.
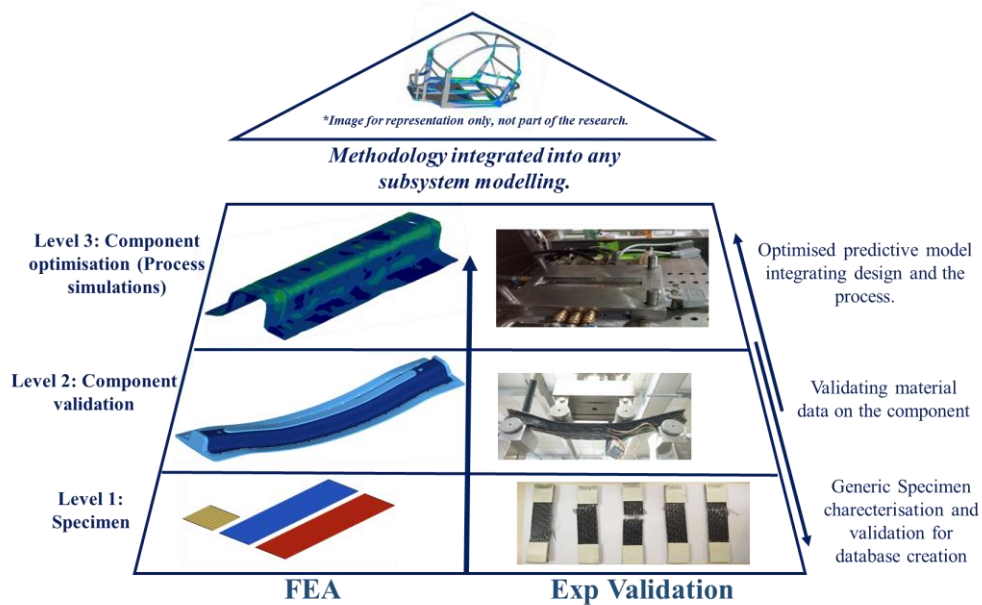
Figure 8 Building Block approach used for the research [Adapted from 23]

Traditionally, product design involves a detailed conceptual and embodiment design followed by detailed prototype manufacture and testing. This trial and error procedure gives an acceptable output but is repetitive, expensive and time consuming with additional labour costs, machine time and many scrap products from repetitive testing. Issues such as tool modifications to overcome the forming problems in the testing phase will result in expensive replacements of the entire tooling setup. To minimise these product development costs and to save time exponentially a robust modelling protocol with a reliable FEA tool needs to be employed to predict the product development stages including its early design phase. These predictive capabilities in the thermoplastic composite industry are examined in this thesis.

To summarise, the objectives of this thesis are

1. To experimentally characterise continuous fibre and short fibre composite materials for FE material card generation.
2. Structural FEA analysis on the chosen composite overmolded component using appropriate composite failure criterion.
3. Comparison of experimental and FEA results.
4. To investigate the possibility of increasing the accuracy of the FE structural model to better match the experimental results by integrating process simulations.

5. To characterise the material for process simulation focussing on tensile, intra-ply shear, tool-ply friction, ply-ply friction and bending.
6. To assess the predictive capability of forming simulations.
7. To explore the scope of mapping the process simulation results on the FEA model to create an all-inclusive predictive model.

The research findings aim to create an explicit industrial protocol to be implemented in the product design process for a thermoplastic composite component in its early stage, which is currently lacking in the industry.

2.4 State of the art and previous research.

The principal reason that initiated the interest in the composite materials in the 1950s, was the demand for the lighter parts with high stiffness in the automotive and aerospace industry. Despite the advantages and years of research, industries have not fully achieved the ability/knowledge/skills to predict the behaviour of composite parts under loading conditions. [25] This is primarily due to the complex behaviour of composite structures that is dependent on various parameters which includes the failure modes associated with composite damage and the effects of manufacturing process. Composite failure can happen due to its complex geometry, loading conditions, the material layup, the material properties itself and the manufacturing process. The effects can vary from fibre failure and matrix cracking to delamination and buckling in extreme cases.

2.4.1 Composite material characterisation

The material properties of the chosen composite material determine the primary failure limits. The experimental procedure for determining the material properties can be adopted from the accepted international standards such as the ASTM (American Society for Testing and Materials) and ISO (International Standards Organisations). These standards however are limited to the strength parameters of the chosen material and the failure properties are not entirely determined. [25]. A 3-DOF multi axial testing methodology was developed to identify more than one material parameters on each loading conditions. [26]

2.4.2 Composite Failure Criterions

The failure criterions for composite materials are classified under failure criteria associated with failure modes and not associated with failure modes. The ideal failure criterion can predict fibre and matrix failure under different loading conditions (normal and shear) and delamination initiation and growth under tension or compression.

For a basic analysis, a maximum strength/ strain criterion from the limits obtained from material tests could be used. For accurate failure analysis many researchers have come up with more detailed criterions. A quadratic interactive criterion has been developed by Hashin for the fibre failure considering the inplane shear [27] and by Hashin and Rotem for matrix failure [28]. Chang and Chang upgraded the quadratic failure criterion by including nonlinear shear behaviour. [29] Puck and Schürmann used the maximum strain criterion by including a stress magnification factor on the transverse normal stress. [30]. A fully interactive criterion was developed by Tsai and Wu in which individual plies are not considered and failure of the entire ply thickness is considered [31]. As the interactive criterion is developed from metals, it is often criticised, but is commonly used when the total ply thickness is smaller and when the accuracy post failure is not critical [32]. Pinho developed a set of failure criteria named as LaRC04, considering each failure modes and the nonlinear matrix shear behavior. It has a set of six relations which can be implemented directly for a range of load combinations. [33]

Advanced modelling can be possible by predicting initiation and propagation of the delamination. The traditional failure approaches can be used for delamination modelling, using the tensile/ shear parameters along the thickness of the individual plies, with quadratic criterions. All the detailed delamination criterions consider the strain energy release rate and compare it with the threshold strain in mode I, mode II and mode III [34]. The delamination criterions for prediction are listed in references [35 to 39]. Damage mechanics can be further modeled which shows the effects of damage on the material definition. [40]

For an accurate analysis of composite structures by FEA, it is necessary to understand the load conditions and the composite structure. For example, for a composite part with multiple plies, for predicting damage in different failure modes, LaRC04 could be used and for a simple part with less plies a Hashin failure criterion could give sufficiently accurate results.

2.4.3 Composite Process simulations

A composite thermoforming process involves woven textile fabric impregnated with resin heated to its melting / forming temperature, then draped to the required geometry and finally cooled to obtain the desired part. As the composite fabric is completely anisotropic and due to resin recrystallization, the resultant part maybe distorted and may have residual stresses in it. This makes it necessary to do composite process simulations to predict all aspects of the final part. [41]. The drapability of composite laminates mainly depends on the composite fabric reinforcement used. The formability of thermoplastic composite laminates was investigated by de Luca et al [42], experimentally and by FEA using a double dome geometry. A comparison study was done between woven composite fabric with unidirectional fabric demonstrating the occurrence of wrinkles. The comparison was repeated by Haanappel [43] using a similar geometry. A series of study was done by Haanappel to quantify the deformation behaviour of composite laminates and fabric [44 to 46] to prove that the deformation mechanism of a composite fabric is dependent on the inter-ply, intra ply, friction and bending rigidity of the laminate. The literature specifically related to process simulation is limited but the tendency of the composite laminate to have process induced defects during the manufacturing process makes it necessary to predict for complimenting the structural FE analysis. Although there are a lot of commercial tools for process simulations with varying levels of accuracy, the challenge lies in mapping the results of the process simulation to the FE structural model.

2.4.4 Previous research at the IEHV research group

This thesis is a continuation of two PhD research thesis focused on two main aspects of thermoplastic composite materials, performed in the IEHV research group, DIMEAS (Dipartimento di Ingegneria Meccanica e Aerospaziale), Politecncico di Torino. The main research goal for the team is to create a knowledge base in all aspects of thermoplastic composite materials.

The PhD research of Andrea Airale, IEHV research group, focused on material characterisation and experimental testing including aging UV cell, climate and corrosive on composite materials with DMTA analysis, ATR, light and electron microscopy. [48]. The PhD thesis of Alessandro Ferraris, IEHV research group focuses on the developing a lightweight thermoplastic composite automotive part by optimising the NVH performance, by considering the case study of a lightweight automotive door panel [47]. A range of design, testing and FEA has been done for

the development of a damped door using interlaminar composite materials. A good correlation has been achieved between the FEM and physical damping tests.

Chapter 3

Literature review

3.1 Thermoplastic composite part

A state-of-the-art overmolded composite component was made for this research, Fig 1. In the fast-evolving thermoplastic composite technology, the latest trend in the automotive sector is the use of hybrid composites structures where the mechanical properties of multiple composite materials give the structural feature to a single component [1, 22, 49, 50]. The design flexibility combining the ease of tailoring high-strength and stiffness components with elevated functional integration including crack propagation resistance [51], better acoustic and damping properties, enhanced protection against collapse in a crash [52] and cost savings with its hybrid process [53] makes this an enabling technology [54]. The obvious significant benefits are the decreased cycle time and the ability to realise complex profiles and to contrive the reinforcements with a continuous fibre prepreg. This combination of the moldability of short fibre composite materials with the high strength of continuous fibre composites to a single component opens many new possibilities for thermoplastic composites. The only drawback for a hybrid over-moulding process is its difficulty in anticipating the combined strength and bond quality of the component [55].

The focus of recent academic and industrial researchers is to recognise completely the process parameters associated with composite materials during manufactures such as in-plane fabric deformations, fibre direction change, thickness variations and the tendency to develop internal stresses and strains during production. [56 -59].

The desired shape of the reinforcement for the composite laminates is obtained by using a punch and die setup to deform the continuous fibre prepreg (e.g., compression moulding) or composite fabrics to its required shape [60]. The component under review as shown in Fig 1. It is thermoformed to the required geometry and the short fibre reinforced polymer compound is over-moulded with a single step process. The substrate being TEPEX® Dynalite 104-RG600(2)/47% [61] (Bond-Laminates), a continuous fiber twill 2/2 E-glass impregnated with

polypropylene and the over-mould is Xmod™ GD301FE [62] (Borealis), a 30% glass fiber polypropylene compound intended for injection moulding.

Further detailed study was done specifically on the substrate by characterising the continuous fibre twill 2/2 E-glass fabric separately as a part of the process characterisation. (WVR 600T supplied by Crystex composite materials) [63].

3.2 Material properties of Anisotropic Composite materials

To characterise an anisotropic composite material a series of tests need to be done to study its tensile (0° and 90°), shear and bending properties. Initially, material testing should be done in quasi-static strain rates in the range of 10^{-4} to 10^{-3} s^{-1}. The material should then be tested under dynamic loading using a Split Hopkinson Pressure Bar or drop tower testing machine for multi-strain rate results for crash simulations. However, for this research, the results from the dynamic loading is not included, as it does not contribute to the static load tests and the forming simulations considered.

The available literature for the characterisation of composite materials is well established with standards as detailed in Fig 9, which provides consistent results. In the first part of the research, a complete material characterisation is done on two materials chosen.

a: Tensile Test
ASTM D 3039

b: Compression Test
ISO14126:1999

c: Bending Test
ISO 14125:1998

d: Shear Test
ISO 14129: 1997
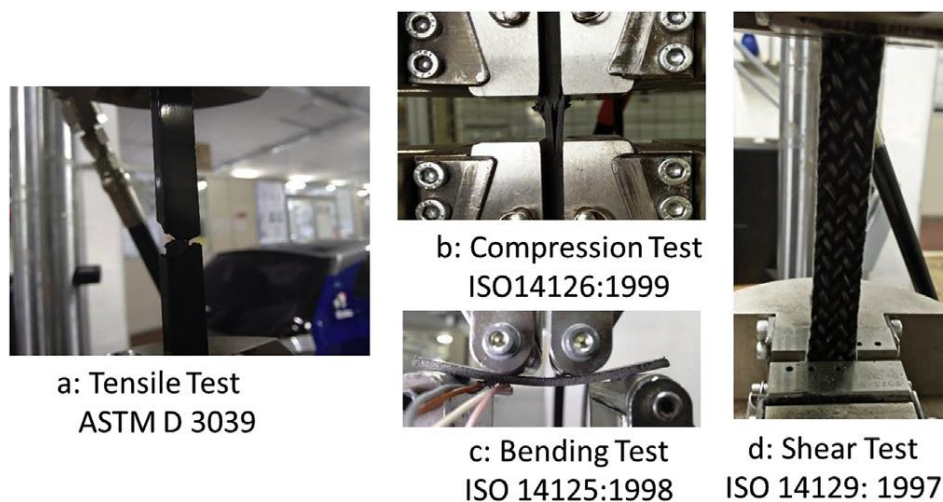
Figure 9 The characterisation tests employed for composite laminates [64, 65, 66, 23, 1, 67]

3.3 Card fitting for creating material model

The experimental results are further used for developing the FE material cards model by a method called card fitting [7, 23, 1]. This is done to convert the principal values obtained by physical characterisation tests to structural response and formation of damage of the material during impact in FE simulation. The response of composite material under load in FE analysis can be divided into two stages, the first being the "damage resistance" and the second being the "damage tolerance" [68]. Choosing the right composite failure criterion is the critical step here to replicate the material properties exactly.

Currently, all the composite failure criterion falls into two categories that will be explained in the following.

3.3.1. Failure criteria not associated with failure modes.

This group uses a single mathematical expression, a polynomial and tensorial criteria, to represent the composite failure surface as a function of the material strength. All the failure criterions in this section is a derivative of Tsai Wu failure criteria [69], in which the damage occurs when the following condition is satisfied.

$$F_i.\sigma_i + F_{ij}.\sigma_i.\sigma_j + F_{ijk}.\sigma_i.\sigma_j.\sigma_k \geq 1 \tag{1}$$

Where the F_{i-k} are lamina strength in the principal directions

Crasurv failure criterion, [70] an improved version of the Tsai-Wu, is one of the adopted failure criteria for this research. An orthotropic plastic hardening criterion, which follows a linear elastic behaviour until the yield stress value followed by a plastic behaviour. Plastic hardening is denoted as a function of plastic work with strain rate dependency. It also allows the possibility to define plastic work for each direction (representing the absorbed energy of the composite).

$$F = \sum F_{ii}(W_p)\sigma_{ii} + \sum F_{ii}(W_p)\sigma_i^2 + 2F_{12}(W_p)\sigma_1\sigma_2, \tag{2}$$

Where:

$F(\sigma) < 1$, elastic state
$F(\sigma) = 1$, Plastic admissible state
$F(\sigma) > 1$, Plastically inadmissible stresses

$$F_i(W_p) = \frac{-1}{\sigma_{iy}^c(W_p)} + \frac{1}{\sigma_{iy}^t(W_p)}, \tag{3}$$

$$F_{ii}(W_p) = \frac{1}{\sigma_{iy}^c(W_p)} \cdot \frac{1}{\sigma_{iy}^t(W_p)}, \tag{4}$$

$$F_{12}(W_p) = -\frac{\alpha}{2}\sqrt{F_{11}(W_p)F_{22}(W_p)}, \tag{5}$$

Where:

$$\sigma_{iy}^t = \sigma_{iy}^{t0}\left(1 + b_i^t W_p^{n^{it}}\right)\left(1 + c\ln(\frac{\dot{\varepsilon}}{\dot{\varepsilon}_0})\right) \tag{6}$$

$$\sigma_{iy}^c = \sigma_{iy}^{c0}\left(1 + b_i^c W_p^{n^{ic}}\right)\left(1 + c\ln(\frac{\dot{\varepsilon}}{\dot{\varepsilon}_0})\right) \tag{7}$$

F_i, F_{ii}, F_{ij} are coefficients describing elastic/plastic transition envelope
W_p is the global plastic work
$\sigma^{t0,c0}{}_{iy}$ is the initial tension and compression yield stresses in direction i
$b^{t,c}{}_i, n^{t,c}{}_i$ are the hardening coefficient and exponent

During an event of exceeding yield stress, stresses are plastic inadmissible and is projected on to the yield surface as in Fig 10 [71].
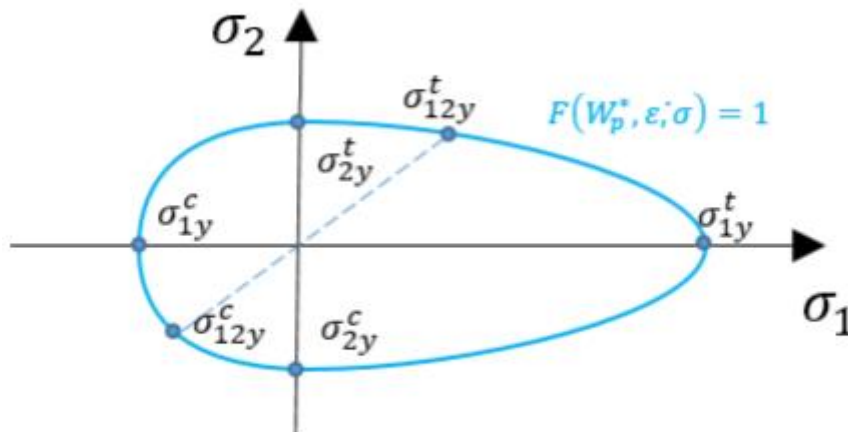
Figure 10 The yield surface for Crasurv formulation [72]

3.3.2. Failure criteria associated with failure modes.

The failure criterions associated with failure modes directly considers the material strength and the non-homogeneous nature of composites leading to different failure modes such as fibre fracture, transverse matrix cracking, shear matrix cracking. The major criterions coming under this category include maximum strain- criterion, maximum stress criterion, Hashin criterion, Puck Etc [73].
Hashin Criterion [74] is considered from this group, as it can determine different failure modes separately, considering the material stresses as shown in Fig 11.
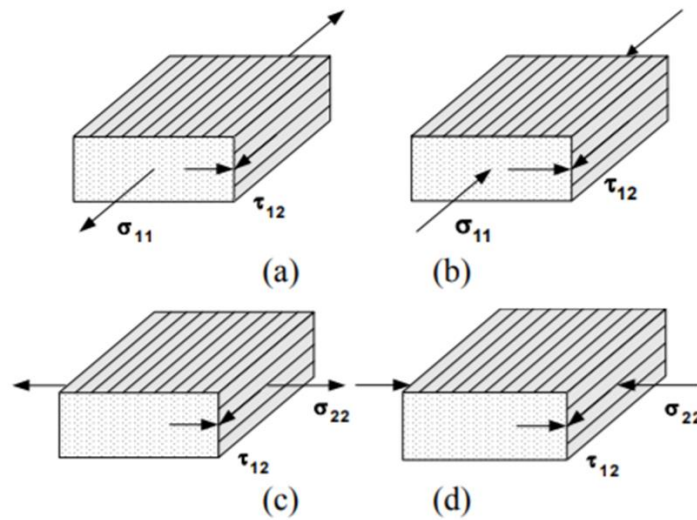
Figure 11 Failure modes distinguished in Hashin criterion [73] (a) tensile fibre failure, (b) compressive fibre failure, (c) tensile matrix failure and (d) compressive matrix failure

Fibre failure in tension: $\sigma_1 > 0$:

$$\left(\frac{\sigma_1}{\sigma_{1T}^u}\right)^2 + \frac{\sigma_{12}^2 + \sigma_{13}^2}{(\sigma_{12}^u)^2} = 1 \qquad \text{or} \qquad \sigma_1 = \sigma_{1T}^u \qquad (8)$$

Fibre failure in compression $\sigma_1 < 0$:

$$-\sigma_1 = \sigma_{1C}^u \qquad (9)$$

Matrix failure in tension $(\sigma_2 + \sigma_3) > 0$:

$$\left(\frac{\sigma_2+\sigma_3}{\sigma_{2T}^u}\right)^2 + \frac{\sigma_{23}^2-\sigma_2\sigma_3}{(\sigma_{23}^u)^2} + \frac{\sigma_{12}^2+\sigma_{13}^2}{(\sigma_{12}^u)^2} = 1 \qquad (10)$$

Matrix failure in compression $(\sigma_2 + \sigma_3) < 0$:

$$\left[\left(\frac{\sigma_{2C}^u}{2\sigma_{23}^u}\right)^2 - 1\right]\frac{\sigma_2+\sigma_3}{\sigma_{2C}^u} + \left(\frac{\sigma_2+\sigma_3}{2\sigma_{23}^u}\right)^2 + \frac{\sigma_{23}^2-\sigma_2\sigma_3}{(\sigma_{23}^u)^2} + \frac{\sigma_{12}^2+\sigma_{13}^2}{(\sigma_{12}^u)^2} = 1 \qquad (11)$$

The FE material models should be created with failure criterions, specially made for composite materials, strain rate dependent, non-linear, orthotropic, and have options for advanced material damage and failure. Once the material models are chosen, a shell or a solid finite element model is created using the selected FE tool.
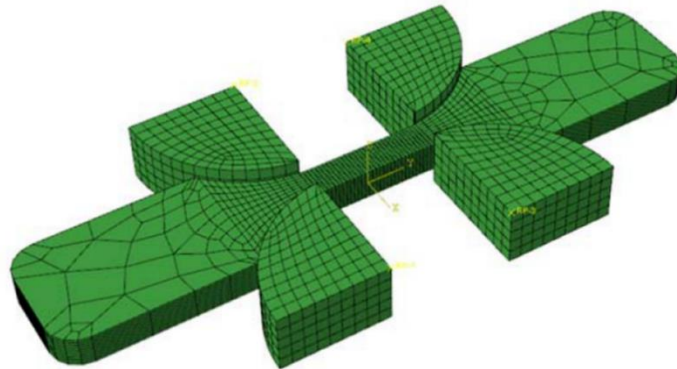
Figure 12 Sample solid FE model of short fiber composite tensile test [75]

The FE model tries to simulate all the experiment done on the specimen with the same dimensions, with the direct inputs from the experimental results. Variations were checked for after the test, which is then adjusted to create an accurate material model. Fig 12 shows the FE specimen model made for card fitting done by Helga et al. [75].

3.3 Composite Fabrics and pre-impregnated composite laminates (organo sheets)

The forming process of composite laminate involves deforming the laminate to the required 3D shape at the exact forming temperature and cooling it back to the room temperature to let it retain the deformed state. Composite parts, while production can lead to shape distortions which can alter the material properties, characterised such as spring back, distorted/altered fibre distribution, wrinkling, etc [60, 76, 77, 78]. This mainly depends on the geometry of the part, process temperature, material property and friction. To efficiently determine and optimise the manufacturability, a separate study on all the associated deformation mechanisms is done, as displayed in Table 2.

Table 2 Different composite deformation modes during forming [79, 76, 78]

Deformation	Description
Intra- ply tensile loading	▪ Tension parallel to the yarn direction ▪ Primary source of energy dissipitation
Intra-ply shear	▪ Rotation between warp and weft at tow crossovers ▪ Key deformation mode
Inter-ply and tool-ply friction	▪ Friction between the adjoint plys and tools during forming
Ply bending	▪ Bending of composite layers
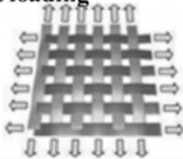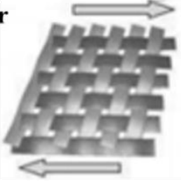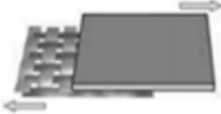
The fabric is heavily bent during draping, and the intra-ply or inter-ply deformation is restricted and leads to out of plane buckling [79]. Buckling is due to in-plane compressive stresses and is measured per unit width of the sample in in-plane compression. Wrinkling can occur post-buckling phenomenon, which is then

triggered from the moment a critical compression force or strain is reached. The shear strain and elongation strain can be classified as the microscopic deformation mechanisms [79], were as the deformations including fibre bending, resin percolation and transverse fibre flow can be identified as deformations on mesoscopic deformation mechanisms. Additional deformations such as the fibre redistribution and the laminate thickness variations can be tagged as macroscopic deformation mechanisms regarding ply bending, in-plane and inter-ply shear. Forming behavior is determined by the combination of resistance to all these deformation mechanisms [79, 6].

Ideally, for an accurate prediction inter-ply slippage (in-plane), ply bending, and intra-ply shear (interface) need to be found out to determine the global deformation of a composite laminate under forming conditions as described in Table 3. The resistance against these deformations determines the formidability of a composite material at forming states [76].

3.4 Experimental Composite Fabric and composite laminate characterisation (at forming temperature)

Although the actual thermoforming process takes place under non-uniform deformation rates, currently the characterisation tests are done at a constant temperature and speed/angular velocity. The results obtained are for isothermal material properties, and validation done by comparing the experimental results with FEM (which is detailed in chapter 4).

As previously stated, for a macro scale model, any deformation in the entire composite laminate is assumed homogeneous. The dominant deformation mechanism of fabric deformation is in-plane shear [76, 80] and tensile properties, especially with composite fabric with the high stiffness of yarns on the tensile direction and much lesser stiffness on the shear. Bending stiffness is also considered and has been known to influence the occurrence of wrinkles associating with shear properties. [81]. Friction between the adjacent plies and between the tool and the laminate plies is also a critical factor contributing to the final structure of the composite part which needs to be addressed with specially designed testing setups. [79, 78, 82, 83]

Table 3 Basic principle values required for composite forming simulations

Composite Fabric	Composite Laminate

▪ Tensile modulus
▪ Shear modulus
▪ Shear angle
▪ Thickness
	▪ Shear modulus
	▪ Bending modulus
	▪ Frictional Coefficient (Static and Dynamic)
	    ▪ Tool-ply
	    ▪ Ply-ply
	▪ Shear angle

3.5. Process FEA Simulation approaches

Even with all the advantages of composite materials as mentioned before, a composite part is only as good as its design. To utilise all the unique properties of a composite material, it must be made sure that there are no wrinkles and excessive thinning on the part. The final fibre orientation should be aligned with respect to the distribution of the load. Currently thermoforming and RTM (Resin Transfer Molding) have been identified as the production technology suitable for mass production of composite materials [84].
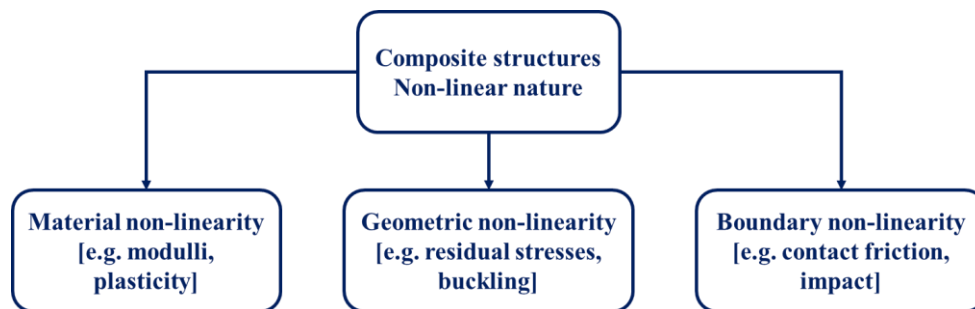
Figure 13 Classification of non-linear problems [adapted from 85]

Conducting process simulations for thermoforming of two-dimensional composite laminates into a three-dimensional product is considered a very complicated process mainly due to the anisotropic nature of the blank. The quality of any process simulation depends on the mechanical properties of a composite fabric that needs to be characterised as explained in the previous sections. Other

important factors that influence the simulation are temperature, binder pressure, punch velocity, punch pressure, etc.

Thermoforming of a thermoplastic composite part is complex and can induce various defects on the final part. While some flaws can be tolerated like thinning on non-structural areas of the part, critical defects will lead to discarding or worse, unexpected failure during load conditions [84]. As shown in Fig 13, process simulation checks for geometric non-linearity and boundary non-linearity to an extent. Critical evaluation of the integrity of the part by checking for errors and deformations is the primary purpose or process simulation. With this approach, adjustments can be made quickly to the part on a geometric level to get an optimum design for the part, and the tools can be made accordingly. This effectively eliminates the traditional, expensive and time-consuming trial and error approach. [86].

a. Fibre Wrinkling

b. Fibre thinning

c. Out of plane wrinkling
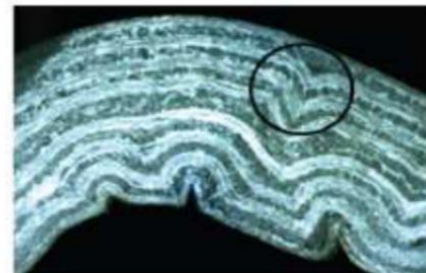
d. Interply fibre wrinkling

Figure 14 Defects in Composite Laminate Profiles during thermoforming operation [adapted from 87, 88, 89]

Fig 14 shows the common defects in composite laminate profiles originating during the thermoforming operation. All the defects need to be addressed in the process simulation, and the deciding factor is the ability to efficiently map these results to a standard mesh for further load or crash simulations.

3.6 Mapping

After forming composite components, the accumulated plastic strain may increase or decrease the yield for further loading depends on the load direction. Also, for a regular load and crash simulations, a constant thickness along the surface of the part is assumed which is not usually the case as thickness variations or thinning may occur during the forming operation. The most critical criteria that affect the simulation is evidently the reorientation of the fibre in the composite part post-forming. All the mentioned critical aspects are missing from usual crash/ load simulations leading to reasonably inaccurate results.

Mapping is done to transfer simulation data between the results from the process simulation results having different discretisation, element types, material models etc. to the crash model. This efficiently transfers the resultant stresses & strains developed in the model during production and more importantly the change in the fibre orientations during forming including any associated thickness change on to the actual model [71].

| Mapped Plastic Strains on the Crash Component | Physical Test Results | S1 - FE Results without forming effects | S2 - FE Results with forming effects |
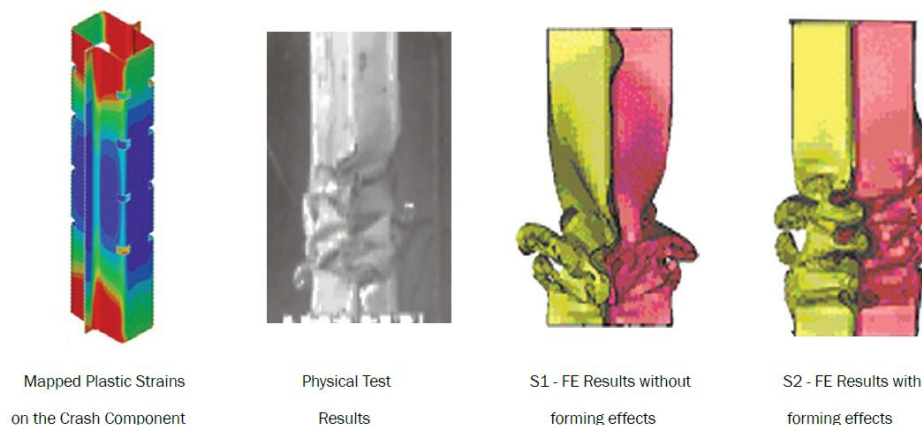
Figure 15 Effectiveness of using mapping on a metal component [adapted from 71]

Fig 15 shows mapping done on an isotropic metal component, based on a case study done by Altair [71], demonstrating the apparent match between the physical test and the FE model with and without the process simulation results mapped on to it. The effect of residual stresses has an evident impact of the model as per the set of images, showing the importance of mapping for structural simulation accuracy.

Mapping is studied in detail in chapter 4, for composite fibre reinforced thermoplastic components.

Chapter 4

Experimental characterisation and structural analysis

The primary case study for the research thesis, as shown in figure 2, is an over-molded part constituting a continuous glass fiber reinforcement consolidated with a polymer layer as a substrate over-molded with short fibre reinforced polymer compound. The continuous fiber reinforcement used is TEPEX® Dynalite 104-RG600(2)/47% supplied by Bond Laminates [61] and the short fiber impregnated polypropylene over-mold used is Xmod™ GD301FE provided by Borealis [62]. The two materials were chosen because the base resin for both the composite material is polypropylene which will result in good inter-material bonding.

4.1. Characterisation tests

The mechanical characterisation of the two materials: TEPEX® Dynalite 104-RG600(2)/47% & Xmod™ GD301FE was done separately considering them as orthotropic-elastic until rupture and nonlinear afterwards. A set of tensile tests (0^0 and 90^0 Direction), shear and compression (0^0 and 90^0 Direction) tests were done on the specimen. An additional bending test was done on the specimen for further validation of tensile, compression and shear properties obtained.

The standards used for each test are mentioned in Table 4. Five specimens were tested for each test, and the detailed specimen description including the dimensions is given in Appendix 1.

Table 4 Basic principle values required for composite forming simulations [64, 65, 66, 67]

Tests	Standard	Description
Tensile tests	ASTM D 3039	Standard Test Method for Tensile Properties of Polymer Matrix Composite Material
Compression tests	ISO 14126:1999	Fibre-reinforced plastic composites -- Determination of compressive properties in the in-plane direction
Shear tests	ISO 14129:1997	Determination of the in-plane shear stress/shear strain response, including the in-plane shear modulus and strength, by the plus or minus 45 degree tension test method
Bending tests	ISO 14125:1998	Fibre-reinforced plastic composites -- Determination of flexural properties

All the experiments were done using an Instron Model 8801 machine with a maximum load of 100 kN. For each specimen, the force-displacement curves and stress-strain were calculated along with elastic modulus, maximum stress, strain at break and maximum load using the data obtained directly. An extensometer, capable of recording longitudinal deformation up to 25 mm and transverse up to 1 mm per side, or a strain gauge attached to each specimen (HBM LY-48-3/350 Ohm) was attached to each specimen to sample the strain measurements. For further elaboration of the experimental results, a dedicated Matlab code allowed to obtain mean value curves and the standard deviation. It calculates the ideal stress-strain curves for further FEA analysis and filtering out any noise on the curve, then the stress-strain curves output curves are obtained accordingly for further curve fitting.

Fig 16a to Fig 16d shows the raw data from experimental results for the continuous fibre laminate (TEPEX® Dynalite 104-RG600(2)/47%) showing its vital material properties. As the laminate is balanced, the properties are assumed the same for both 0° and 90°. The properties are summarized in Table 5.
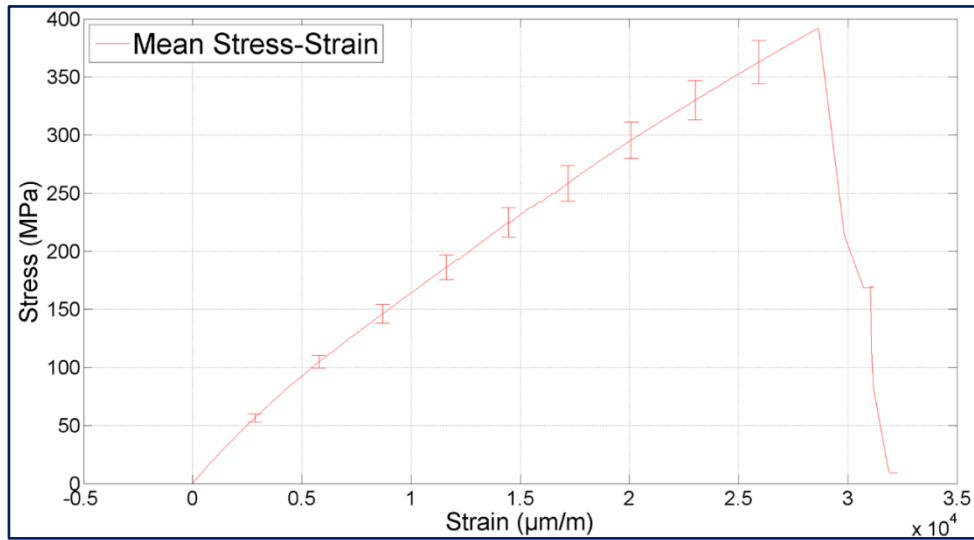
Figure 16.a Experimental results for the continuous fibre laminate: Tensile tests
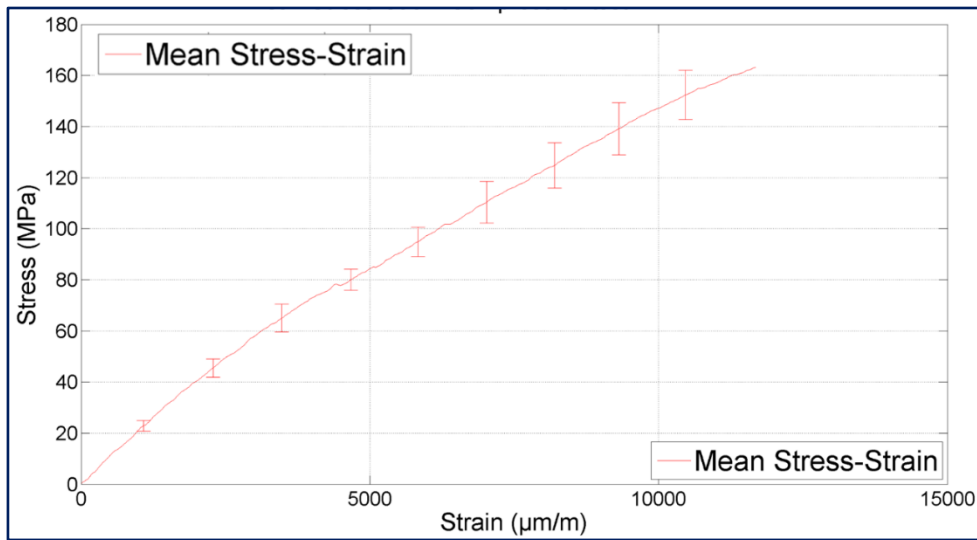
Figure 16.b Experimental results for the continuous fibre laminate: Compression tests
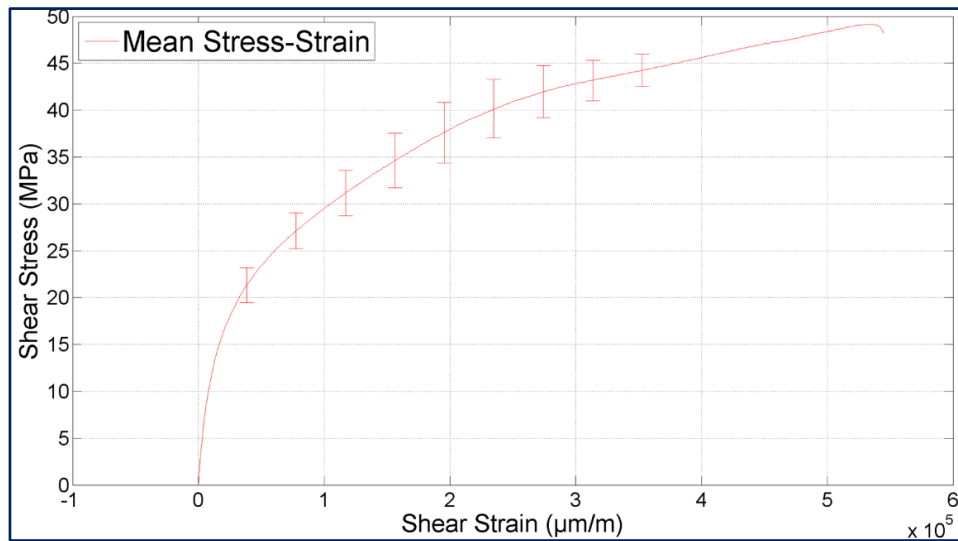
Figure 16.c Experimental results for the continuous fibre laminate: Shear tests
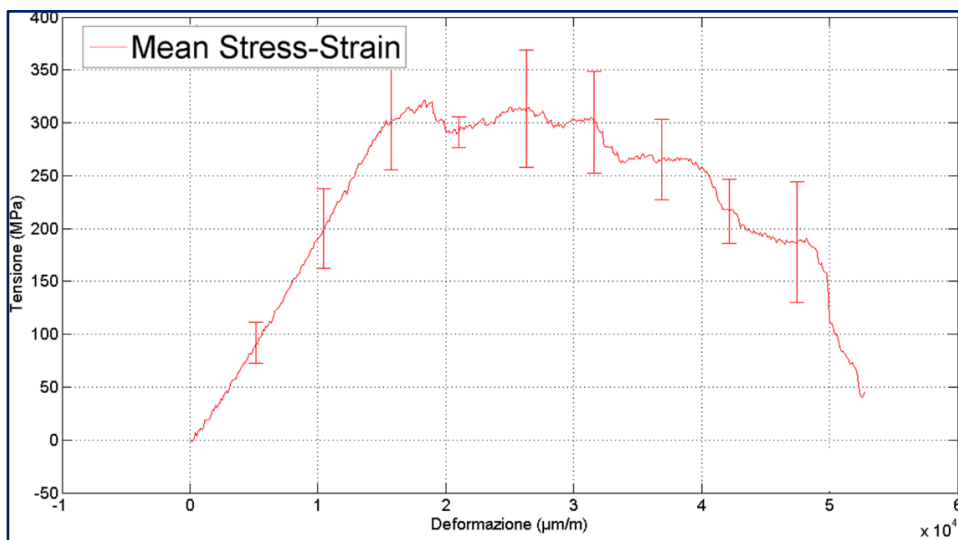
Figure 16.d Experimental results for the continuous fibre laminate: bending tests

Table 5 Properties for continuous fibre Laminate

Fig 17a to Fig 17e shows the raw data from experimental results for the continuous fibre laminate (Xmod™ GD301FE) showing its key material properties. The properties are summarized in Table 6.
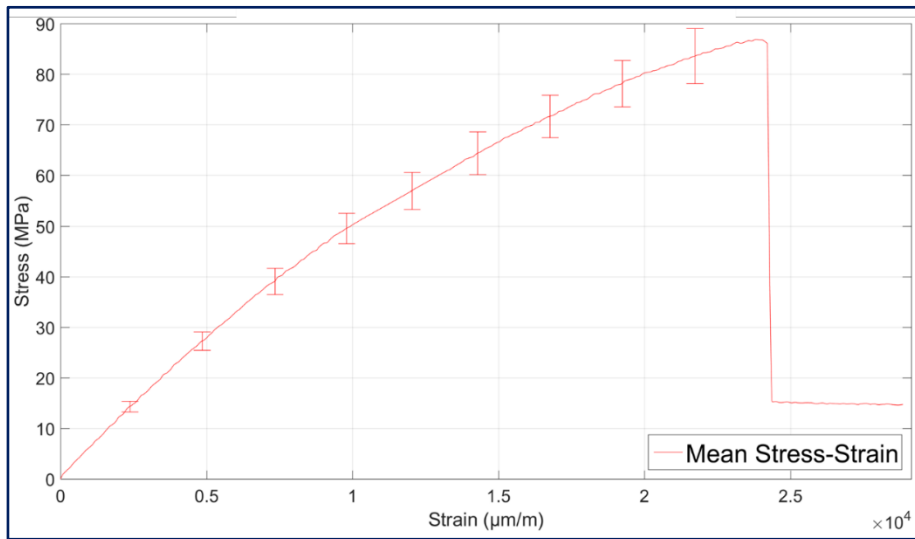
Figure 17.a Experimental results for the short fibre composite: Tensile test 0°
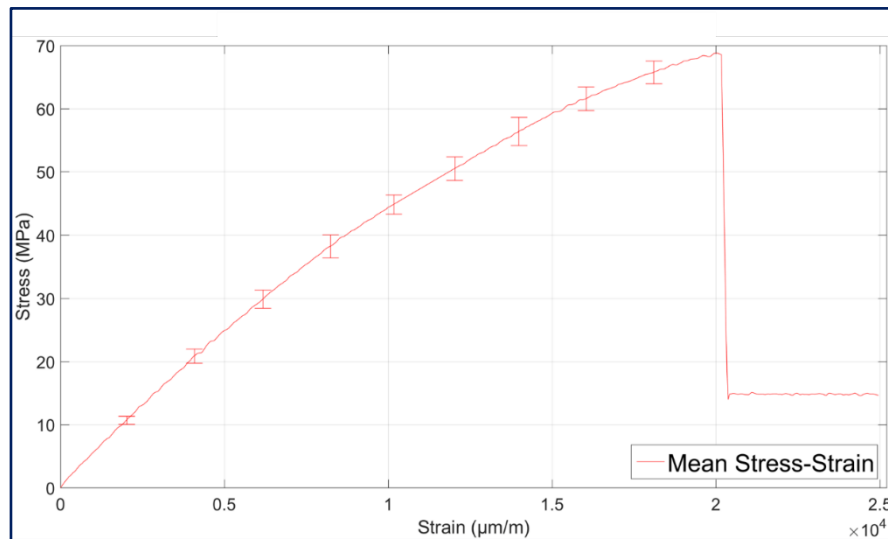
Figure 17.b Experimental results for the short fibre composite: Tensile test 90°
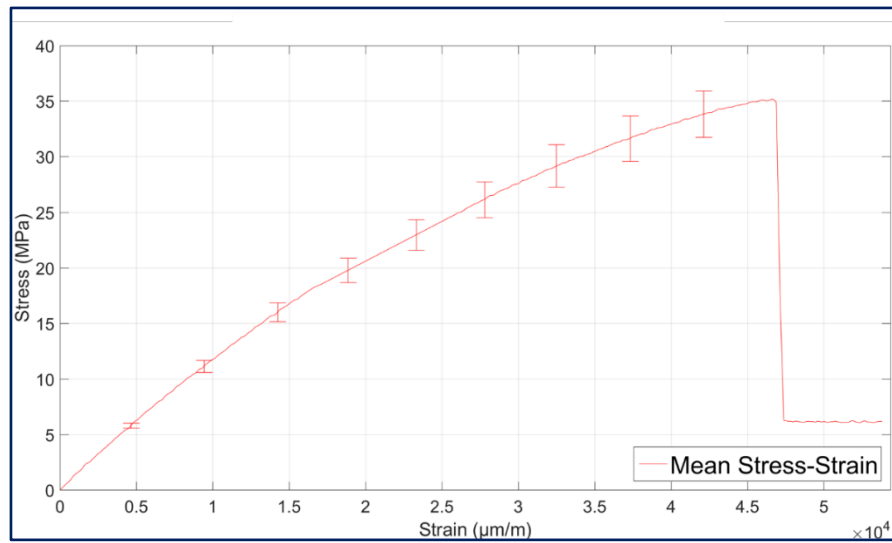
Figure 17.c Experimental results for the short fibre composite: Shear test
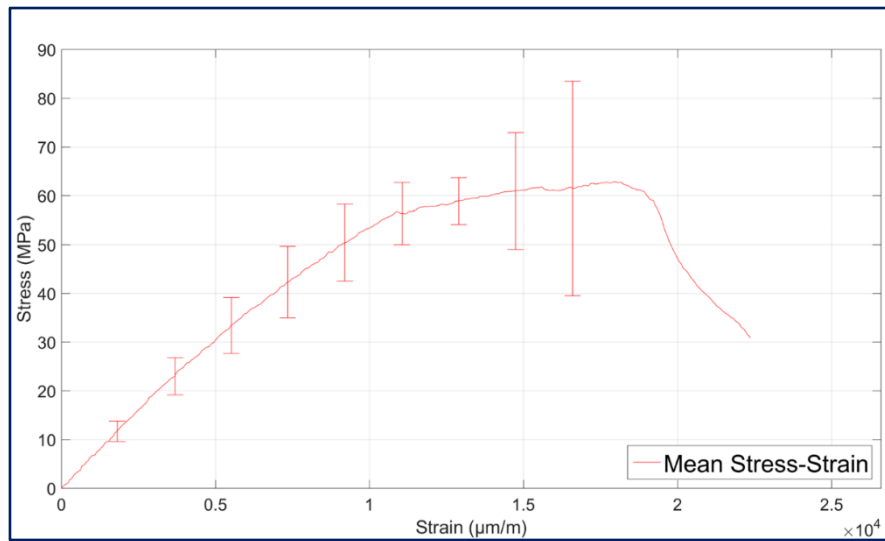
Figure17.d Experimental results for the short fibre composite: compression test 0°
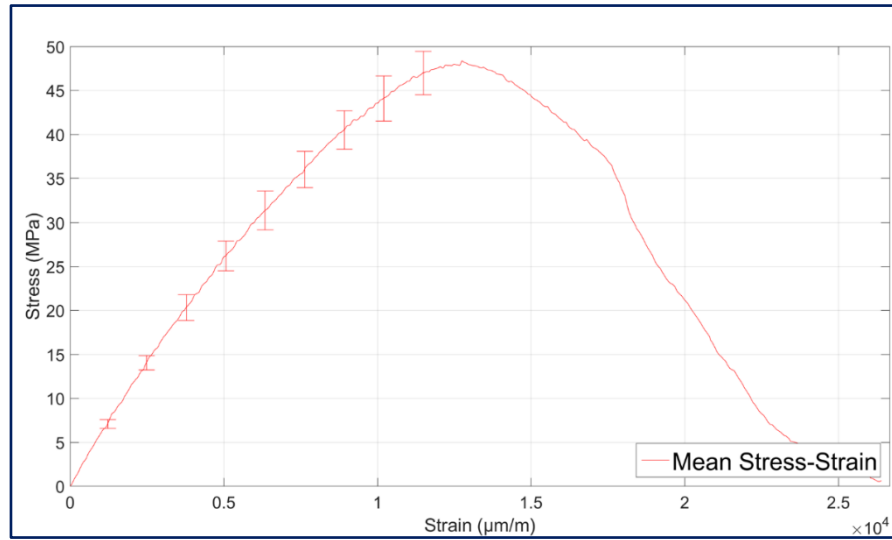
Figure 17.e Experimental results for the short fibre composite: compression test 90°
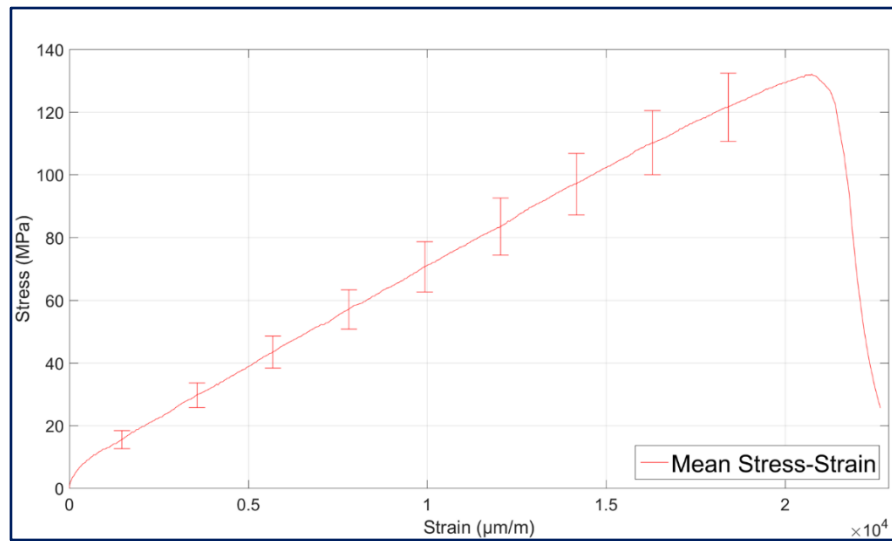
Figure 17.f Experimental results for the short fibre composite: bending test 0°

From the material properties obtained, the next step is to make the associated FE material cards for it, which is detailed in the next section.

Table 6 Properties for short fibre composite

4.2. Card fitting

An extensive card fitting study has been conducted as reported in Fig 18, 19 and 20, aiming to match its tensile, compression, shear and flexural properties, as closely as possible to the FE card. Card fitting is a technique used to create a precise FEA characterisation of the material by keeping the characteristic properties as its design variables, to match the FE simulation results to the experimental data.

This step is more challenging for fibre composites, due to their anisotropic and their inhomogeneous nature. The aim is to match FEA stress/strain curves to the experimental stress/strain curves obtained for all its defining material property separately like its tensile, compressive, shear, etc. The accuracy of the finite element analysis done on the actual parts depends on how closely the curves are matched.

(a) Compression test
(b) Shear test
(c) Tensile test
(d) Flexion test validation
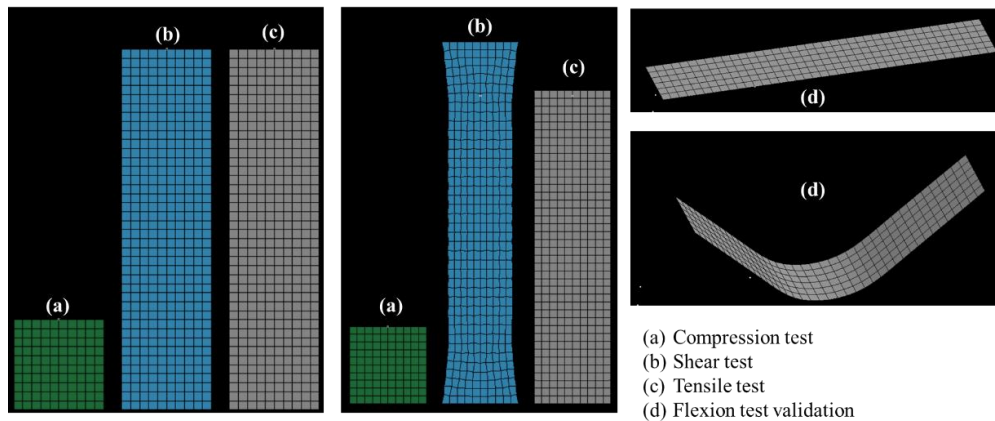
Figure 18 FE specimen for the continuous fibre laminate

As detailed in Section 3.3 of the literature review, two failure criterions are implemened in this reseach. Crasurv (failure criterion not associated with failure modes) and Hashin (Failure criterion associated with failure modes).

The FE material card Law 25 integrating the Crasurv failure criterion in Radioss Hyperworks [71] was used for curve fitting as displayed in Fig 19. [Appendix 4] The red curves denote the FE results from the Crasurv criterion and the results appear to be satisfactory with a good fit for the curves. A problem, which is anticipated with the Crasurv criterion, is that it does not distinguish between the different failure modes leading to inconsistencies in the result. The curves show perfect fit for the tensile, compression and shear, with a comprehensive match for flexion validation.

An additional, separate material card was also developed, the Law 58 in Ls-Dyna solver integrating a modified Hashin Criteria [90, 74] [Appendix 5] was implemented separately. As visible from the curves, the direct input of the experimental curves leads to a good fit for the tensile and the compressive properties of the card Fig 19.a & Fig 19.b, but the fit is lacking for the shear and the bending validation as in Fig 19.c & Fig 19.d, although further optimisation is required for that.
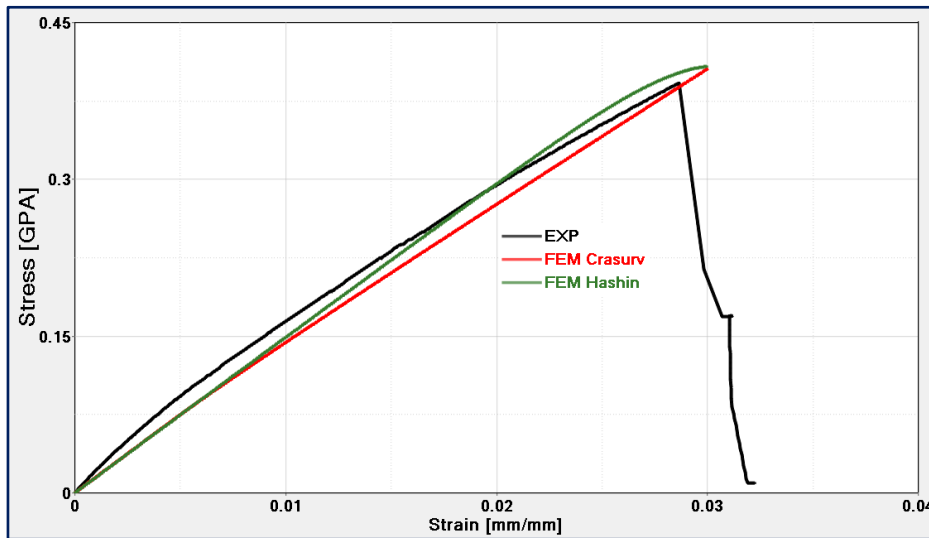
Figure 19.a FE material card for the continuous fibre laminate, Tensile test: first result
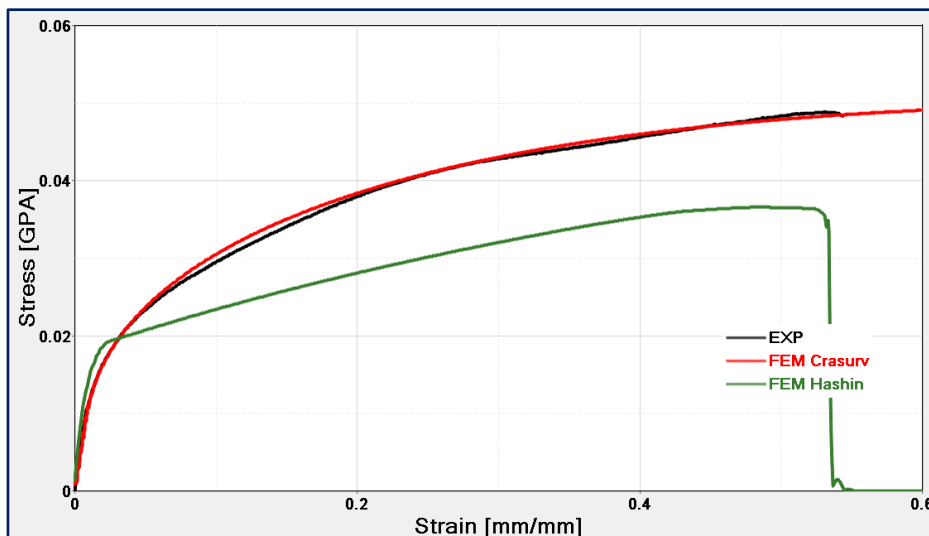
Figure 19.b FE material card for the continuous fibre laminate, Shear test: first result
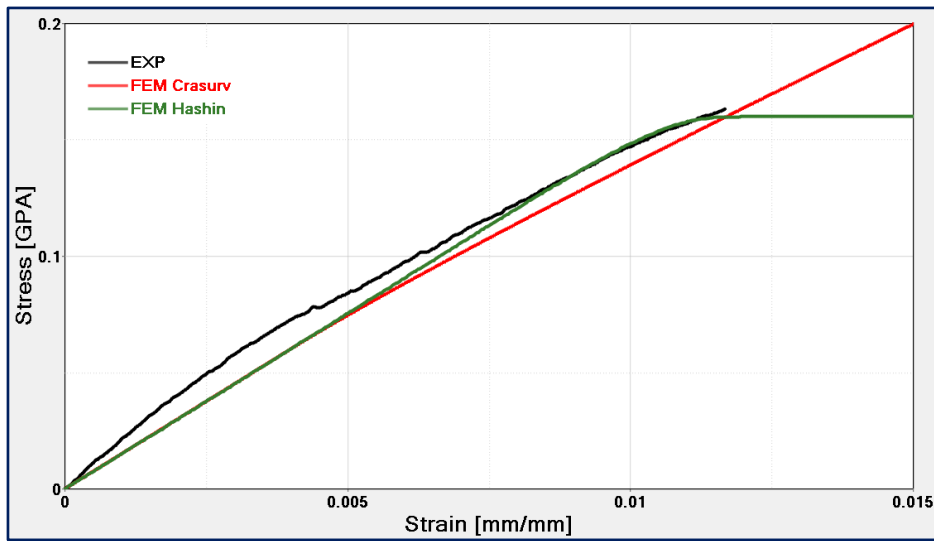
Figure 19.c FE material card for the continuous fibre laminate, Compression test: first result
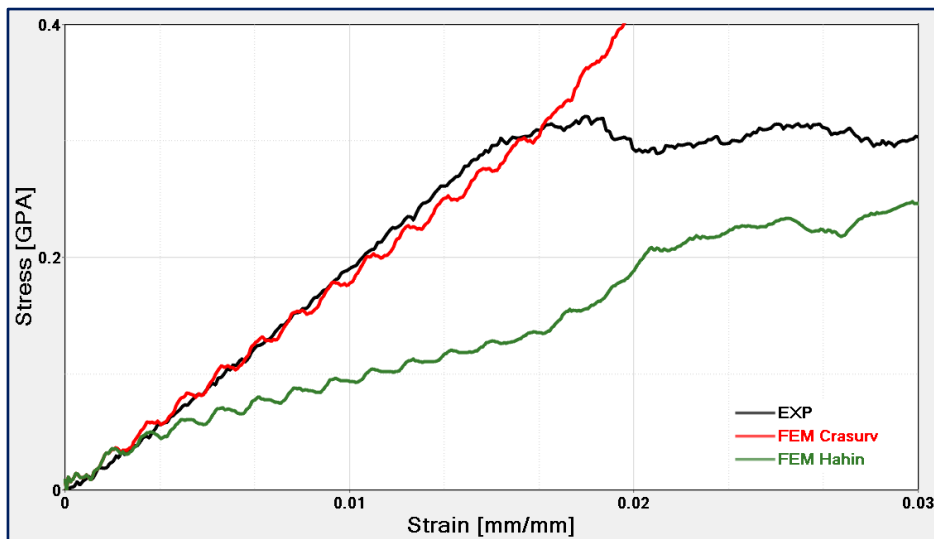
Figure 12.d FE material card for the continuous fibre laminate, Bending Test: first result

The FE material card associated with Hashin criterion is further optimised for a better curve fit by implementing different breaking point (Yield point from the experimental curves Fig 16.a to Fig 16.d) or point of failure on the card for each of the principal properties as shown in Fig 20.a to Fig 20.d. The shear strength has been adjusted slightly as well for a better curve fit with the experimental one.
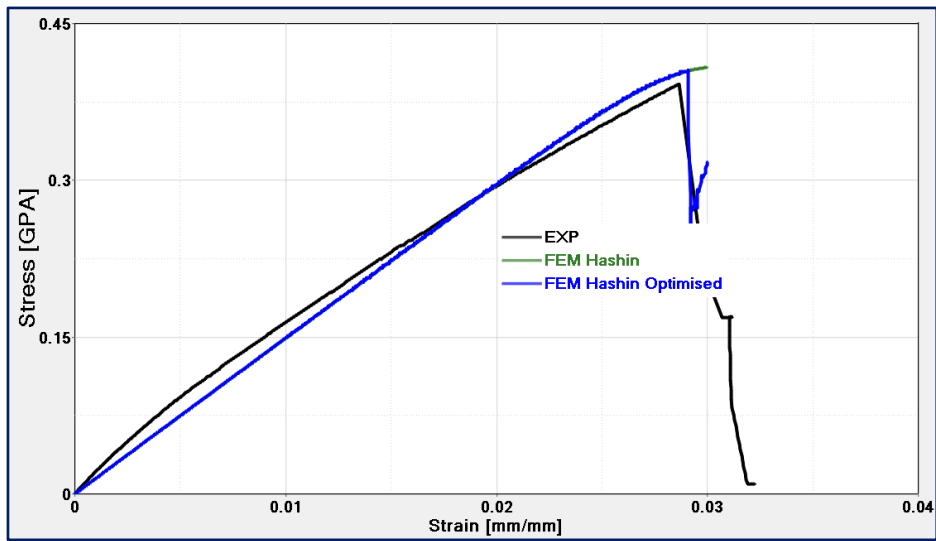
Figure 20.a FE material card for the continuous fibre laminate, Tensile Test: optimised result
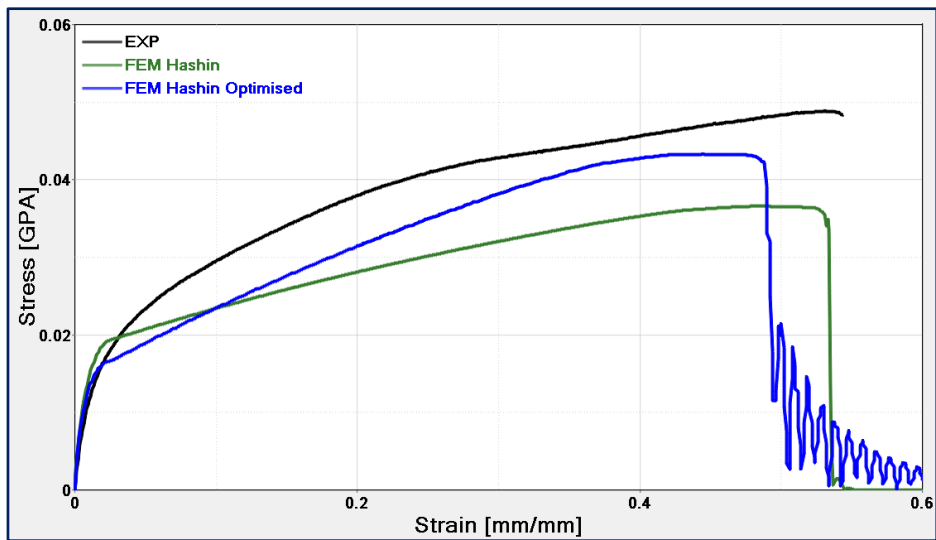
Figure 20.b FE material card for the continuous fibre laminate, Shear Test: optimised result
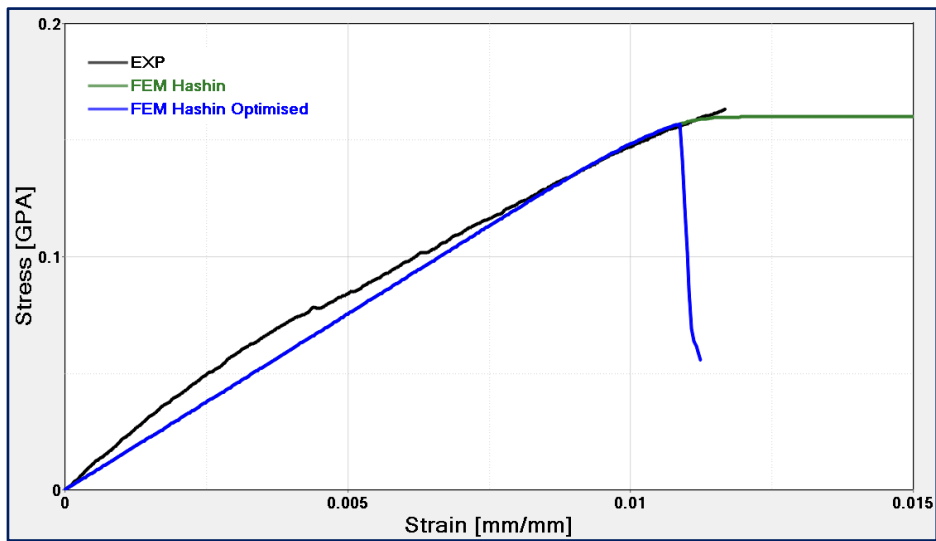
Figure 20.c FE material card for the continuous fibre laminate, Compression Test: optimised result
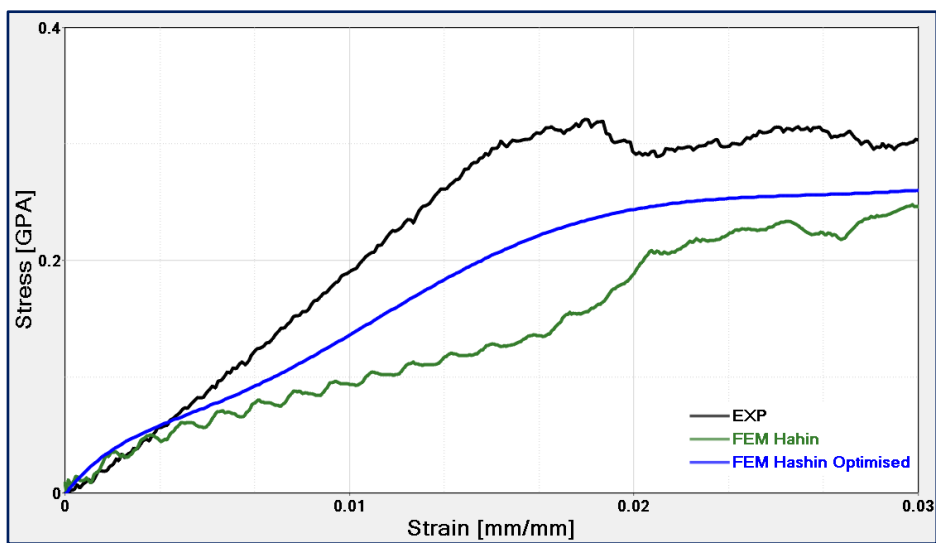
Figure 20.d FE material card for the continuous fibre laminate, Bending Test: optimised result

The credibility of the acquired FE material cards (the Crasurv, and the optimised Hashin) are all tested and demonstrated in the structural simulation (detailed in chapter 4.4).

The Card fitting for the short fiber composite part [62] is included in the [Appendix 2], as the focus of research from now on will be on continuous fiber laminate.

4.4. FEA Structural simulations and comparison with experimental results.

A four-point bending test is used for the experimental validation of the FEA. Specifically, the ISO 14125:1998 [4] for testing the flexural properties of the chosen laminate reinforcement for the overmolded component (Fig 2). Bending test is quite simple to perform, but the state of stresses and the associated failure modes is very complicated. The tensile and the compressive strength of fibre reinforced composites can be contrasting and is fibre direction dependent as well. Therefore, for bending test of a composite part, it undergoes both compressive stress (at the top) and tensile stress (at the bottom) of the composite part.

Once card fitting creates the matrial database, the FE model of the component is made with this material data using appropriate properties. Interfaces and constraints are designed to match the actual physical four-point bending tests to get a good comparability of the results. Flexural strength and stiffness are the combined effects of a material's tensile, compressive and shear properties.

The specimen is loaded in the horizontal position, which results in the application of compressive force on the upper side and tensile force on the lower side. There are two load points at equal distances from the support points for the four-point bending test, and the gap is kept 1/3 of the 250mm span.

4.4.1. Four-point bending experimental tests

The Laminate reinforcement part shown in Fig 8 was subjected to load with appropriate four-point bending fixtures using an Instron testing machine. The four-point bending fixture was customised to minimise the shear stress deformation and to limit inter-laminar shear failure, which is done by making the support span considerably longer than the specimen thickness. The specimen will be deflected at a constant rate of 2 mm/min until it fractures. The machine is equipped with automatic hydraulic grips that allow substantial contact with the specimen and ensuring their grip without sliding. The force and displacement were acquired directly from the testing machine.
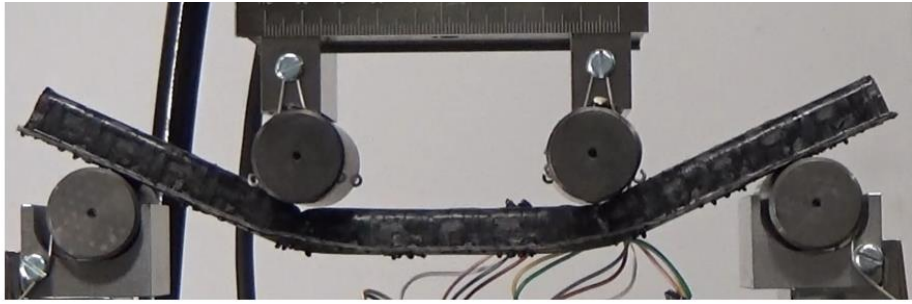
Figure 21 Composite component, structural four-point bending test

Although the component was tested in various orientations, only the results when normally tested to the component as in Fig 21 were considered for this thesis. A set of five specimens were tested giving an average maximum force of 600 N at its breaking point with a displacement of 7.7 mm. The average force-displacement curve is plotted on fig 23. Because of the curved nature of the laminate part and the slightly angular base, it was made sure there were four points of contact when the test was started to avoid erratic results.

The machine displacement is assumed to correspond the real displacement suffered by the sample at the contact points. Initially, there were some doubts about the reliability of the displacement recorded by cross head displacement for bending tests with no external device such as an extensometer. The crosshead displacement suffers some noises, including the effect of machine compliance, which may amplify the reading, depending on the sample compliance. This doubt was eliminated by doing some physical tests comparing the recorded crosshead displacement to the actual crosshead displacement by obtaining a sequence of photographs in fixed short interval proving the assumption correct. More details on the test done is included in Appendix 3.

4.4.2. Four-point bending tests by FEA

After the extensive card fitting done, four-point bending FE tests were done to simulate and compare with the experimental results. The element size was kept as 2mm, the same as during the card fitting of the material. The component was subjected to imposed displacement with the two cylinders to replicate the four point bending test with no additional boundary conditions.

Flexural strength and stiffness are the combined effects of a material's tensile, compressive and shear properties. The laminate FE specimen is subjected to pure flexion with two cylinders with the exact specifications of the physical four-point bending tests done as shown in Fig 22.

As explained in the card fitting, two composite failure criterions have been exhaustively studied for the composite laminate substrate. The two cards are implemented separately, compared against each other and with the experimental results.
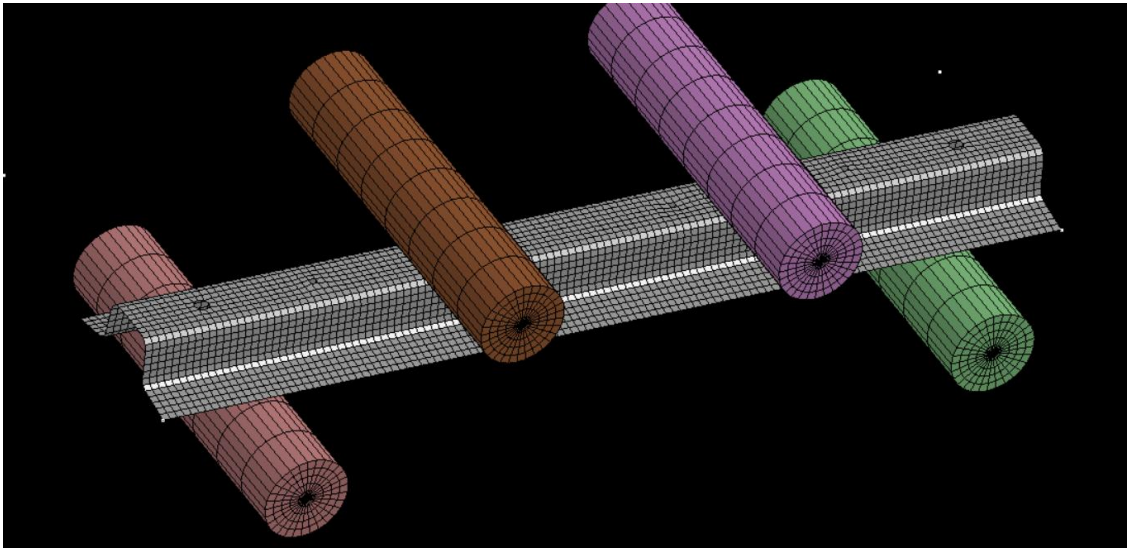
Figure 22 Composite part, structural FE Four-point bending simulation model
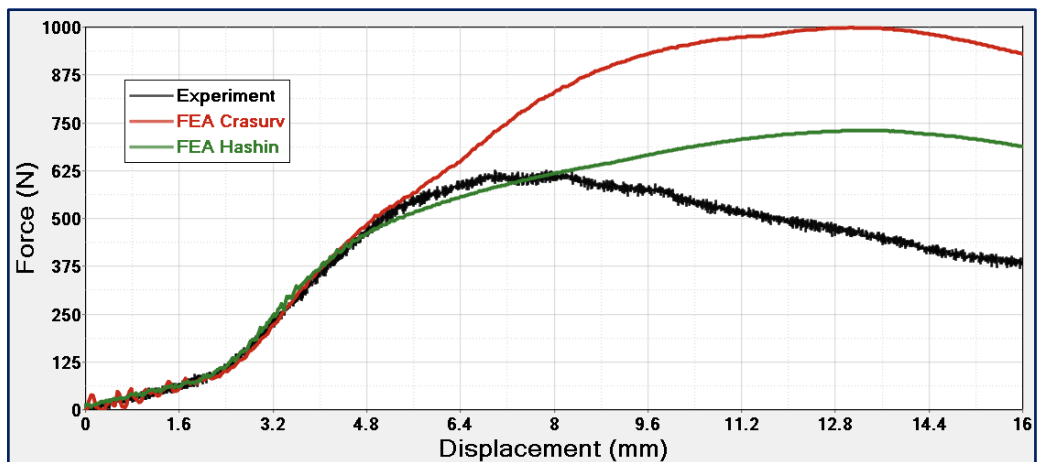
Figure 23 Composite part, four-point bending results comparison among experimental, FEA Crasurv and FEA Hashin

Fig 23 shows the FE material card implemented from the initial results presented in Fig 19, comparing the Crasurv criterion and Hashin criterion against the

experimental curve. This was done to find the ideal failure criterion that can be implemented efficiently on to a composite part under review. From the curves, it is evident that both the failure criterions hold good for its elastic behaviour, but the curve with Crasurv criterion diverges upwards in the plastic strain zone compared to Hashin criterion. At this stage, it is conspicuous from the comparison that the Hashin failure criterion would be better suited for this application.
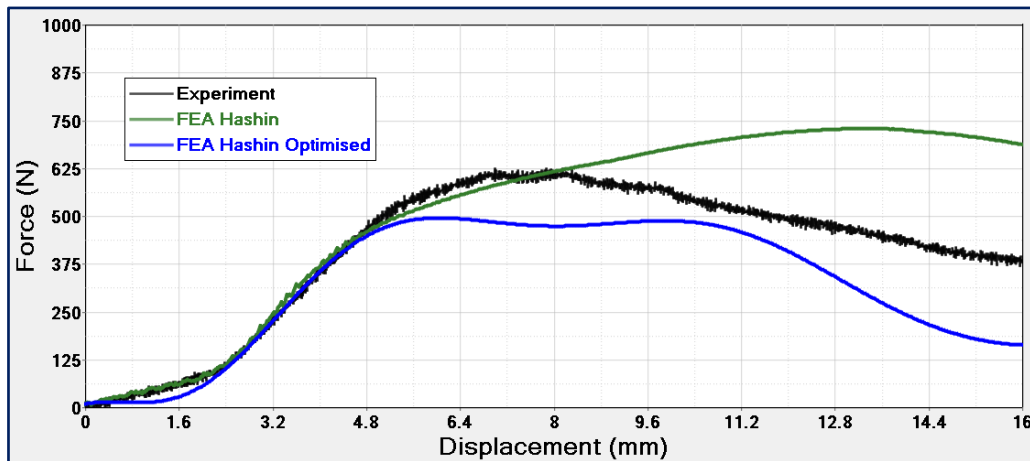
Figure 24 Composite part, four-point bending results for experimental, Hashin and Hashin optimised

The Hashin failure criteria are further optimised in Fig 24 as per the FE card developed in Fig 20. After the optimisation, the force-displacement curve converges downwards underestimating the strength of the component; making it the most accurate result so far.

4.4.3. Results and discussion

The results obtained with the Crasurv criterion were not very satisfactory as shown with the four-point bending test of the laminate component compared with the experimental results as shown in Fig 23. The problem being the criterion does not distinguish between different modes of failure.

This drawback for the Tsai-Wu/ Crasurv criterion has been studied by John Hart, [91] where demonstrates the compressive stress states of a submarine hull could be increased by decreasing the transverse strength on the same laminate; which of course is physically incorrect. Therefore, the conclusion is when multiple failures occur on a part at the same time as in the four-point bending, the results

may not be accurate in the plastic zone. The results after implementing Hashin criterion is much better as shown in Fig 24 showing a massive improvement from the Crasurv criterion.

To conclude, the Crasurv criterion which considers isotropic nature of the composite materials is not very accurate for the component considered in this thesis undergoing multiple failure modes at the same time. While the Hashin criteria which consider the non-homogeneous nature of the composites is visibly more accurate. The final result of Hashin criterion gives an underestimated strength of the component which is accepted in the Industry. However, the aim is to increase further the accuracy of the result, which is further studied in the following chapters.

Chapter 5

Process Simulations

By concluding chapter 4, the maximum possible accuracy of the model was reached by considering only the material non-linearity, as detailed in the building block in Fig 6. Additionally, to increase the efficiency of the model boundary and geometric non-linearity of the model needs to be considered. Considering the inclusion of residual thermal stresses, change in fibre orientation while forming, stiffness degradation models, and delamination failure, etc. For the composite laminate part under review as detailed in Fig 8, the effect of delamination and degradation is limited as there are only two plies, so fibre orientation change and residual thermal stresses are further investigated which is the results from the process simulations.

Process simulation for thermoforming involves shaping the thermoplastic prepreg by heating it above its glass transition temperature to form it into a three-dimensional part. It involves heating the material first to its glass transition temperature for shaping, then transferred to the press where it is hot pressed [57]. The formed part is then cooled under the same pressure to ensure dimensional stability and then removed. However, for forming simulations, to reanimate or predict the process, a complete material characterisation needs to be done at all the temperatures the blank will be exposed to. The results greatly depend on the property of the resin concerning temperature, so a multiple temperature strain dependency input curve for the resin determines how close the output will be to the actual scenario [92, 93].

The commercially available software for thermoforming of composites are LS-Dyna (MAT_249 model) [90], Abaqus (Fabric Material model) [94], Radioss (Mat_58) [95], Aniform [96] and PAM-FORM (Mat 140) [97]. A table comparing the different features of all the FE codes are shown in Table 7. The comparison study was done partly based on a benchmark study done by researchers from various companies including AUDI, Volkswagen and BASF [98].

Table 7 Process simulation results compared with the actual part (partially adapted from [98])

Feature	PAM-Form	AniForm	LS-Dyna	Abaqus	Radioss
Defining bending behaviour seperately	Yes	Yes	No	Yes: user defined	No
Implimenting charectersitc curves	Yes	No	Yes	No	Yes
Deformation described by constitutive models	No	Yes	No	Yes: user defined	No
Rate dependent bending behaviour	Yes	Yes	No	Yes: user defined	No
Rate-dependent interface mechanisms	Yes	Yes	Yes	Yes: user defined	No
Thermo-mechanical Modeling	Yes	Yes	Yes	No	No
Modeling of grippers / clamp holders	Yes	Yes	Yes	Yes: user defined	Yes
Tailoring determination	Yes	Yes: user defined	Yes: user defined	Yes: user defined	No
Export fiber orientation	Yes	Yes: user defined	Yes: user defined	Yes: user defined	Yes

The comparative study explores all the essential and important capabilities that are expected to be fulfilled by FEA. Although the FE codes are relatively similar, the central aspect to consider is the availability of the proficiency on how to implement them, also how credible and repeatable the results are. Another crucial deciding factor is the operability of the FE codes, which includes how user-friendly the FE code is, how time-consuming it can be and how easy it is to make changes on the simulations.

For the current research, initially, all the simulations were run in Radioss and were later changed to LS-Dyna. This was because the Radioss does not have a specific material model yet for composite forming and is currently combining two material models to obtain the required results. (Law 58 fabric card and Law 59 cohesive element card) [99]. LS-Dyna was more accessible with more robust results with their new material model Mat 249 for thermoplastic composite forming [Appendix 6]. Aniform was initially tried giving reasonably good results, as part of the research as well and is now kept for future trials due to the current time restrictions.

The deciding factor was the ability to map the process simulations results to a standard mesh for further load or crash simulation. With Ls-Dyna the linkage of multiple commercial tools for mapping the process simulation results could be avoided, as the mapping code could be directly implemented as detailed in the Chapter 4.

5.1. Experimental characterisation for process simulation

The material characterisation tests are done based on the literature review to complete the chosen FE material card (Law 249 in LS-Dyna).

5.1.1. Tensile Characterisation

Tensile tests are done only on dry composite fabric and not on the composite laminate (fabric + resin) because material parameters such as tensile Young's modulus are fibre dominant and exhibit limited change with respect to temperature. This is based on the study done by Melo and Radford [92].

During tensile tests, two deformation modes can be observed when the fabric is tested axially as shown in Fig 25. The first deformation mode (Fig 26) appears when the yarns are undiluted leading to the tightening of the yarns in the pulling direction. The second mode initiates after the full extension of the yarns leading to axial stretching of the yarns. When defining the tensile curve of fabric it is necessary these to deformation modes which is critical for further study and FEA simulations.
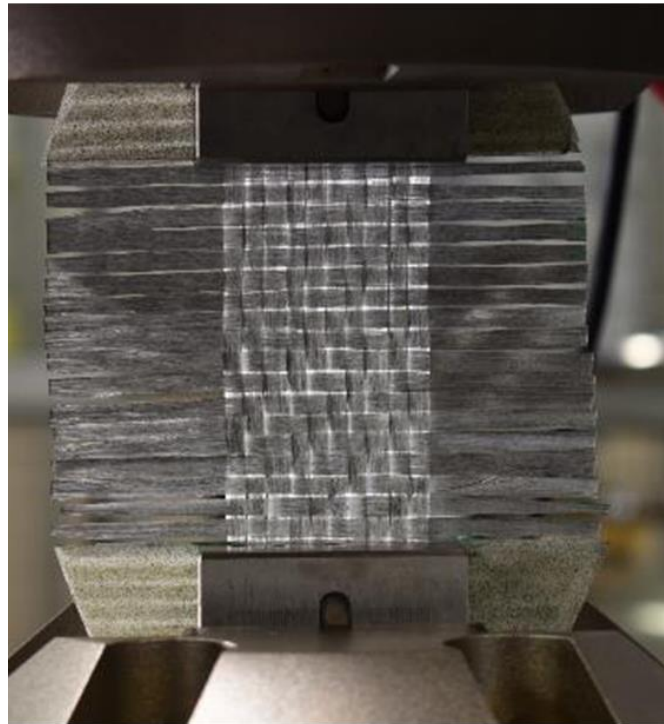
Figure 25 Tensile Fabric specimen
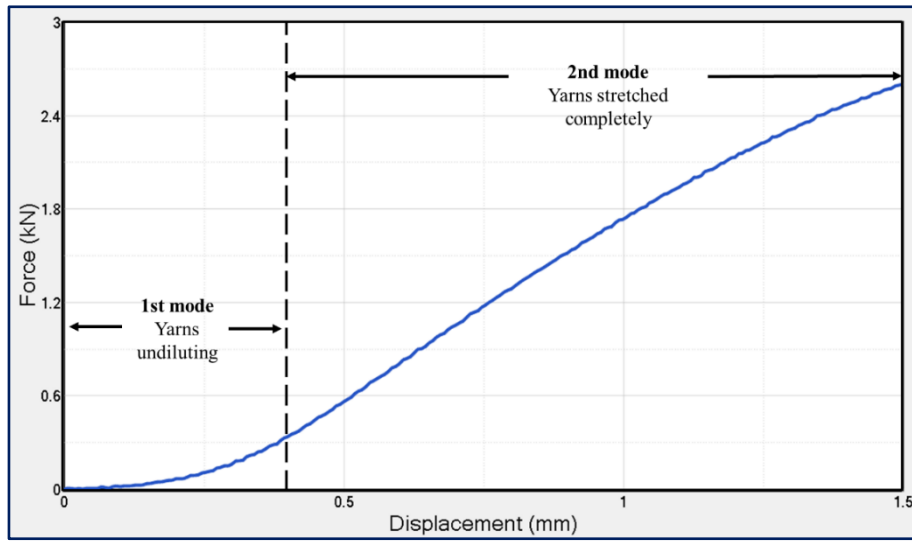
Figure 26 Typical tensile test result of a dry composite fabric as per ASTM D5035 (E-Glass twill fabric) [100]

The primary challenge is the difficulty in handling the fabric specimen and the requirement of powerful clamping force as the tensile load is usually incredibly high for composite fabrics. The fabric tensile tests are done at room temperature and the specimen following ASTM D5035 [100]. Exceptionally steep stiffness curves are usually observed for tensile curves for composite fabrics.
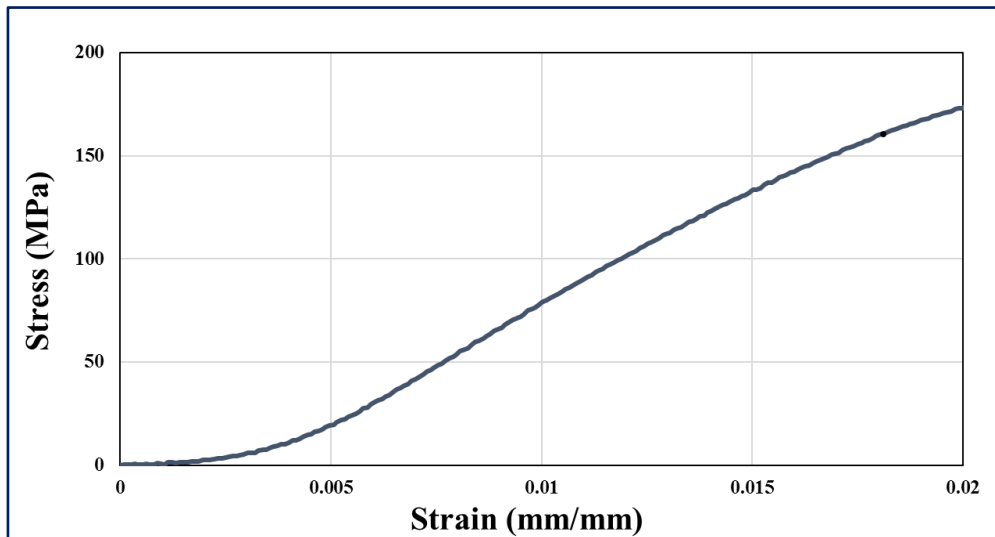
Figure 27 Tensile Fabric stress vs. strain

The associated stress-strain curves from the tensile tests are as shown in Fig 27. From the experimental curves, the card fitting is done to obtain the FE curves. The

card fitting displayed in Fig 28 shows an accurate fit for both force displacement and stress-strain confirming an excellent tensile match.
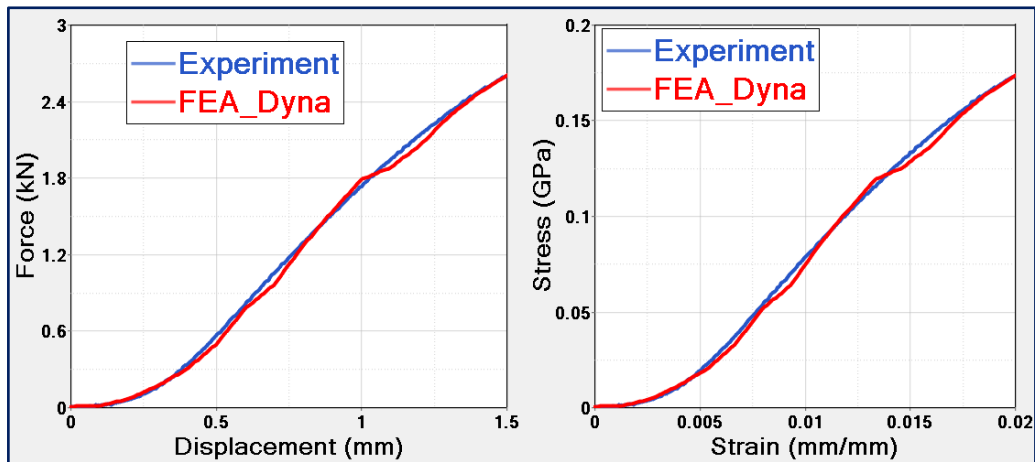
Figure 28 Tensile Fabric card fitting Force-Displacement & Stress-Strain.

5.1.2. Shear characterisation

Intra-ply shear is considered the primary deformation mechanism during the thermoforming of composites. It occurs when the fibre orientation changes when the yarns are rotated at their crossovers. This change in fibre orientation is denoted by shear angle, which starts at zero and increases or decreases when the angle between the warp and the weft yarn changes. A typical shear compliance curve for a composite fabric is as shown in Fig 29, which is divided into four regions.

During low shear angles denoted in the pure shear zone, the force required is meager is almost parallel to the x-axis which is mainly due to the friction between warp and weft yarns undergoing rigid body rotation. [101, 102]. The shear angle keeps on increasing till the yarns cannot rotate freely leading to compression of the yarns in contact which leads to a rapid increase in the shear stiffness. [101]. This point is denoted as shear locking angle, and the shear locking zone is the transition area of the shear zone of the fabric. The wrinkling post shear locking zone region shown in Fig 29 is where the shear angle is reached for the entire shear area leading to out of plane deformations such as stretching and wrinkling. All the load applied post shear locking is a combination of predominantly tensile, then yarn compression at the shear locking edges and some shear as well.
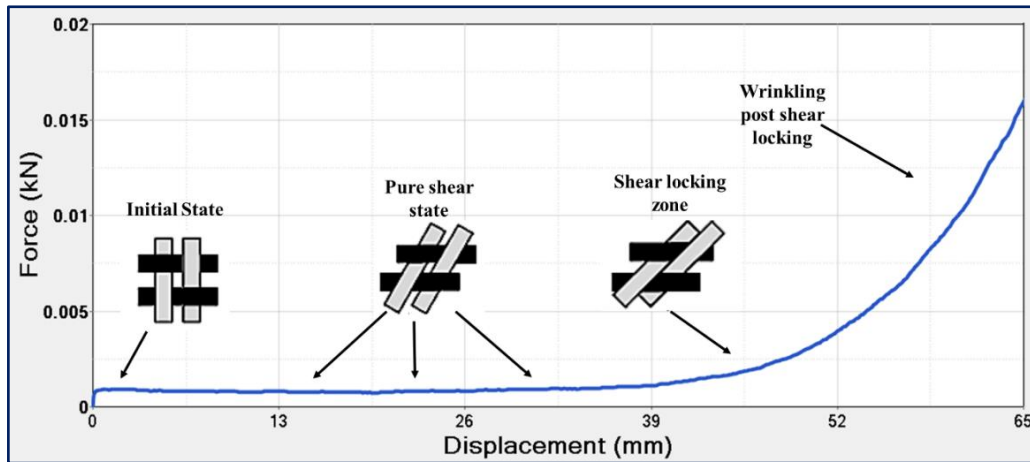
Figure 29 Typical shear curve for dry composite fabric

A benchmark study had been done to characterise the in-plane shear behaviour of composite fabrics [60]. Although there was slight variability in the results, based on the extensive tests conducted, some critical best practice methods and recommendations can be observed, such as the importance of the preparation of specimen in the right way, avoiding preload on the specimen, etc. Based on this study two methods are used to determine the shear behaviour, so that the results can validate each other. The methods are Bias-extension test and Trellis frame test, which is detailed in the following subsections.

Bias Extension tests (Fabric)

For Bias extension tests rectangular specimens of 200 x 100 mm^2 (with additional gauge area of ~ 50 x 100 for clamping) were tested as shown in the Fig 30 b. The warp and the weft of the specimen are initially oriented at ±45° to the applied force in the tensile direction. The speed of the test was fixed at 10 mm/min. The grippers were custom made as well to accommodate e-glass composite fabric and gauge area width of at least 100 mm.

During the testing, the measured force from the bias extension test is not pure shear deformation but a combination of partial shear and full shear forces. As the specimen is extended each fibre yarn is assumed to be inextensible, and the crossing acts as a possible rotation point developing three distinct regions as denoted in Fig 30(a). During the test, around the area of pure shear deformation, the shear angle increases gradually until it reaches a critical angle known as shear locking angle leading to out-of-plane deformation possibly leading to wrinkles. For the ease of

normalisation, the kinematics on the specimen undergoing bias extension are described using three different regions a, b and c. Fig 31. [103, 104]. The shear in the zone 'a' is expected to undergo pure shear, whereas the region 'b' is approximated to have half shear and the region c does not have any shear; remaining un-deformed during the test. This assumption of kinematics holds valid for the test specimen undergoing tensile force until the specimen is deformed leading to an intra-fibre slip and secondary crossover slip. This error is estimated equal to ±2° from the calculated results with a 50° shear angle [105]. However, this kinematic normalisation is necessary for isolating the shear stress further analysis.

Figure 30 a) Sample specimen shear force distribution, b) Bias extension test setup

Although from the initial analysis, it was proved that it is difficult to perform the test on the chosen material specimen; multiple tests were conducted to obtain at least five good results. The difficulty was mainly involved in handling the specimen as during the bias extension test the specimen is only supported on two sides leading to easy intra-ply slippage. This again is due to the specific nature of the chosen glass fibre fabric with its slippery nature and thicker yarn size.

The shear angle and shear force are calculated based on the relationships developed as a function of fabric size and displacement.
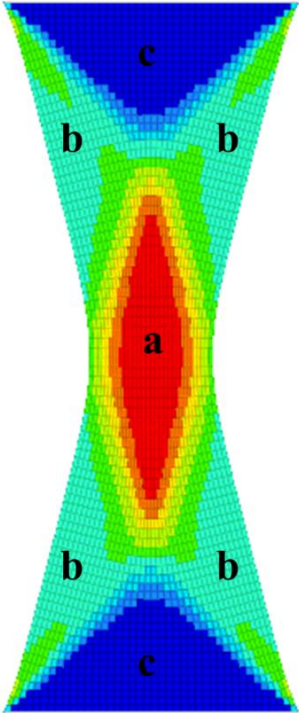
Figure 31 Bias Extension test setup
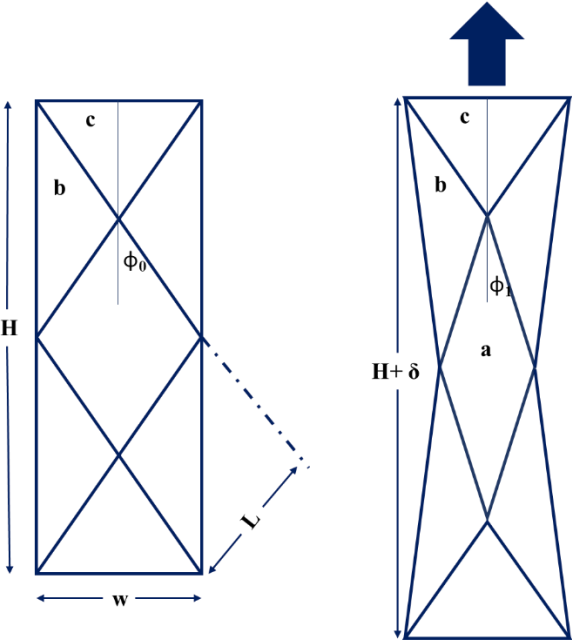
Figure 32 Bias Extension specimen representation for kinematic analysis

From the kinematic analysis of the bias extension sample shown in the Fig 32, the shear angle θ can be deduced as a function of the displacement δ, and the specimen size [106] through the equation:

$$\theta = 90 - 2\cos^{-1}\left(\frac{(H-W)+\delta}{\sqrt{2}(H-W)}\right) \tag{12}$$

Where, H is the tensile length of the specimen and W is the width. For normalising the shear force for bias extension, the energy required to deform the three deformation zones are considered for the specimen. The relationship is derived based on the assumption of pure shear kinematics on the fabric specimen.

$$F_n = \frac{(\lambda-1)f_A}{L_{eff}(2\lambda-3+2X)} \tag{13}$$

$$\lambda = \frac{H}{W} \tag{14}$$

$$X = \frac{(\cos\theta)^2\left[1+3\left(\sin\frac{\theta}{2}\right)^2\right]}{\left(\cos\frac{\theta}{2}\right)^2[1+3(\sin\theta)^2]} \tag{15}$$

Based on the normalisation steps done with the equations, the average result obtained showing the shear stress, and shear angle are presented in Fig 33. Additionally, the experimental results obtained are fitted on the FE material card fitted with MAT_249 Ls-Dyna material card as shown in Fig 34. The curves fit is not accurate post 35 mm displacement of the specimen. This may be because as the shear force is calculated analytically by the energy method, the result may not be accurate post the shear locking of the fabric. Although this is a point of concern, this is ignored for now to try a different shear test to compare the shear results [107].
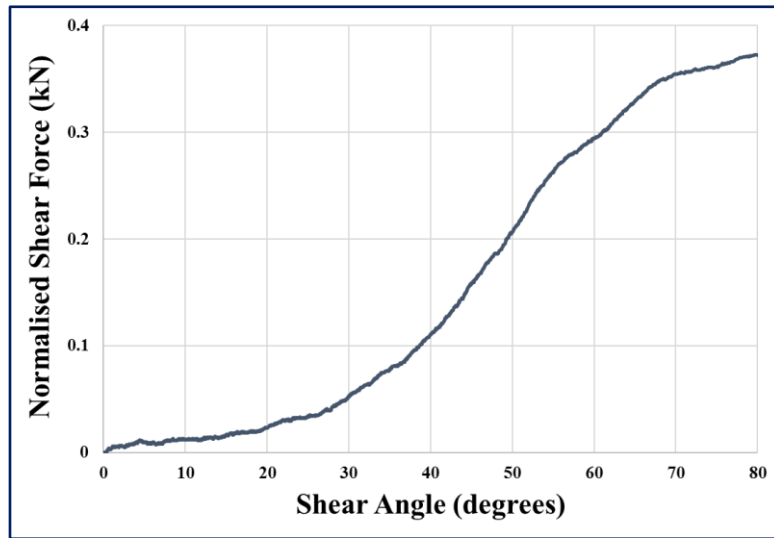
Figure 33 Bias Extension: Normalised shear force vs. Shear Angle
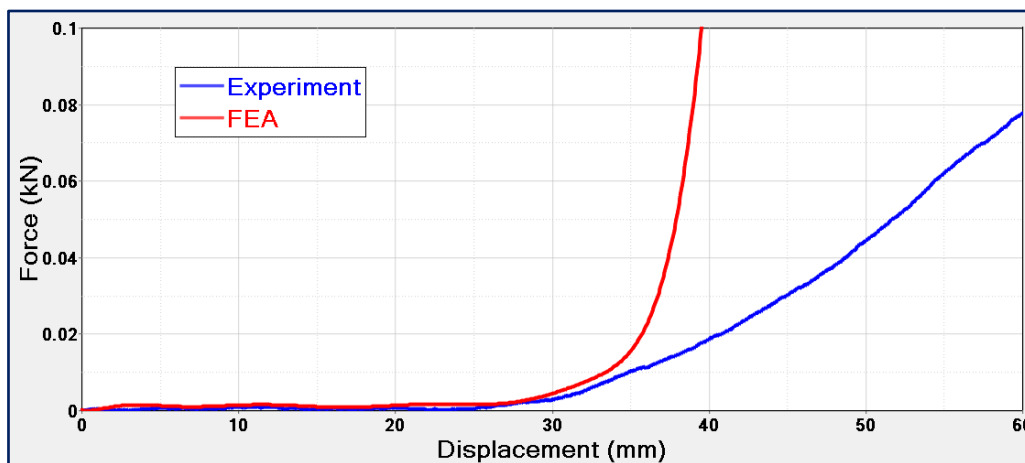
Figure 34 Bias Extension: Card fitting FEA vs. Experimental results

The loss of accuacy for experimental curves is due to the intra-ply slippage, which makes the results unreliable post shear 35 mm.

Trellis Frame tests (Fabric)

A trellis frame shear test has been additionally done for validation, and the setup is shown in Fig 35. The specimen is cut to have at least 100 mm^2 pure shear zone in the centre. Initially, the test is done only on the composite fabric to obtain its shear characteristics.
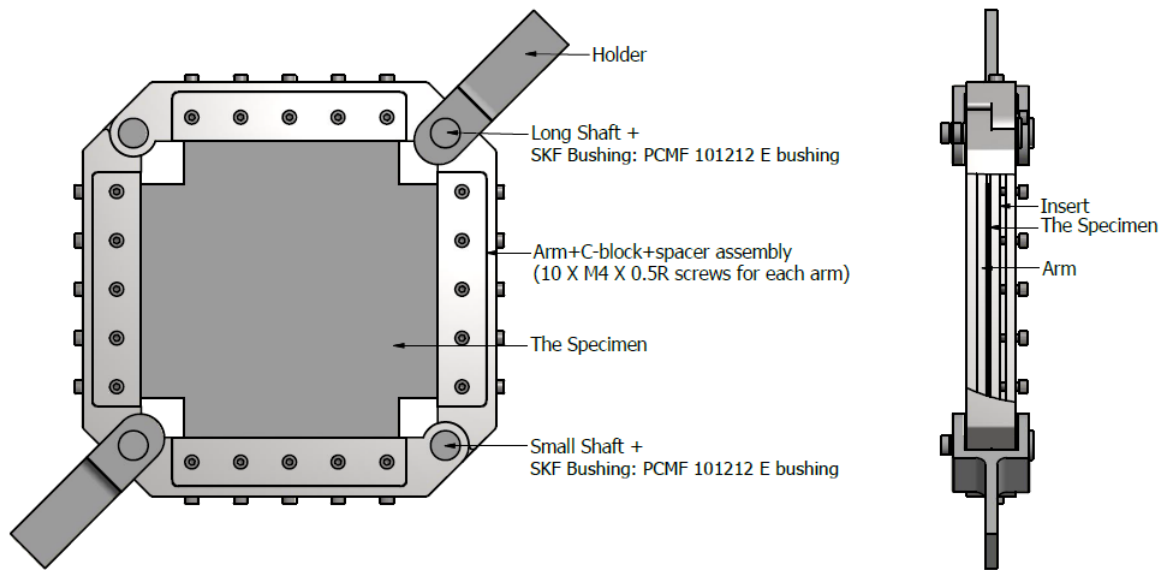
Figure 35 Trellis Frame setup

Extra precautions were taken while cutting the specimen to confirm and validate the number of yarns and its orientation. Additionally, two yarns were removed to isolate the shear zone in the trellis specimen as shown in Fig 36. To make sure the specimen undergoes uniform shear a sensitivity study was done to minimise the applied compressive and tensile force on the specimen, just enough to keep the element in place [108]. A high precision screw gauge was employed to do it as shown in Fig 37. Tow buckling due to the edge effects at the point of contact between the fixture and specimen is also minimised by doing the sensitivity study.

Figure 36 Trellis Frame fabric specimen setup

Figure 37 Trellis Frame specimen setup for good results

Yarn rotation is the predominant deformation for fabric when conforming to final geometry. This rotation is denoted as the shear angle which is initially set at zero when the fibers (the warp and the weft yarns) are perpendicular. The shear angle from the trellis frame is obtained trigonometrically using the relation [109]:

$$\theta = \frac{\pi}{2} - 2\cos^{-1}\left(\frac{1}{\sqrt{2}} + \frac{d}{2L_{frame}}\right) \tag{16}$$

Where: L_{frame} is the frame length and d is the displacement of the frame.

The shear force, F_s, can be calculated from the measured pulling force F and the global shear angle [109]:

$$F_s = \frac{F}{2\cos\theta} = \frac{F'' - F'}{2\cos\theta} \tag{17}$$

To avoid considering the inertia and weight of the trellis frame, the 'net' shear force F is obtained by deducting an offset value F' from the machine-recorded value F'' during the test. The offset value F' is obtained by testing just the trellis without a specimen, which records the weight and the inertia of the fixture including the inertia of the fixture**.**

Based on the normalisation steps, the result obtained showing the shear stress, and shear angle is presented in Fig 38.
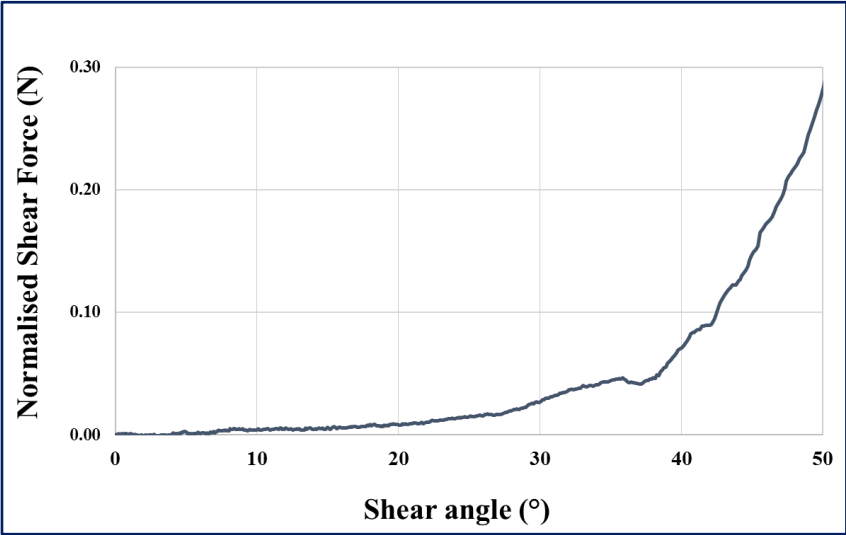
Figure 38 Trellis Frame Fabric Experiment: Normalised shear force vs. Shear angle

Additionally, the experimental results obtained is fitted on the FE material card fitted with MAT_249 Ls-Dyna material card as shown in Fig 39. The model was made as shown in the Fig 40 to simulate the trellis frame for curve fitting.
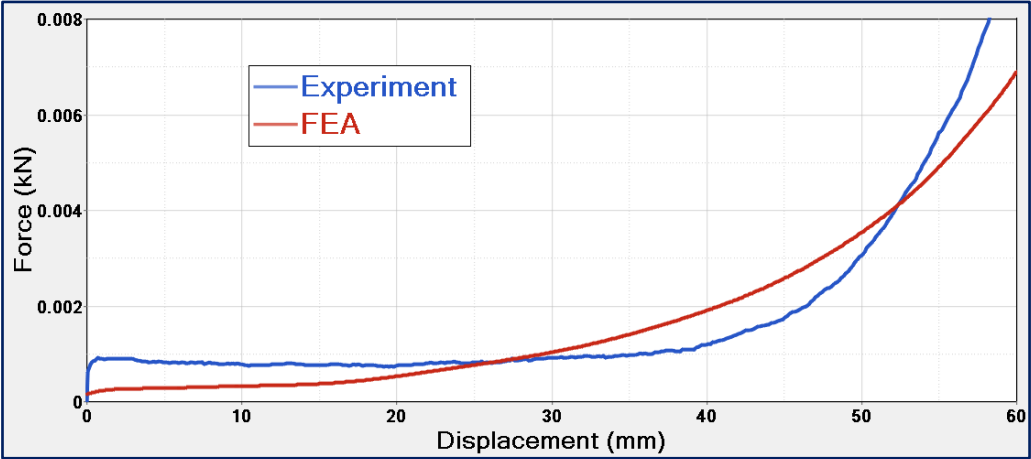
Figure 49 Trellis Frame fabric: card fitting curves FEA vs. Experimental
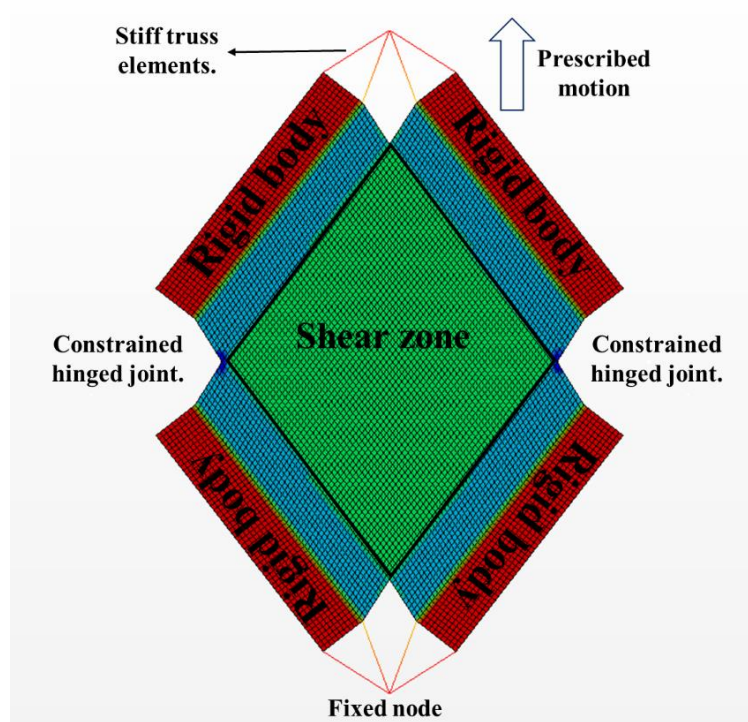
Figure 40 Trellis Frame FE specimen setup

Trellis Frame tests (Laminate)

After the trellis tests on the fabric, the trellis test on the entire laminate was done inside a thermal chamber, to simulate the properties of the laminate at its forming temperature (Fig 41). The only difference being the trellis laminate is the combination of shear properties of the fabric and the properties of the matrix, while the trellis fabric influenced only by the shear properties of the fabric. The properties of the matrix were obtained by comparing both the results of the ongoing FE analysis.
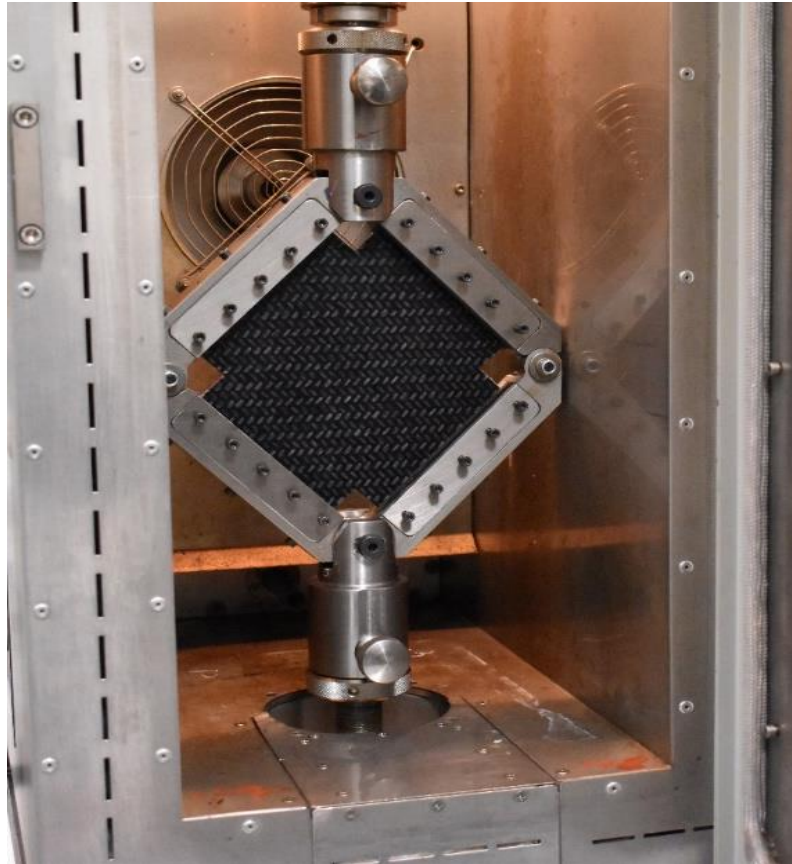
Figure 41 Trellis Frame laminate specimen setup

The specimen was cut with the same dimension of the trellis frame fabric to enable a shear zone of 100 mm^2. The force was made to make sure the specimen is oriented at ±45° to the force direction. Similar to the trellis frame: fabric, a sensitivity study was done to obtain the minimum compressive force required to achieve the ideal shear characteristic curve. The experimental result obtained from the trellis frame laminate is shown in Fig 42.
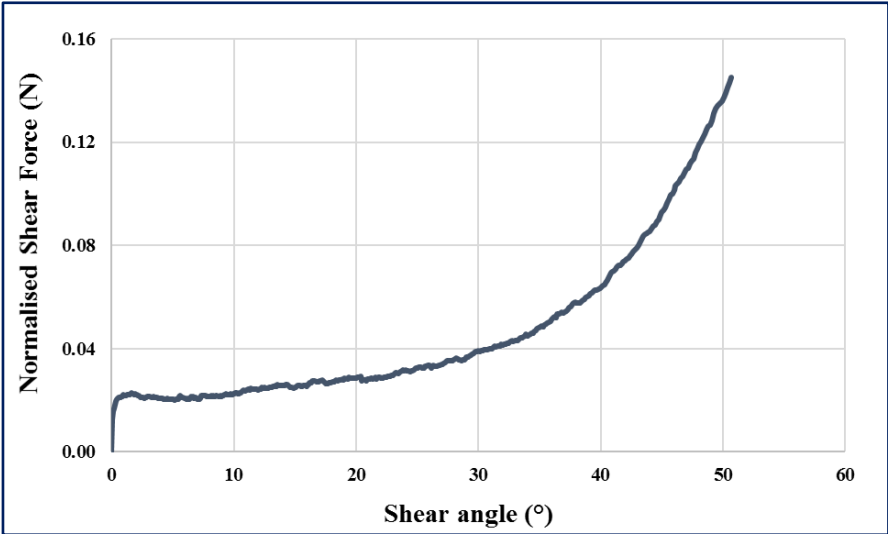
Figure 42 Trellis Frame Laminate Experiment: Shear Force vs. Shear angle
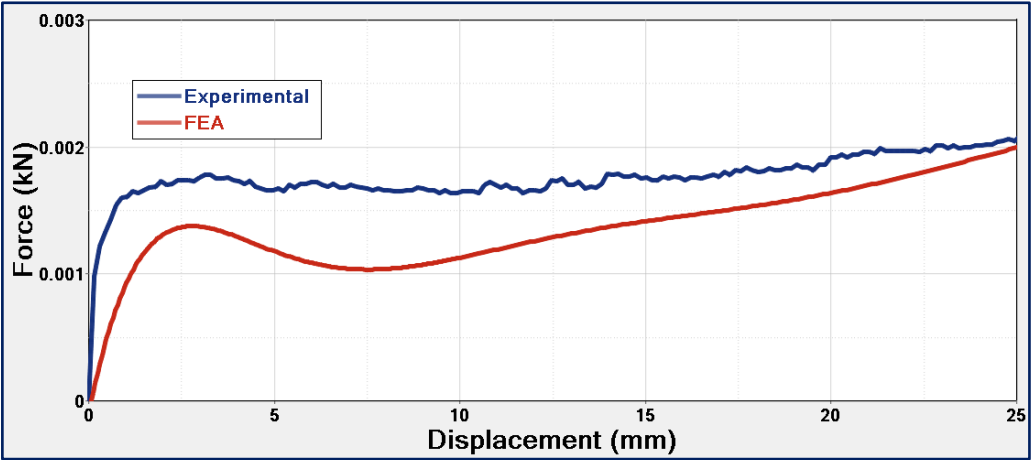
Figure 43 Trellis Frame Laminate: Initial matrix behaviour card fitting

The result with the closest match attained is shown in fig 43 to represent the matrix behaviour in the laminate during forming. The initial behaviour of the curve is intentionally kept underestimated to compensate for the initial inertia of the trellis fixture.

Shear results

After fitting the shear curves in the bias extension and the trellis fixture, the result can be validated by comparing the results after normalising the shear force obtained. The idea being, since both the tests were done to obtain the shear characteristics of the curve, matching results will self-validate the shear data [107].
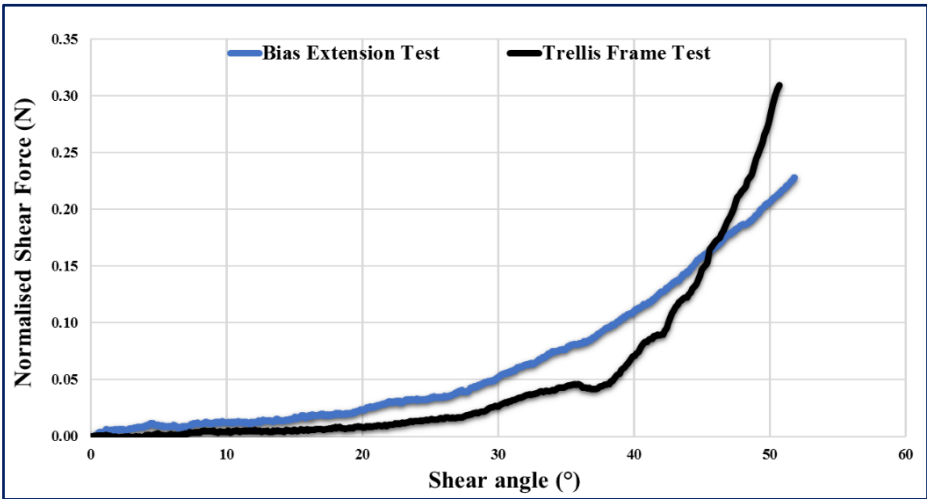
Figure 44 Bias Extension and Trellis frame test results comparison

Fig 44 shows the normalised results from the trellis frame 'fabric' and the bias extension compared giving identical results. The shear stress was calculated from the calculated shear force, shear angle and the specimen dimensions as shown. The shear curve is further modified to normalised shear stress vs. shear angle in both positive and negative axis as a direct input representing shear characteristics for the material card Mat_249 in Ls-Dyna for accurate results Fig 45.
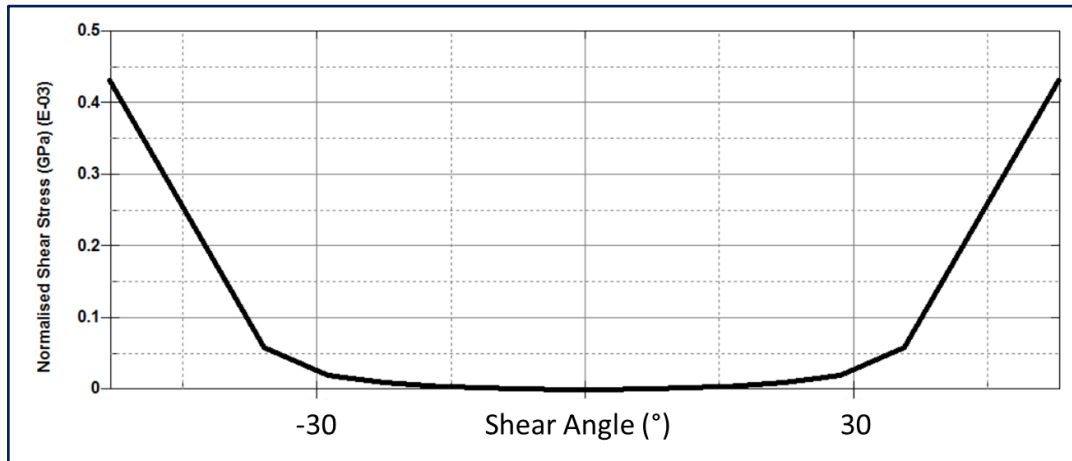
Figure 45 Shear Curve input for FE material card

.

Trellis frame test is recommended for further trials as the intra ply slippage dominant during the bias extension test can result in unreliable results and a lot more tests required to obtained usable data. Trellis frame test is relatively simple if a proper procedure is implemented giving repeatable results.

5.1.3. Friction characterisation of woven fabric and laminate

Another significant deformation due to the traction of continuous fibre reinforced composite is inter-ply slippage and tool ply slippage [78, 110].
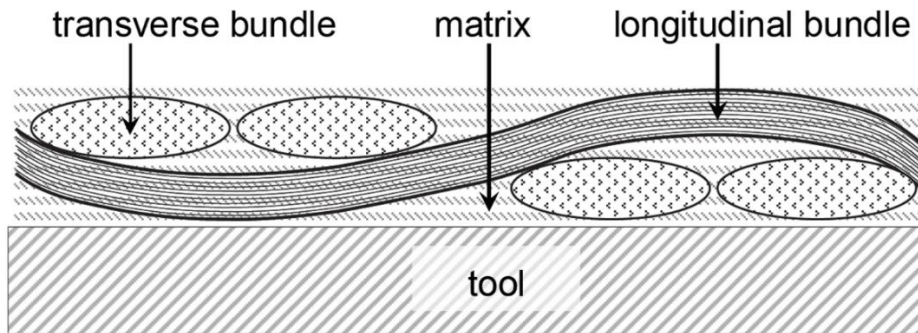
Figure 46 Schematic cross-section of a 2x2 Twill ply on a tool surface (adapted from [78])

Fig 46 shows a cross-section of the composite laminate in contact with the tool surface where a hydrodynamic lubrication is expected on the interface between adjacent plies and between the tool and the ply.

Fig 47 shows the representation of tool-ply friction and ply-ply friction setups.
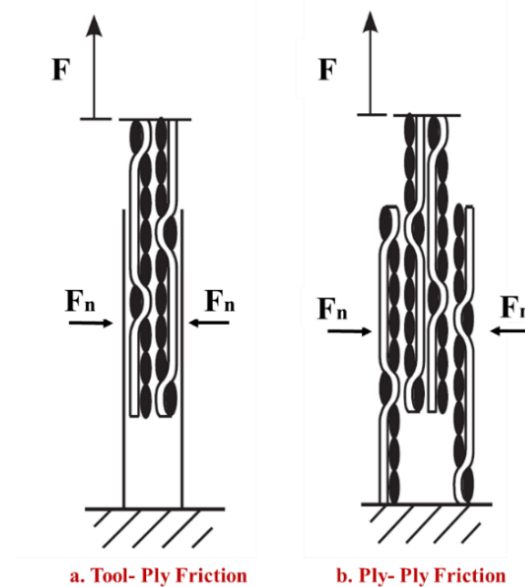
Figure 57 Friction testing experiment setup representation (adapted from [79])

The required output is the nominal force required to pull the specimen gripped with a fixed force measuring the frictional coefficient. Although there is an absence of a test standard to build a setup, a benchmark study had been conducted by different research groups to develop a testing rig to evaluate the friction tests under

nominally equal conditions on the same test material [78]. The testing setup used for the thesis was designed and fabricated, after reviewing the benchmark research.

The required design characteristics of an ideal friction testing rig for optimum results includes avoiding a larger friction area to prevent the influence of the edge effects, uniform pressure and homogeneous temperature distribution. Another critical design requirement is the importance of a very robust test setup configuration with strict constraints on the test specimen. This is done to make sure the sliding interface have consistent contact with the frictional interface and should not detach or rotate. An important constraint here is that the polymer matrix may be influenced by the degradation at high temperature in an oxygen-rich environment, so effort should be taken to minimise the operation time [111].

Figure 68 Friction testing experiment setup

Fig 48 shows the friction-testing rig setup developed for this thesis research. The gripping force (normal load) required to hold the specimen is supplied using the four high-temperature cylindrical collar screws along the four corners of the 'Internal Block' that goes all the way through the entire thickness of the specimen. The gripping force is recorded using a high-temperature piezo-electric sensor sandwiched between 'External Block' and 'Internal Block'. A tensile force is applied to the specimen using an Instron testing machine, enabling it to slide out of the friction testing setup. The specimen is made by two composite laminate sheets (Fig 49) that is cut and stuck on to the metal plate with high-temperature adhesive.
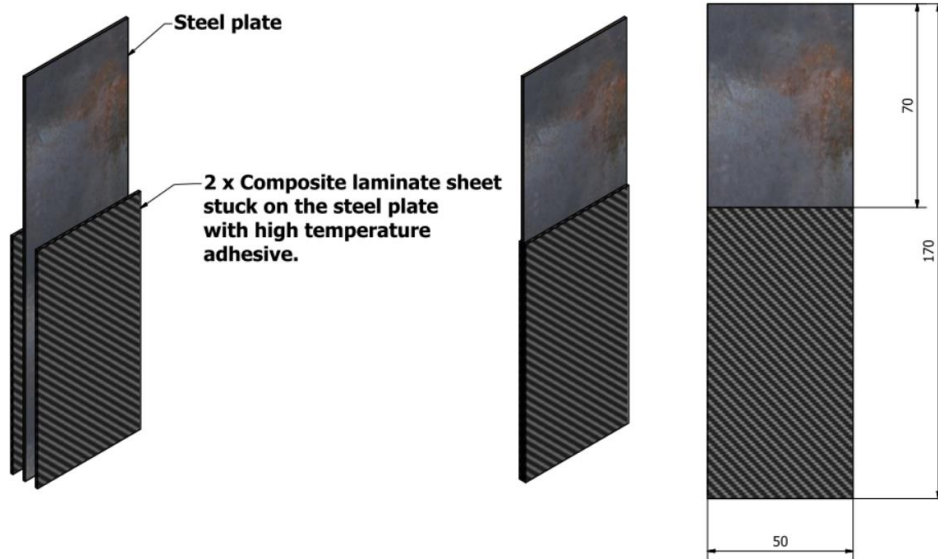
Figure 49 Friction testing specimen setup

The test is conducted inside a thermal chamber kept at 180°C representing the forming (process) temperature of polypropylene composite, and it starts to degrade above that temperature. The sliding velocity is kept at 100 mm/mm, with a constant contact surface area of 5000 mm^2. Two thermocouples are placed very close to the specimen to make sure a uniform temperature was achieved throughout the specimen. An extremely sensitive torque wrench of the range of 1 Nm to 5 Nm was employed to achieve the required normal gripping force of 300 N for both the tests.

The maximum frictional force F when the plies are sliding with respect to another ply or tool or when in limiting equilibrium is the product of its frictional coefficient and the normal reaction force:

$$F = \mu R \tag{18}$$

Where: μ is the frictional coefficient and R is the normal reaction force.

Tool - Ply test setup and coefficient.

For the tool-ply setup, the specimen is in direct contact with the metal part of the fixture, representing the tool. The assembly is placed inside the thermal chamber to achieve the required temperature of 180° C. Once the necessary temperature was

reached, the test is initiated, and a tensile force is induced on the specimen to induce friction between the laminate and the metal surface.

The curve displayed on Fig 50 shows the frictional coefficients plotted against the displacement for the tool-ply friction test showing the initial static coefficient and the later steady-state coefficient representing dynamic frictional coefficients.
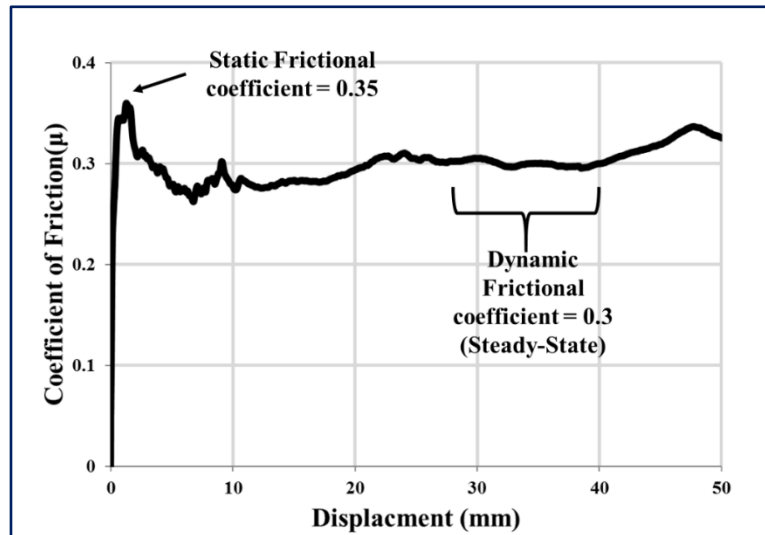
Figure 50 Frictional coefficients vs. displacement for tool-ply

The results obtained, and the estimated frictional coefficients are as reported in Table 8 summarising the entire tool-ply process.

Table 8 Tool-ply test setup and coefficients

Ply- Ply test setup and coefficients.

For the ply-ply setup, the laminate part of the specimen is in contact with laminate fixed on to the 'Internal Block' as described in Fig 51 and in Fig 52, to enable the interface between two plies. After loading the specimen, the entire assembly is placed inside the thermal chamber to achieve the required temperature of 180º C. The test is initiated then, and a tensile force is induced on the specimen to induce friction between the laminate sheets.

The curve displayed on Fig 53 shows the frictional coefficients plotted against the displacement for the ply-ply friction test showing the initial static coefficient.
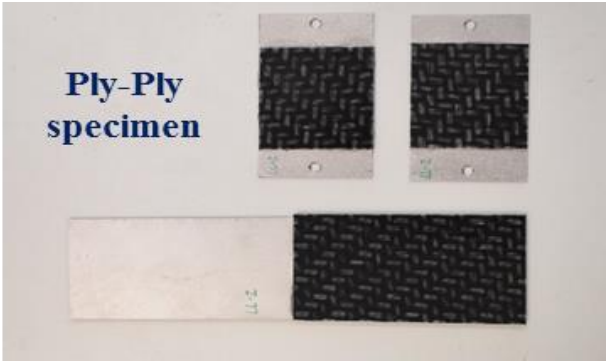
Figure 51 Ply-Ply specimen
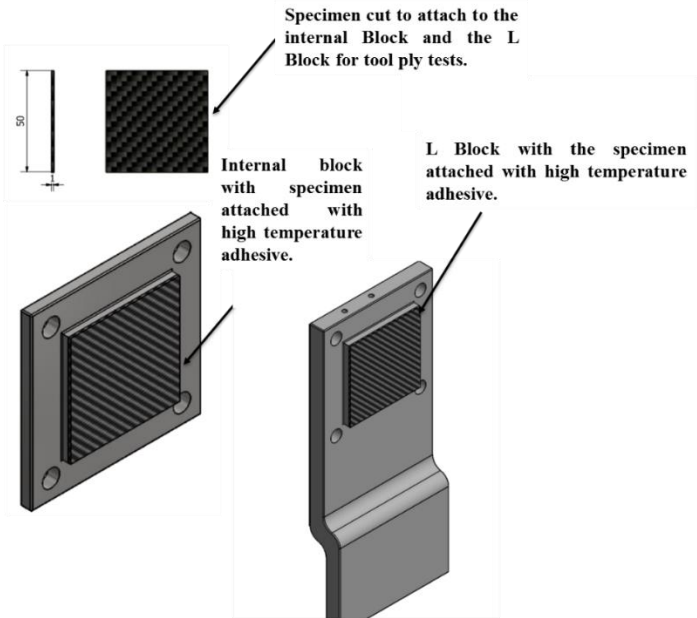
Figure 51 Ply-Ply specimen setup
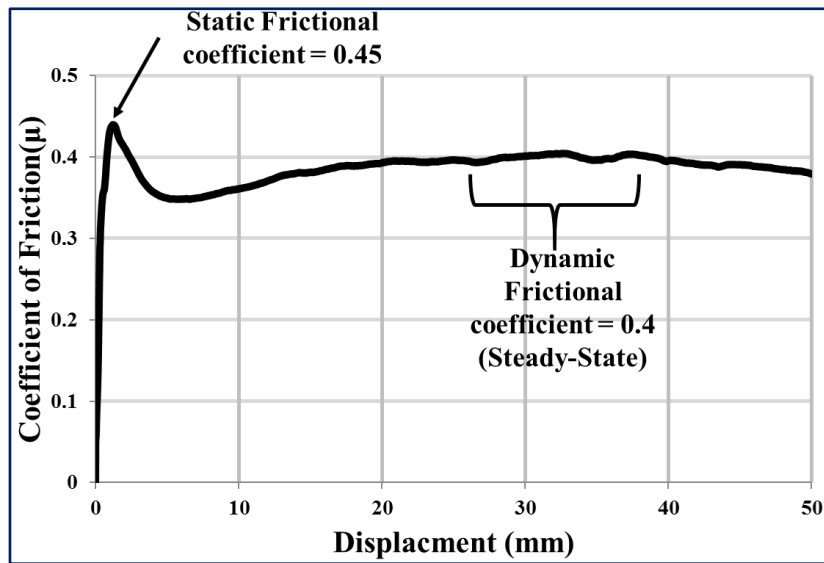
Figure 53 Frictional coefficients vs. displacement for ply-ply

The results obtained, and the estimated frictional coefficients are as described in Table 9 summarising the entire tool-ply process.

Table 9 Ply-ply test setup and coefficients

Friction tests conclusion

Tool-ply and ply-ply friction test had been done to obtain the static and dynamic coefficients for composite forming simulations supplementing the Mat_249 material card in Lsdyna. The hydrodynamic lubricated friction can be represented accurately using the Stribeck curves, but there is no current provision to make it usable in the FE tool adopted [112].

5.1.4. Bending test

The bending behaviour is another essential deformation mechanism that influences the thermoplastic part during the thermoforming. Traditionally for composite laminate characterisation, the bending characteristics of a thermoplastic composite laminate have been neglected owing the bending characteristics to the intra-ply shear and inter-ply friction. Any literature on the general study on bending characteristics of a composite laminate at melting temperature is limited, up until

recently by P. Boisse and the bending fixture developed by Sachs [83, 113]. This research examines the possibility of designing and fabricating a bending setup for composite laminate in thermoforming conditions that can be operated with relative ease to obtain accurate measurements. The conventional three point or four point bending tests are impractical due to the very low bending stiffness and the molten state of the specimen making it impossible to handle.

The primary requirement here is that the specimen should not be tightly fixed in the fixture and the supports should only act as a guide to allow sliding and to avoid forced bending of the specimen as shown in the Fig 54. The specimen should be rested between the fixtures enabling free movement along the circular path to avoid tensional or compressional strains. The image shows the specimen sliding when the fixture is rotated, avoiding any imposed torque on the specimen keeping the bending nature of the specimen similar to the traditional three-point or four-point bending tests. Some other vital requirements are well controlled and sensitive deformation rate, the uniform temperature along the specimen, provision for accurate measurement and short test period to avoid thermal degradation. An important constraint here is the oxidising effect of the polymer matrix on prolonged exposure to high temperature, because of this effort should be made to limit the test time to a minimum [111].

Based on the study done, a bending test rig was developed as a part of the current research. The setup can be easily mounted inside a commercial rheometer, exploiting its capabilities, equipped with an electric coil heater to heat the specimen up to its process temperature. The fixture is divided into two main parts, one stationary holder and one movable holder as described in Fig 55. The rectangular specimen is measured 35×25 mm^2 is bent by rotating the portable holder with precise control. Heat resistant polyimide tapes are stuck on to the edge of the specimen to avoid the molten resin sticking to the holders at its process temperature as detailed in Fig 56.

- Specimen not clamped: specimen free to slide to provide lateral movement and facilitate free bending
- fixture mounted onto the rotating shaft of a rheometer.
- Thermal tapes used to avoid specimen sticking
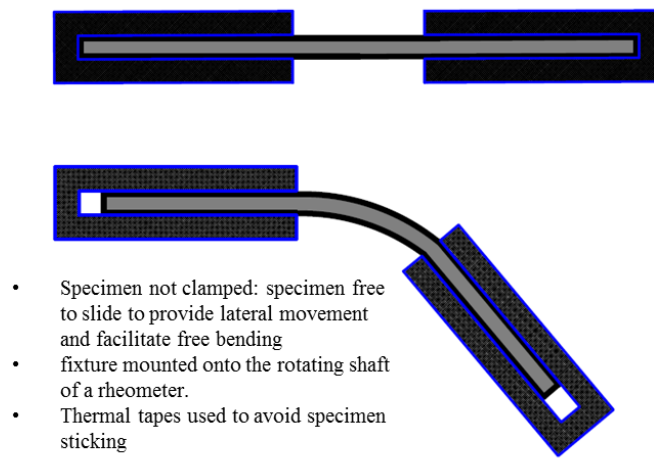
Figure 54 Schematic representation of the bending set-up

Once the specimen is loaded the temperature, the rheometer is closed, and the temperature is raised to 180°C to heat the specimen. The thermocouple placed close to the specimen confirms the temperature of the specimen and the test is initiated. The applied torque is plotted against the rotation angle for the entire duration of the test, which serves as the output.

Based on the tests, the FE model of the bending setup was developed for validating the bending nature of the laminate. Although for the FE material card there is no provision for a direct input of the bending modulus of the material, the ideal bending nature was fixed by varying the integration points along the thickness of the laminate. 'Integration point position variation method', where a *Integration_shell card was used to control better and optimise the position of the integration points to get the best design behaviour of the laminate.
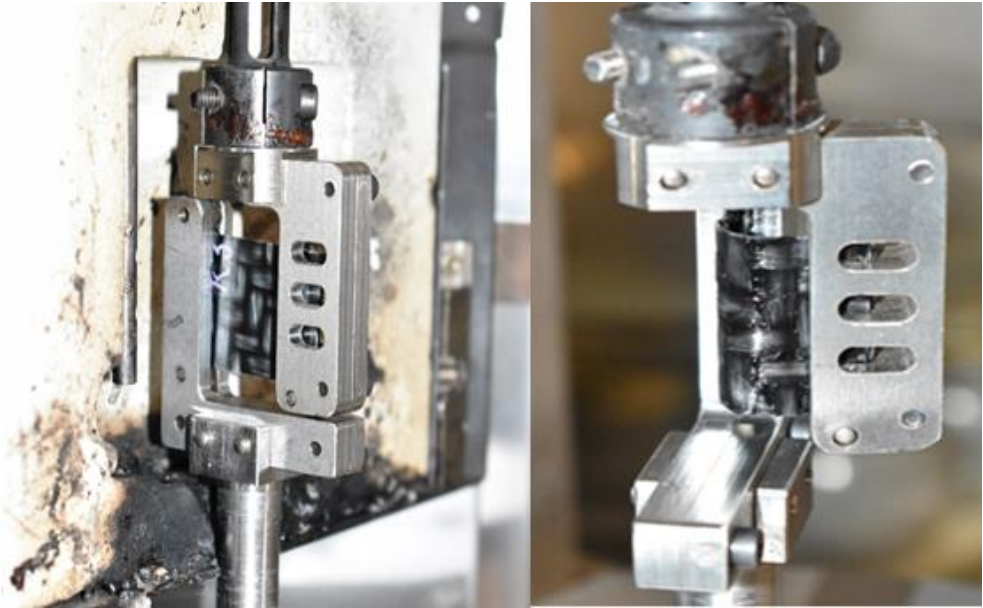
Figure 55 Schematic representation of the bending set-up showing the initial and the final position
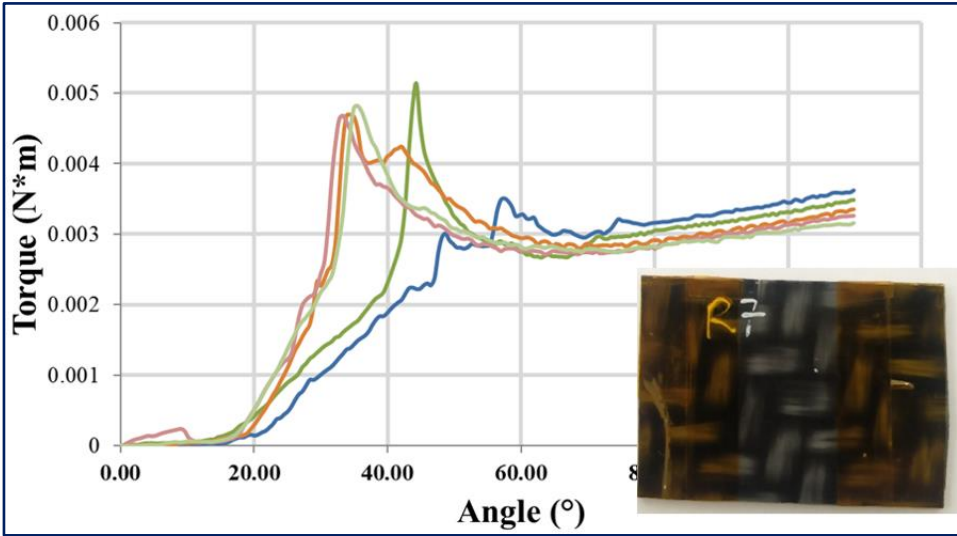
Figure 56 Bending curves with and without the polyimide tape around the specimen
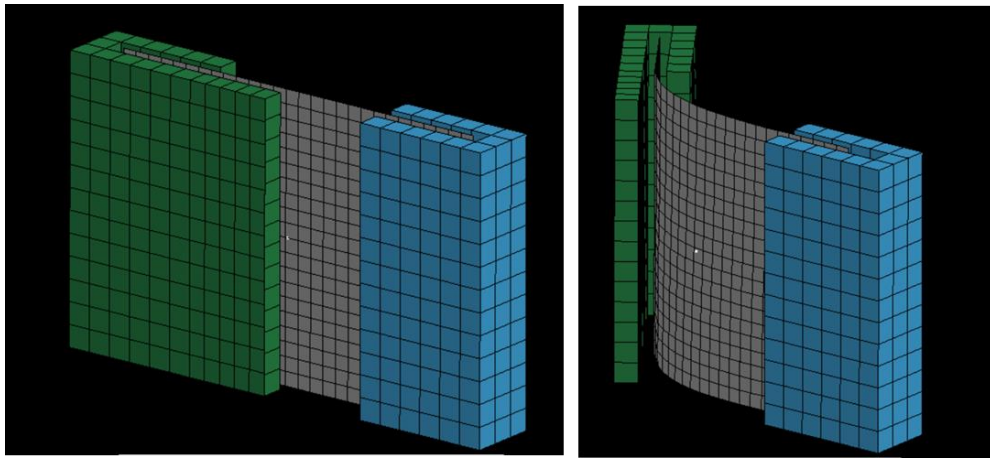
Figure 57 Bending FEA
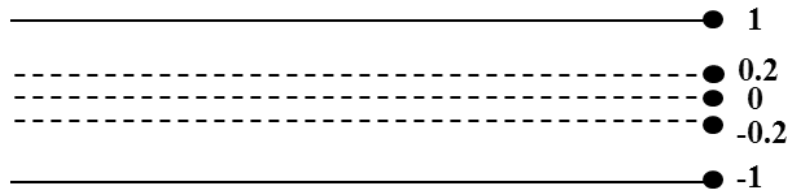
Figure 58 Bending FEA with the adopted integration point position distribution

Based on the bending tests done along with the corresponding FE tests (Fig 57), the number of integration points are currently kept at six as per the interval shown in Fig 58. A general study is currently done to utilize the thickness point variation method for optimum spacing of the integration points as shown in Fig. 58. The integration point concentration at the centre could increase the accuracy, although further testing and evaluations are necessary for accurately validating the bending characterisation.

5.2. Forming simulation setup and results

The process simulations are done to provide a basic understanding, to capture relevant parameters like shear locking leading to wrinkling, fibre direction change, etc [114, 115, 116]. The process simulations were done in Ls-Dyna by using a single action draw with an imposed displacement keeping the die and punch as rigid bodies. The blank incorporates two plies modelled with the Mat_249 material card,

with a Type16 fully integrated composite shell elements defined as anisotropic layered individual shells.

Additional steps to improve the simulation accuracy include:

- The shear input includes both the positive and negative shear angles plotted against the shear force for simulation accuracy.
- Static and dynamic frictional coefficients are given separately for the tool-ply interface and the ply-ply interface.
- Six equally spaced integration points are given for certain bending behaviour, based on the bending tests were done employing the 'integration point variation method'.

The punch moves vertically downwards with an imposed displacement deforming the blank keeping the die fixed (Fig 59 and Fig 60). A binder was used to locate the blank in position and to avoid abnormal behaviour of the blank leading to a failed simulation. Contact is defined between all the interfaces using *Forming_oneway_surface_to_surface card and an additional contact card to avoid self-intersection while forming is given by using a *Automatic_single_surface card. Although global damping was given initially, it was later avoided as it was making the simulation unstable.
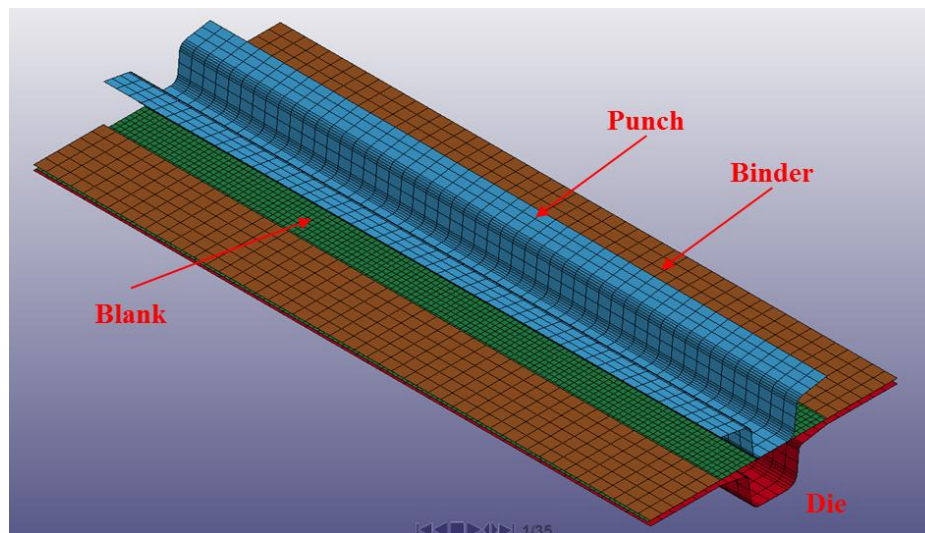
Figure 59 Schematic representation of the bending set-up
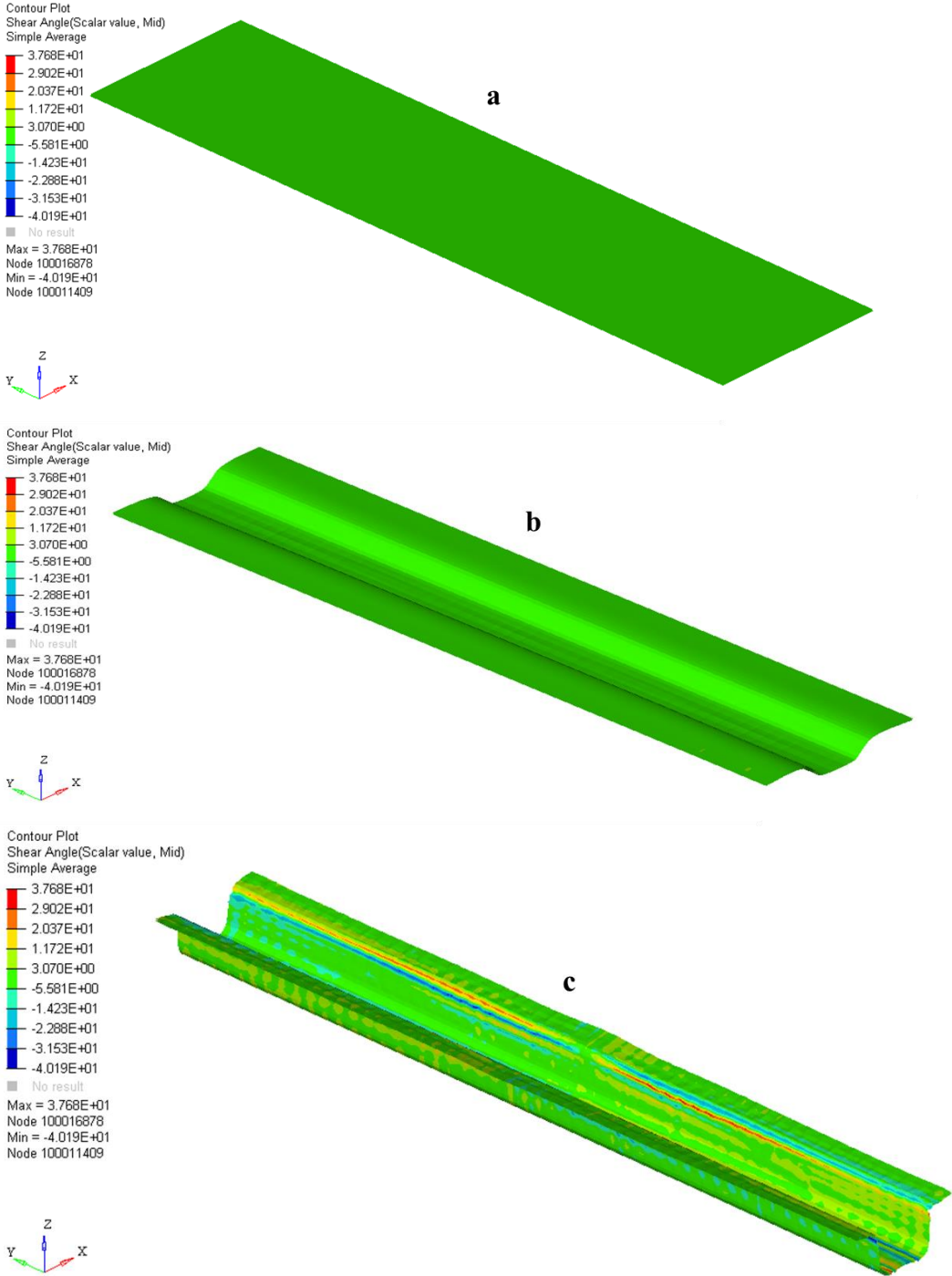
Figure 60 Different stages of forming simulation

5.2.1. Results Discussion

Based on the Forming FE simulations done, the results which directly influences the strength of the component are discussed here, such as the fibre path/ directions, wrinkles, thickness variations, Etc.
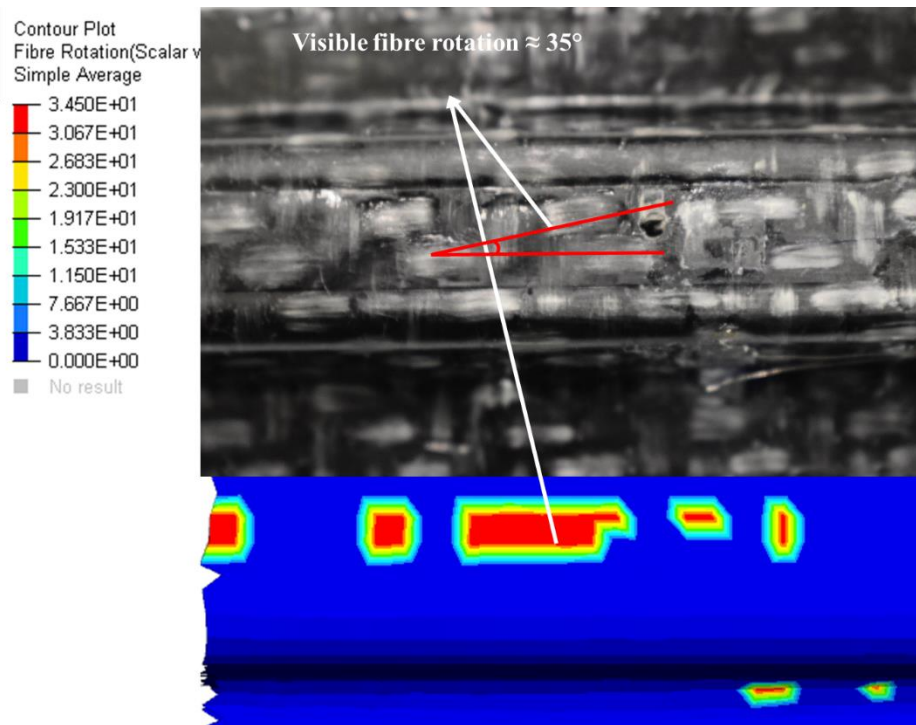
Figure 61 Local fibre rotation comparison

Fibre path/directions: The analysis of the mechanical performance of a composite part is done by assuming the fibre path as constant and uniform. Fig 61 shows that the course of the fibre changes during the process, further validated. An apparent local shift in the fabric direction change can be realised close to 35°.

Wrinkles due to excess in-plane shear: one main reason for developing wrinkles on fabric reinforced composite parts are due to excess shear leading to shear locking or excess pressure distribution on a plane. The FEA process simulation was validated in the component by locating the wrinkle pattern developed on the part as in Fig 62 on areas of the excess shear in the FEA [117].
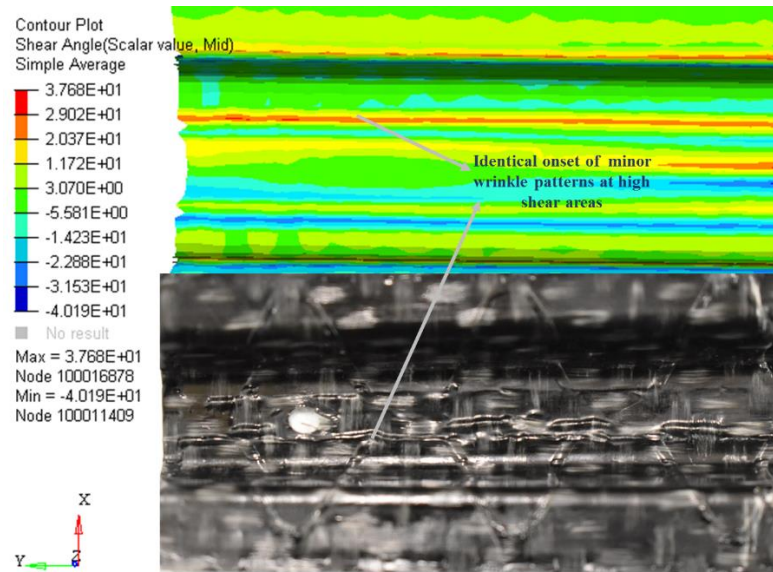
Figure 62 Local wrinkles compared with the FE results

Shell thickness variations: The layer thickness of a composite part may vary due to unequal distribution of pressure by the tool leading to consolidation problems. Identifying this parameter would allow optimising the die mould further to facilitate even pressure throughout the blank during the forming operation.

Fig 63 demonstrates comparable compatibility in the change of the thickness of the laminate. Although it was difficult to determine the thickness variation physically on the laminate precisely, a cross-section of the laminate shows an evident non-uniform thickness pattern. The contour plot shows the percentage thinning demonstrating how much the ply thickness vary compared to its actual output. A general quantitative comparison is currently done to confirm the presence of in-plane thickness variations and local thickness variations with detailed qualitative study is an ongoing study, although not part of this thesis.
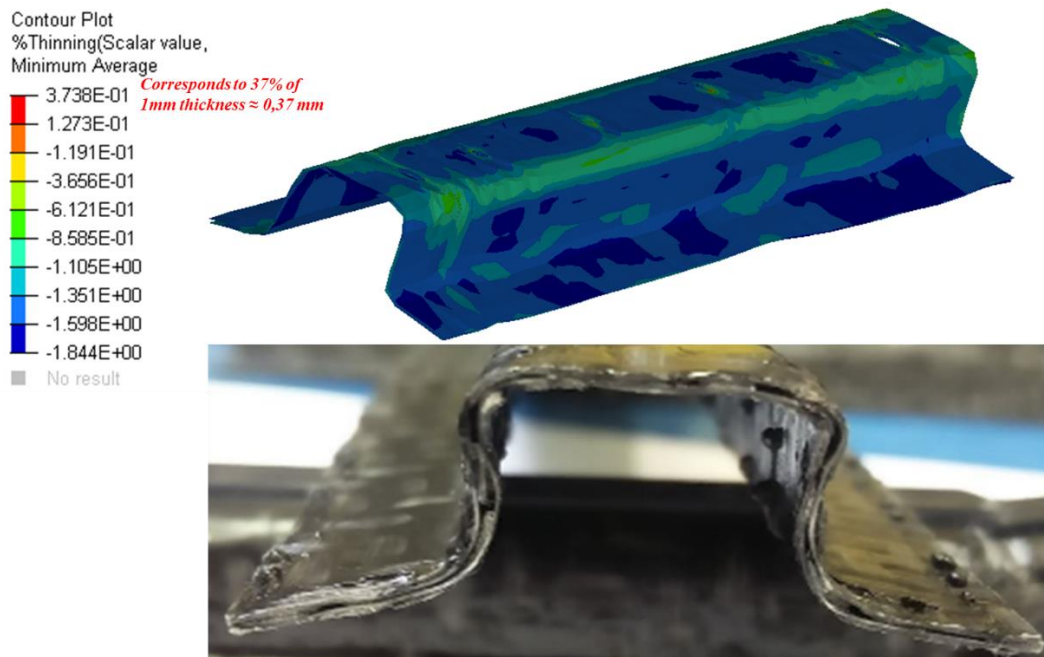
Figure 63 Thickness variation trend compared with the actual component

Residual stresses

Residual stresses occur in a continuous fibre reinforced thermoplastic composite part during its forming/ processing and successive cooling to the room temperature. They are intrinsically present in all thermoplastic composite parts, and it influences its structural integrity [119]. Due to this reason, it is important to include the residual stresses in the analytical modelling of thermoplastic components. The residual stresses can occur at three mechanical levels regarding its origin [118, 119, 120]:

a. Micro-mechanical level/ constituent level.
   Due to the variant coefficient of thermal expansion between the matrix and the composite fabric during thermoforming.
b. Macro-mechanical level/ lamination level.
   Due to the variant coefficient of thermal expansion between adjacent composite laminate sheets during thermoforming.
c. Global level.
   Due to the variant coefficient of thermal expansion along the entire thickness of the part during thermoforming.

Although the three levels are separately stated, the residual stresses developed on a global scale is considered here for analysis. Fig 64 shows the global residual stress that is developed along the surface thickness of the part.
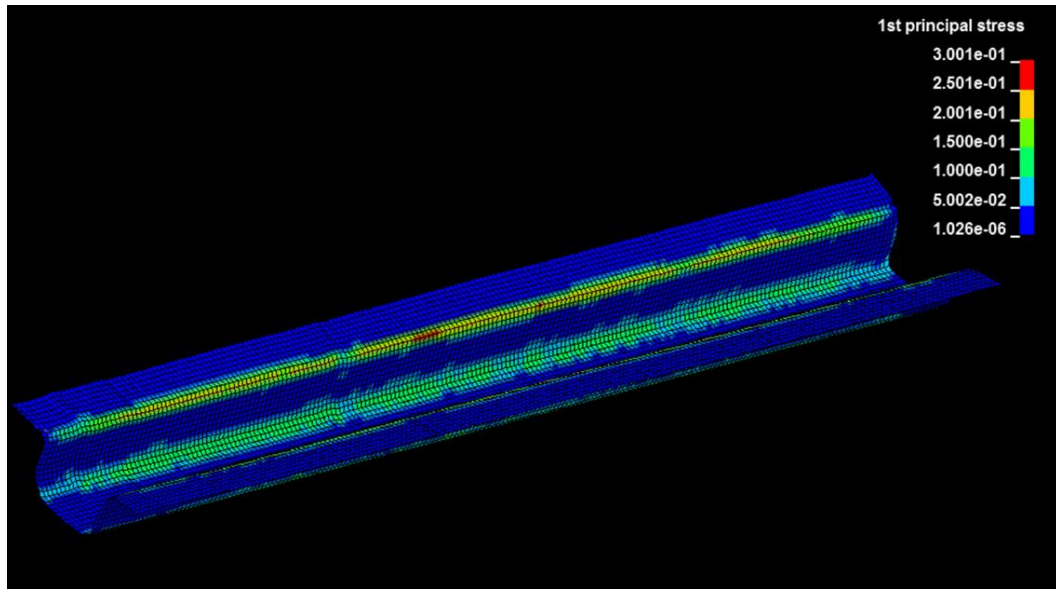
Figure 64 Global principal residual stresses developed on the part

All the manufacturing process parameter results shown here will influence the structural integrity of thermoplastic composite parts, and it is critical all these values are included in the FEM model for accuracy.

5.3. Mapping

The results generated from the process simulations need to be mapped into the component model to investigate its effect on the structural analysis. The possibility to import residual stresses, thickness variations and the fibre orientation post-process has been studied for further structural analysis.

Mapping was attempted by working closely with LsDyna, Germany by testing a new mapping tool under development specifically for mapping anisotropic composite materials models inside LsDyna. It is currently named ENVYO and is not yet available for commercial usage [121]. For accurate mapping, the output from the process simulation can be requested as single result file by enabling the *Interface_springback, including the initial stress, initial strain, and the spatial varying fibre orientation and thickness changes for the composite part. The fibre orientation is written for each integration point along the thickness as six component orientation tensors $\{a_{11}, a_{22}, a_{33}, a_{12}, a_{13}, a_{23}\}$.

Since ENVYO is in its early stage of development, there is no GUI and input request is developed using a notepad. Nodal pairs need to defined or initial mesh alignment between the result and the target mesh. Currently, the transformation model can be achieved with two options [122]:

a. Iterative Closest Point (ICP) a straightforward algorithm to align two free-form shapes given an initial guess for relative transform to create the alignment.
b. Four points Congruent Sets (4PCS) a Random sample consensus-based method for aligning two partially overlapping set of 3D points.

Table 10 ENVYO input sample

```
$#------------------------------- $#----------------------------
$# Main mapping definition        $# Mapping-Options
$#-------------------------------  $#----------------------------
ENVYO=SHELL-SHELL                 ALGORITHM=ClosestPoint
$#-------------------------------  SORT=BUCKET
$# Activate transformation        REPEAT=YES
$#-------------------------------  Shell_Option=Composite
TRANSFORMATION=YES                $#----------------------------
TRAFO_OPTION=ICP                  $# Source - PIDs
NodalPair#1=46555 10800           $#----------------------------
NodalPair#2=44234 10501           NumSourcePIDs=1
NodalPair#3=45394 10957           SourcePid#1=1
NodalPair#4=45433 10646           $#--------------
NodalPair#5=45747 40299           NumFibers=2
NodalPair#6=45801 35822           FiberID#1=1
WriteTransformedMesh=YES          FiberID#2=2
$#-------------------------------  CMPFLG=0
$# In- and output meshes          SourceMaterialModel=249
$#-------------------------------  TargetThickness= 1
SourceFile=dynain                 NumberOfTARInPlaneIPs=1
TargetFile=model.k                NumberOfTARLayers=4
MappingResult=model_mapped_ICP.key ThroughThicknessAveraging=YES
OrientationFile=HISV              NumberOfFiberBundles=4
TransformedMeshFile=trafo_ICP.k   FiberBundle#1:
$#-------------------------------  Lay=1,IP=1,Fib=1
$# Target - PIDs                  Lay=1,IP=2,Fib=2
$#-------------------------------  FiberBundle#2:
NumTargetPids=1                   Lay=1,IP=1,Fib=1
TargetPid#1=1                     Lay=1,IP=2,Fib=2
$#-------------------------------  FiberBundle#3:
$# Mapping-Options                Lay=1,IP=1,Fib=1
$#-------------------------------  Lay=1,IP=2,Fib=2
ALGORITHM=ClosestPoint            FiberBundle#4:
SORT=BUCKET                       Lay=1,IP=1,Fib=1
REPEAT=YES                        Lay=1,IP=2,Fib=2
Shell_Option=Composite            MapStrain=YES
$#-------------------------------  MapStress=YES
$# Source - PIDs                  MapThickness=YES
$#-------------------------------  $#----------------------------
NumSourcePIDs=1                   $# END-OF-FILE
SourcePid#1=1                     $#----------------------------
$#--------------
```

Table 10 shows the input request sample for ENVYO, showing the different parameters, including the transformation options and the nodal pairs defined between the source and the target mesh. The CMPFLG and the POSTV denotes the additional variable that can be written including the shear angles, damage, tri-axiality, fabric strains etc. if required. The thorough thickness averaging option can be enabled, where the user can define the fiber bundles (the number of fiber bundles, the orientation and the integration points) on target mesh, which will be generated by averaging. The option to map strain, stress and thickness need to be additionally specified as shown.

5.3.1. Mapping Results

Mapping was done on the composite part under review with the results generated from the process simulation. Fig 65 shows the source file created by the process simulation, the target mesh and the output mapped file generated from ENVYO after mapping. The residual stresses and strains will be mapped on individual elements by making use of additional cards called *Initial_stress_shell and *Initial_strain_shell.

The mapped model will be generated as *Element_shell_composite to control the specific element direction suitable for the composite which corresponds to the material orientation as in Fig 66.
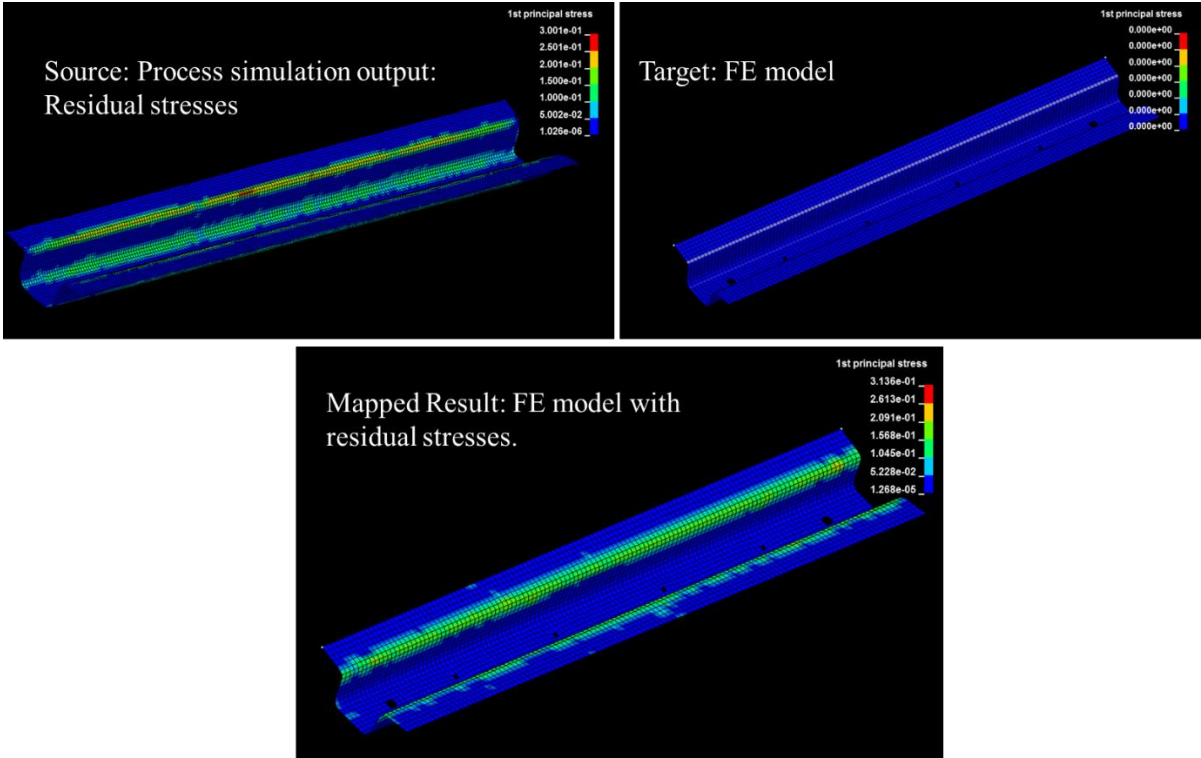
Figure 65 Residual stresses mapped on the part
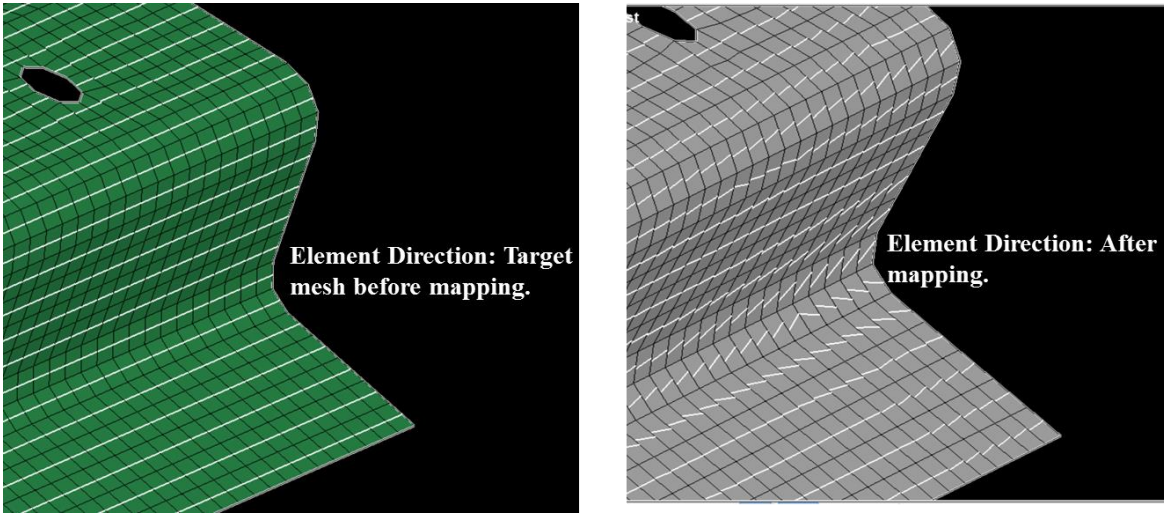
Figure 66 Fibre direction mapped on the part

Four-point bending FEA test on the components were repeated after mapping the results to check for possible influence from process simulations on the model. The analysis was done on the setup as in Fig. 7 with the only difference being the standard component model replaced with the mapped model.
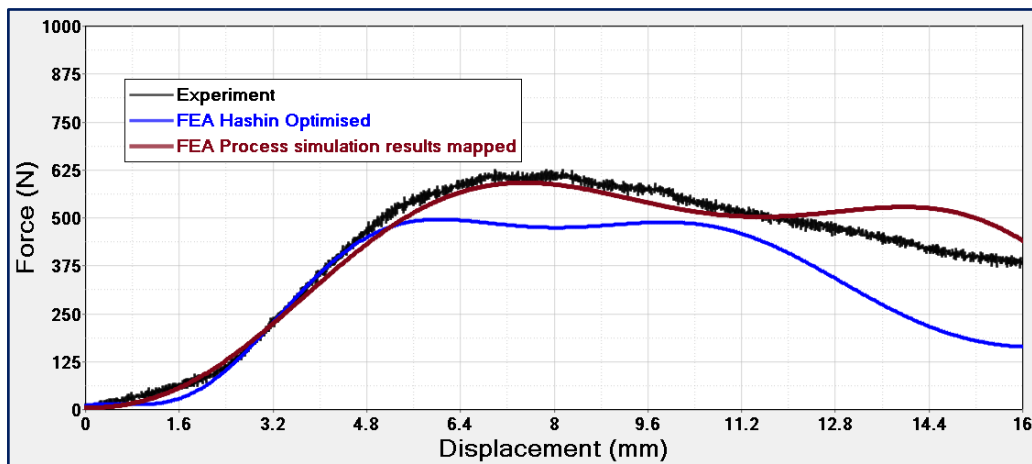
Figure 67 Four-point bending force vs. displacement curves for mapped part, non-mapped FE and experimental

Fig. 67 show the force vs. displacement curves of the Laminate component compared with the standard FEM model (FEA Hashin optimised) to the FEA model with the process parameters mapped on it (FEA process simulation results mapped). The comparison between both the FE curves demonstrates a definite resemblance in the elastic part, and the mapped curve is exceptionally accurate even on the plastic part showing a closer match with the experimental results obtained. This reflects the importance of including the process simulation data on the structural models.

Also, as visually evident in Fig. 68 the specific energy absorbed for the mapped laminate profile which is the area under the load-displacement curve is slightly higher for the mapped model. Hence establishing the need for imposing process material properties for achieving good simulation accuracy. This difference evidently is due to the changes in the direction of the continuous fibre and formulation of yield stresses during the forming operation.
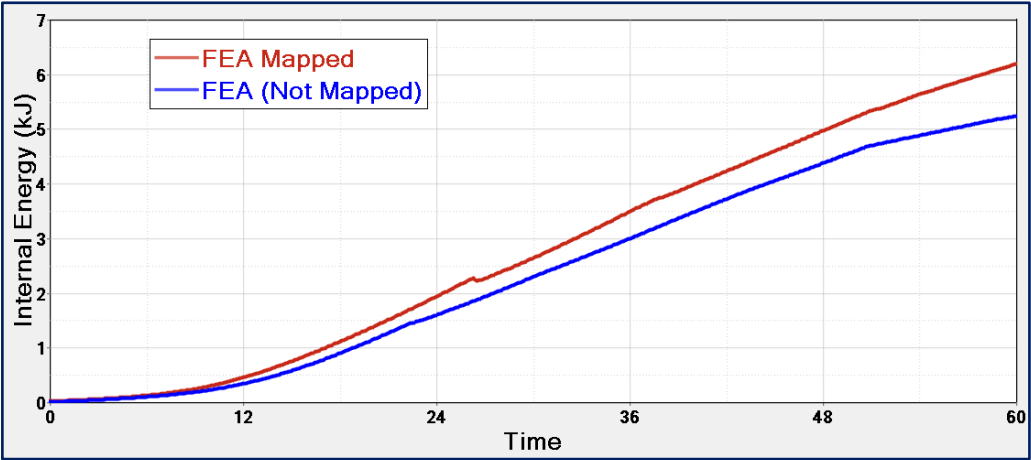
Figure 68 Four point bending internal energy curves for the mapped and the non-mapped part.

Chapter 6
Validation of the process

Following the flow process described in the Phase IV of Fig 1, the entire methodology is validated by considering a complex component as a double dome stressing the importance of integrating a process simulation to get an accurate model. The double-dome model considered is shown in Fig 69.
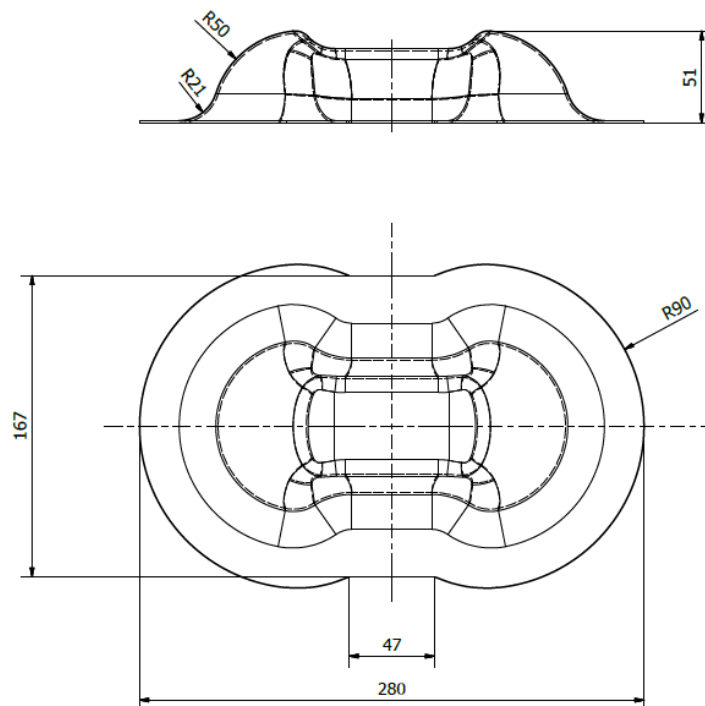
Figure 69 Double dome CAD

The forming setup developed in Ls-Dyna is shown in Fig 70, showing the placement of the Punch, Die and the blank sandwiched in between the binder. The necessary process simulation parameters are detailed in Table 11. The tools including the punch, die and the binder is modelled as rigid bodies, while the blank is TEPEX® Dynalite 104-RG600(2)/47% which is characterised in Fig 18.
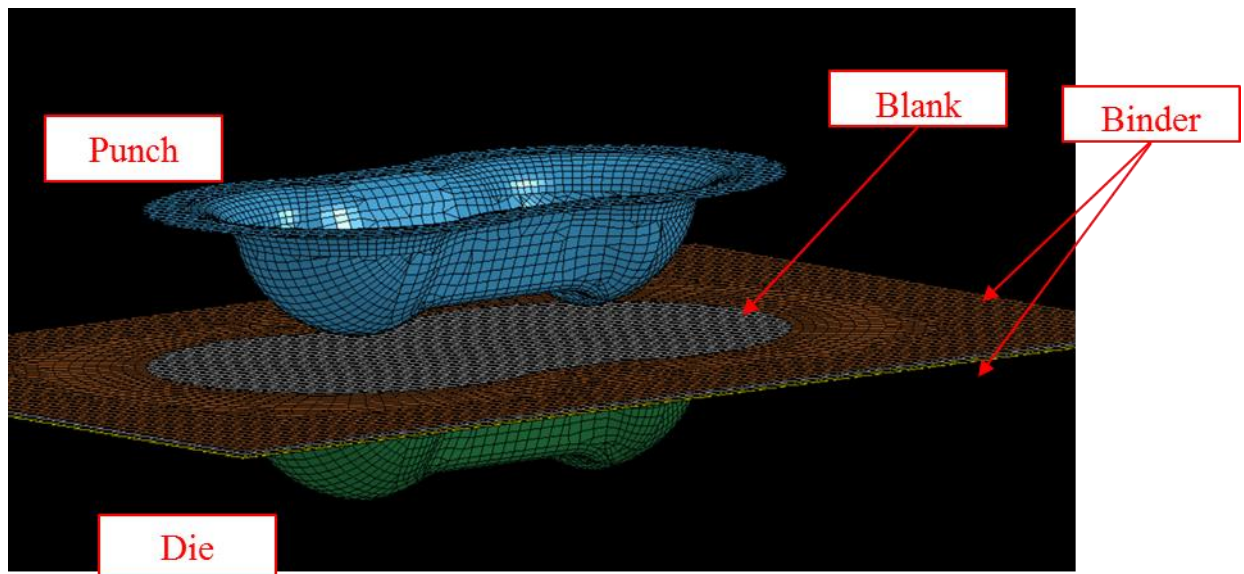
Figure 70 DoubleDome forming setup.

Table 11 Process simulation parameters for the double-dome

Punch Displacement	49.8 mm
Blank	2 Layers
Layer thickness	0.5 mm
Material direction of the fibre	0°- 90°
Binder	Fixed

6.1. Results

The Fig 71, Fig 72 and Fig 73 show the primary effect of the forming operation, including the shear angle variation along the surface of the specimen, the shell thickness and the punch force required.

6.1.1 Shear Angle

The shear angle being the angle between the fibres oriented at the warp and the weft direction, illustrates the in-plane shear. The locking angle occurs at around 43º for the chosen material, resulting in a quick increase in the shear stiffness required for deformation, which may result in wrinkling. Although in Figure 72, there are no visible wrinkles, when the component is tested in this orientation.
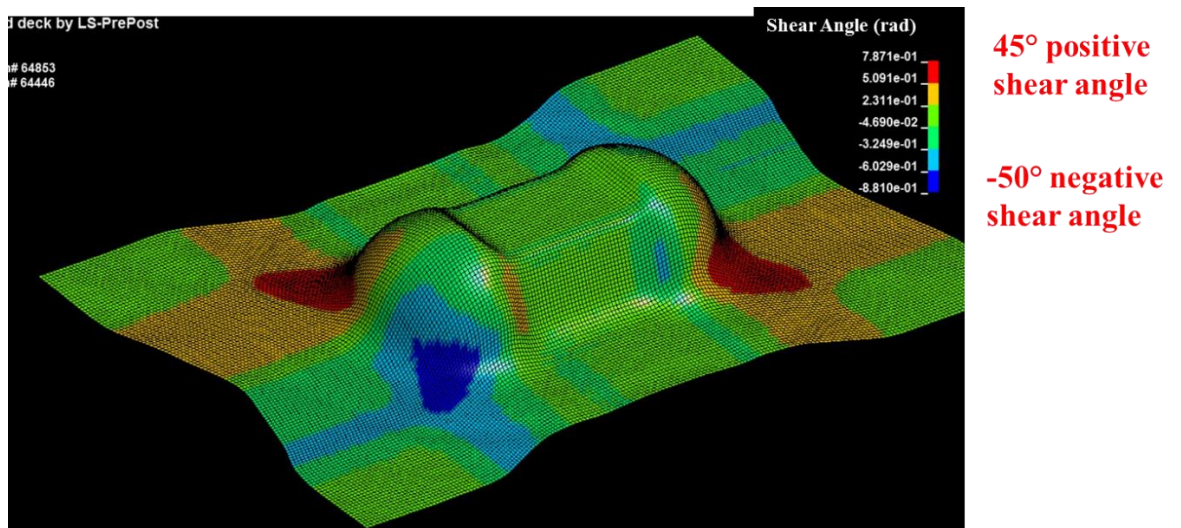
Figure 71 Shear angle developed after the forming operation

6.1.2. Shell Thickness

Like Fig 64, the layer thickness of a composite part may vary due to unequal distribution of pressure by the tool leading to consolidation problems. Fig. 74 shows the thickness distribution of the part along its plane, showing a thickness increase of 0.5 mm at the four corners of the geometrically 1 mm thick part. The contour plot shows the thickness variation demonstrating how much the result can be different from the standard model with a uniform thickness of supposedly 1 mm.
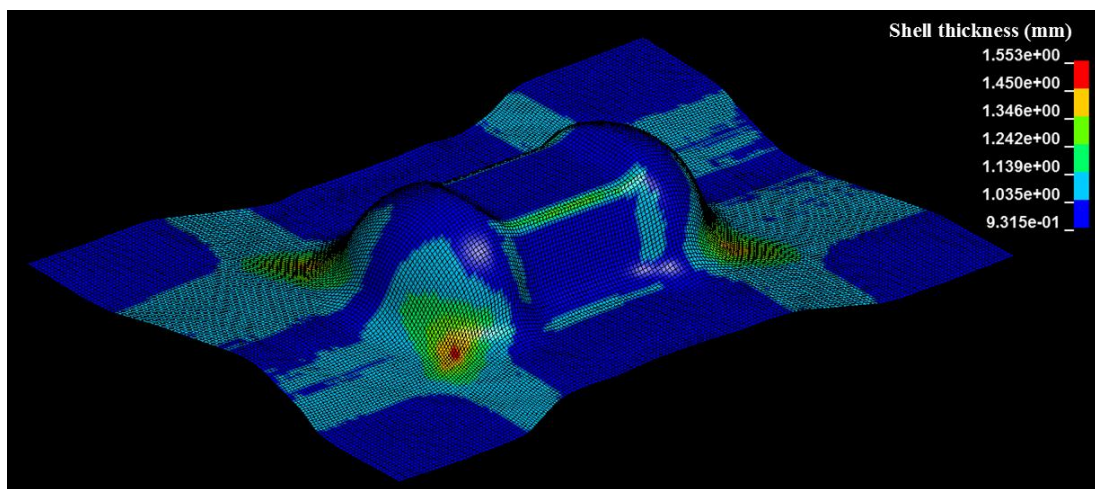
Figure 72 Shell thickness variation after the double dome forming operation

6.1.3. Punch Force

Although the punch thickness does not influence the post-processing results, it is essential to plot it to make sure it is in the reasonable range. It is a way to confirm if the process simulation done is good or not. If there are errors in the input values including the material parameters and the boundary conditions, the punch force plot will provide unrealistic results. Fig 75 shows the punch force plotted against the displacement.
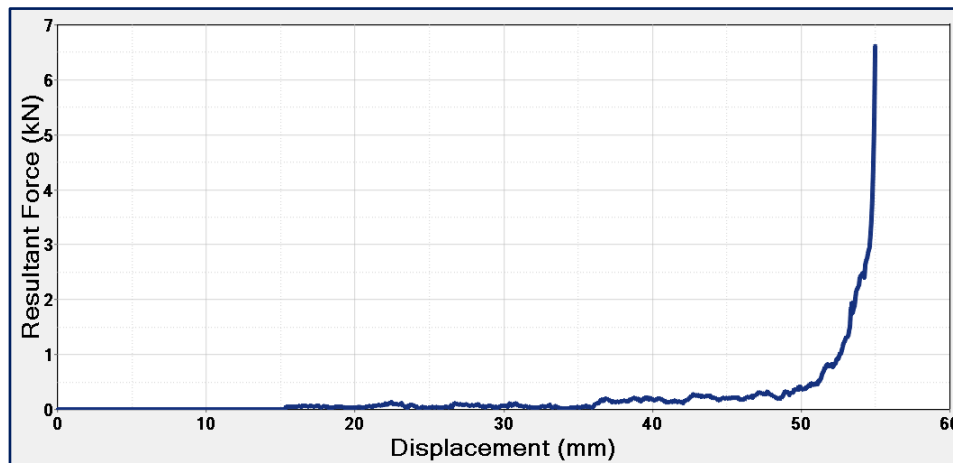
Figure 73 Punch force required for the double dome

6.2. Mapping

Mapping was done on the composite part under review with the results generated from the process simulation. The values that are mapped are the fibre orientation, the thickness, residual stresses and the residual strains.

Similar to the mapping described in Fig 64, the mapping is done in ENVYO, and Table 12 shows the input code written for generating the mapped output. The residual stresses and strains will be mapped on individual elements by making use of additional cards called *Initial_stress_shell and *Initial_strain_shell. The mapped model will be generated as *Element_shell_composite to control the specific element direction suitable for the composite which corresponds to the material orientation.

Table 12 Mapping Script used in ENVYO

```
$#-------------------------------------------------    $#---------------------------
$# Main mapping definition                             $# Source - PIDs
$#---------------------------                          $#---------------------------
ENVYO=SHELL-SHELL                                      NumSourcePIDs=1
$#---------------------------                          SourcePid#1=1
$# Activate transformation                             $#--------------
$#---------------------------                          NumFibers=2
TRANSFORMATION=YES                                     FiberID#1=1
TRAFO_OPTION=ICP                                       FiberID#2=2
NodalPair#1=5684 57379                                 CMPFLG=0
NodalPair#2=36860 57721                                SourceMaterialModel=249
NodalPair#3=31477 44165                                TargetThickness= 1
NodalPair#4=3912 47500                                 NumberOfTARInPlaneIPs=1
NodalPair#5=4028 45888                                 NumberOfTARLayers=4
NodalPair#6=31717 45882                                ThroughThicknessAveraging=NO
WriteTransformedMesh=YES                               NumberOfFiberBundles=2
$#---------------------------                          FiberBundle#1:
$# In- and output meshes                               Lay=1,IP=1,Fib=1
$#---------------------------                          Lay=1,IP=2,Fib=1
SourceFile=dynain                                      Lay=1,IP=3,Fib=1
TargetFile=model.k                                     Lay=1,IP=4,Fib=1
MappingResult=model_mapped_ICP.key                     FiberBundle#2:
OrientationFile=HISV                                   Lay=1,IP=1,Fib=1
TransformedMeshFile=trafo_ICP.k                        Lay=1,IP=2,Fib=1
$#---------------------------                          Lay=1,IP=3,Fib=1
$# Target - PIDs                                       Lay=1,IP=4,Fib=1
$#---------------------------                          MapStrain=NO
NumTargetPids=1                                        MapStress=NO
TargetPid#1=1                                          MapThickness=YES
$#---------------------------                          $#---------------------------
$# Mapping-Options                                     $# END-OF-FILE
$#---------------------------                          $#---------------------------
ALGORITHM=ClosestPoint
SORT=BUCKET
REPEAT=YES
Shell_Option=Composite
```

6.3. Three-point bending

A three-point bending test was performed comparing the results from both the FEA model; mapped double dome Fig 75 and the not mapped double dome Fig 74. Three-point bending was selected over four-point bending, unlike the part tested before, because of the geometrical constraints. Fig 75 shows the global residual stresses mapped on to the model along the fabric re-orientation during forming.
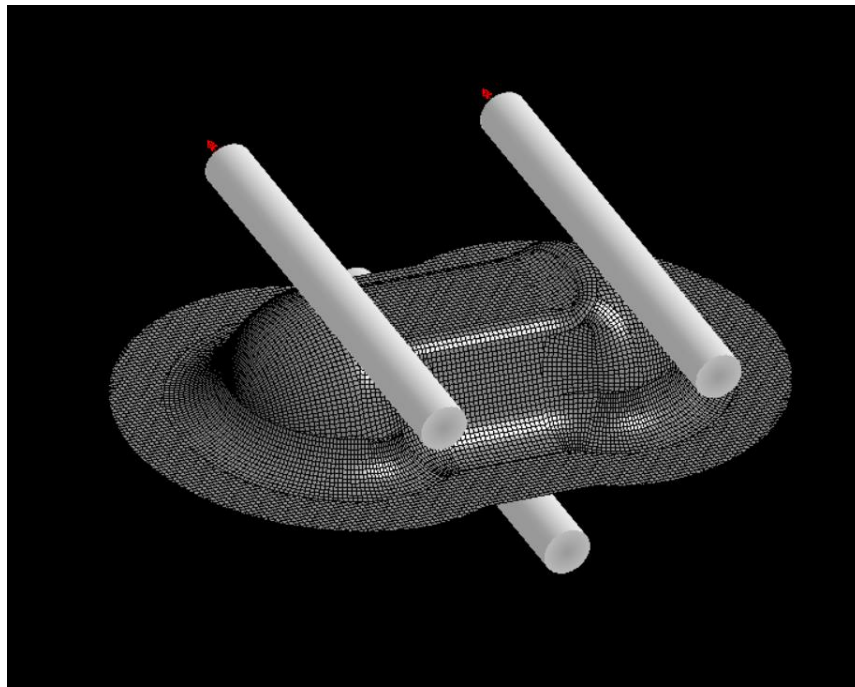
Figure 74 Three-point bending: not mapped
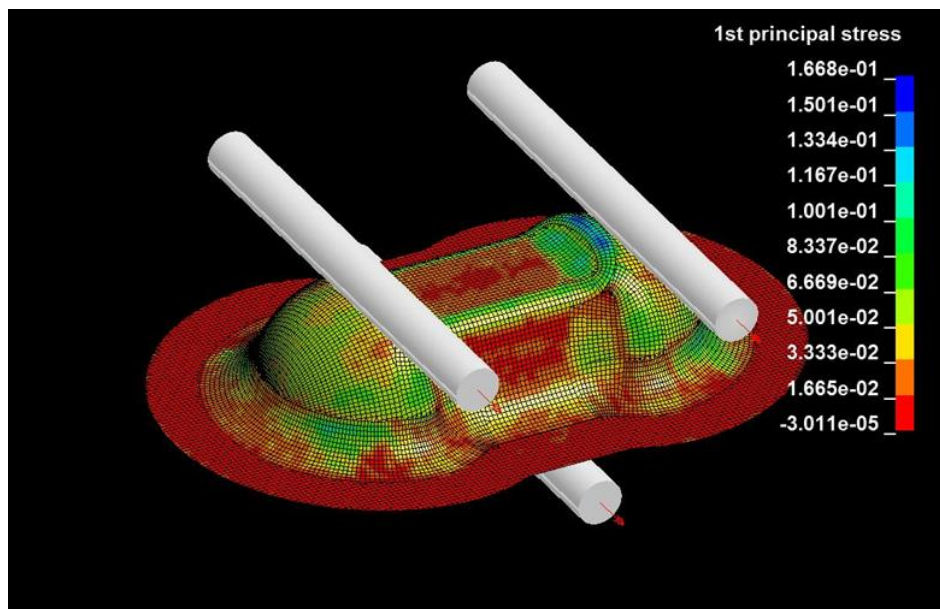
Figure 75 Three-point bending: mapped fibre orientation, residual stresses (in GPA) and thickness variations.

Based on the comparative three-point bending test done as detailed in Fig. 7 and explained in subsection 5.4.1, the force-displacement curve is shown in Fig 76. Identical to the previous part tested, the comparison between both the FE curves demonstrates a resemblance in the initial elastic part, but after a certain displacement the curve diverges upwards slightly increasing the force required to bend the specimen.
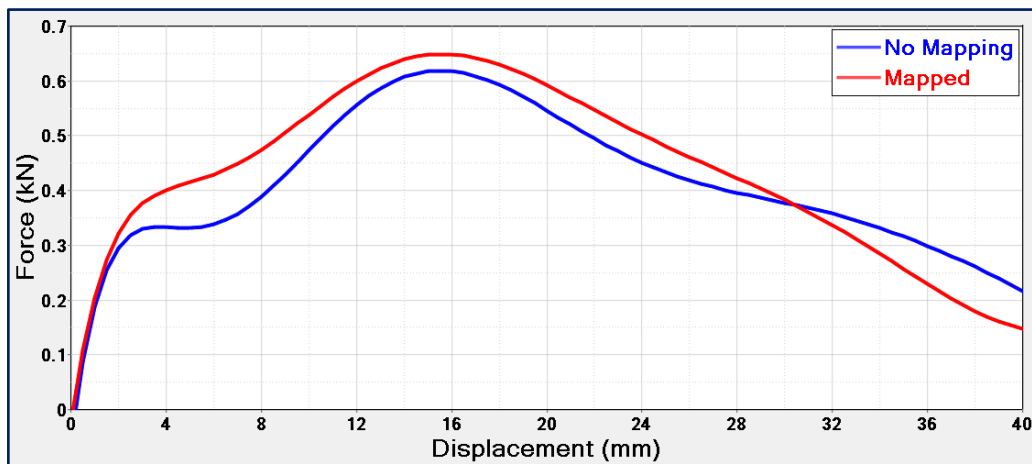
Figure 76 Mapped results of Three-point bending

Also, as visually evident in Fig. 77 the specific energy absorbed for the mapped double dome profile which is the area under the load-displacement curve is slightly higher for the mapped model.
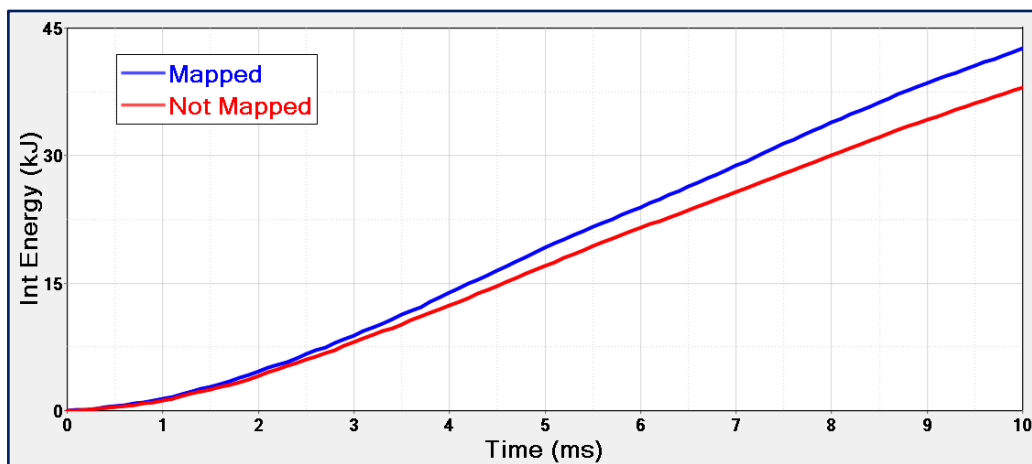
Figure 77 Mapped results of Three-point bending

Fig.1 and Fig.8 has been used as a guideline for the entire validation detailed in this chapter. One of the main advantage in terms of the accuracy for adopting this process flow is the systematic approach for modelling a multi-material composite part. Another main advantage is the ability to visualise the high stress areas after process simulation which gives the ability to modify the geometry or locally increase the stiffness on the part if required.

Chapter 7

Conclusions

The material properties of composite materials are entirely different from typical materials used in similar applications such as metals and other polymers, which means conducting different characterisation tests to identify each of these properties.

To reiterate the research done, the thesis aimed at creating a methodology to create an accurate FE model for structural composite parts. This was done primarily by identifying the key material properties of the composite material that require characterisation at its various phases, with additional steps to optimise the FE model. The process flow diagram presented (Fig 1) along with the building block diagram developed (Fig 8) has been followed closely to develop the process methodology. The adopted technique involves choosing the right composite failure criterion to create the FE material model, considering the structural requirements for the chosen part. An exhaustive FE model was then created then for the composite part. After that process simulations were done to realize the process parameters, which is then mapped on to the FE model.

The mapped FE model was tested to be more accurate by doing a comparative structural analysis with a standard FE model with no mapping. The significant milestones of this research activity concerning the objectives are:

1. Experimental procedures developed from existing standards for testing composite specimens; continuous fibres and short fibre. Sensitivity studies were done to obtain the usable data, and a Matlab code was developed to obtain the mean value curves and standard deviation.
2. A study was done comparing the two common failure criteria for fibre reinforced polymer composites (Crasurv and Hashin). The component test has revealed that the Hashin failure criteria are ideal for the component chosen undergoing out of plane bending enduring both tensile and compressive stresses at the same time.
3. A protocol was developed for realising the composite material model from the experimental results called curve fitting. FE simulations were done

isolating each of the vital material property, to plot a curve to match the experimental results.

4. Principal values required to conduct process simulations were established leading to the detailed analysis of the formability of the composite fabric without resin and the laminate at its forming temperature. Test setups for the Trellis frame shear test, bias extension test, bending test and friction test were designed and developed. This was done due to the absence of experimental standards for specific parameters such as inter-ply shear characteristics, intra ply friction and bending.

5. FE material card was developed for the composite fabric and the laminate at the forming temperature. This involved extracting usable data from the experimental results and doing card fitting to simulate the tests done. FE testing of shear properties of the fabric and laminate at forming temperature was conducted in detail, trellis frame shear tests in particular. A reliable method to obtain the matrix properties of the composite laminate at its forming temperature is presented.

6. Based on the process simulation conducted all the deformations occurring during the forming operation is found, including the fibre orientation change, shear locking leading to wrinkling, thickness variations etc. A reliable methodology was developed for mapping where the process simulation data is transferred to the model to obtain a comprehensive all-inclusive part model.

Fig 78 shows how the process simulation is integrated into the proposed composite modelling methodology, complementing the building block approach (Fig 8). Overall, the proposed plan adopting building block approach shows great promise in having a standardised procedure for developing a prediction model for modelling composite components. The advantage of the proposed method is in its simplicity and systematic approach for the structural analysis of complex composite parts considering the right standards. Essential process phenomena like the fibre direction change and shear locking leading to wrinkling have been captured.
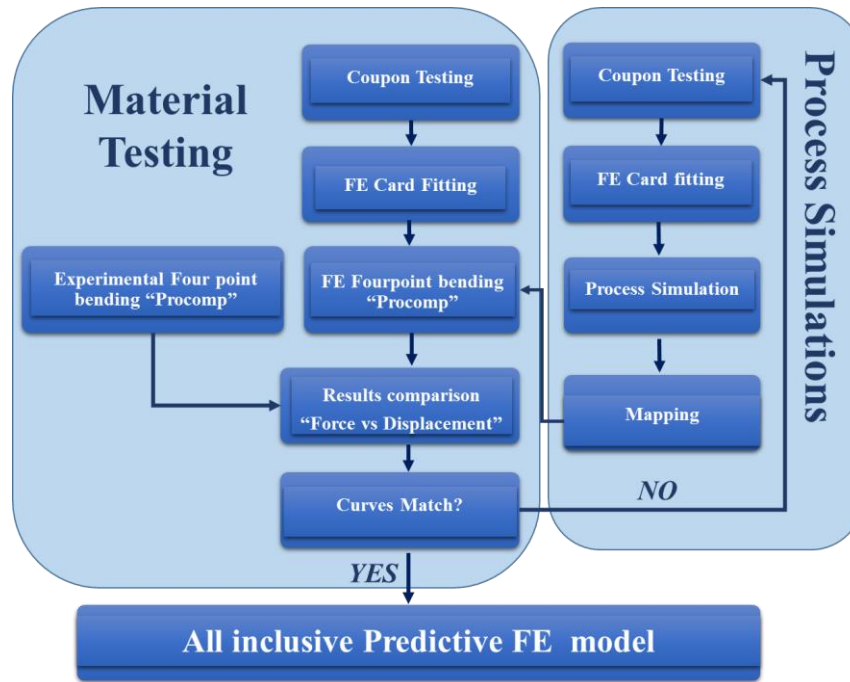
Figure 78 Flow diagram showing process simulation integrated into the composite modelling methodology

The scope of the current research was vast, and some of the steps detailed could be further investigated. The ongoing focus, although not part of this thesis, is to integrate digital image correlation in the building block to record the strain rate for the component and individual characterisation tests, for an augmented and accurate analysis [123, 117]. Another crucial objective is to thoroughly develop the FE material card for the short fiber injection model and develop a methodology to integrate the short fiber fibre direction to the part. Although the method is very similar to the one employed for the continuous fibre composite laminate, it was not included due to time restrictions.

Finally, the methodology proposed will benefit specifically the light weight automotive sector who are trying to integrate composite materials into various structural components. Development of an accurate FE model can limit the dependency on trial and error methods of testing the components till the final design phase.

References

1. N. Amirth Jayasree, A.G. Airale, A. Ferraris, A. Messana, L. Sisca, M. Carello. (2017). Process analysis for structural optimisation of thermoplastic composite component using the building block approach. Composites Part B. (126), 119-132.
2. Compositi ad alta velocità, Proplast. (2016). Available: http://www.plastix.it/compositi-ad-alta-velocita/.
3. Statista. (2017). Global automotive composites material market size from 2015 to 2026 (in billion U.S. dollars). Available: https://www.statista.com/statistics/658766/size-of-the-global-automotive-composites-market/.
4. Goran Djukanovic. (2017). Steel Versus Aluminium: Who's Winning the Lightweighting Battle In Cars? Aluminium Insider. pp 1-2
5. Jeff Sloan. (2016). Composites 101: Fibers and resins. CompositeWorld. pp.1–4.
6. Richar E Lyon, Usman Sorathia, P.N. Balaguru, Andrew Foden. (1996). Fire- Resistant Geopolymer composites. International Conference on Fiber Composites in Infrastructure. 972-981.
7. M. Carello, A. G. Airale, A. Ferraris, A. Messana, L. Sisca. (2017). Static Design and Finite Element Analysis of Innovative CFRP Transverse Leaf Spring. Applied Composite Materials. 1–16.
8. Dr. - Ing. Joachim Starke. (2016, Brussels). Carbon Composites in Automotive Structural Applications. BMW Group. EuCIA: Composites and Sustainability
9. M. Carello, A. G. Airale, A. Scattina. "Carbon fiber monocoque for a hydrogen prototype for low consumption challenge", (2011). Materialwissenschaft und Werkstofftechnik-Special ACE-X Issue, Wiley-VCH Verlag GmbH & Co., vol. 42, No.5, 2011 , pp. 386-392. (DOI 10.1002/mawe.201100793)
10. Massimiliana Carello, Andrea Airale, Alessandro Ferraris & Alessandro Messana. XAM 2.0: from Student Competition to Professional Challenge. (2014). Computer-Aided Design and Applications Vol. 11, Iss. sup,2014

11. Massimiliana Carello & Alessandro Messana. (2015). IDRApegasus: a fuel-cell prototype for 3000 km/L. Computer-Aided Design and Applications Vol. 12, Iss. sup

12. M. Carello, A. G. Airale, A. Messana, (2014). IDRApegasus: a carbon fiber monocoque vehicle prototype, Materialwissenschaft und Werkstofftechnik, Vol. 45, Issue 5, pp. 397-405.

13. Haibin Ning, Uday Vaidya, Gregg M. Janowski, George Husman. (2007). Design, manufacture and analysis of a thermoplastic composite frame structure for mass transit. Composite Structures; 105-116.

14. National Research Council, Division on Engineering and Physical Sciences, National Materials Advisory Board, Commission on Engineering and Technical Systems, Committee on Material for the 21st Century (1993). Materials Research Agenda for the Automobile and Aircraft Industries (Nmab). United States: The National Academies of Sciences, pp. 13-72.

15. M. Carello, A. G. Airale, (2014). Composite Suspension Arm Optimization for the City Vehicle XAM 2.0, Advanced Structured Materials,; Vol. 54, pp. 257-272.

16. National Materials Advisory Board Commission on Engineering and Technical Systems National Research Council. (1987). The place for thermoplastic composites in structural components. Report of the Committee on Thermoplastic Composites as Structural Components. NMAB (434), 1–127.

17. Directive 2000/53/EC. (2014). End of Life Vehicles (ELVS). European Commission, Eurostat, Environmental Data Centre on Waste.

18. James Bakewell. (2016). Recycle route for carbon fibre. Automotive Manufacturing Solutions, http://www.elgcf.com/assets/documents/ams-Recycle-route-for-carbon-fibre.pdf.

19. Marcelo Leite Ribeiro, Volnei Tita, Dirk Vandepitte b. (2011) A new damage model for composite laminates. Composite Structures; 105-116, doi:10.1016/ j.compstruct.2011.08.031

20. Masoud Kazemi Georges Verchery. (2016) Design of composite laminated plates for maximum buckling load with stiffness and elastic modulus constraints. Composite Structures:105-116.

21. Kendra A. Allen. (2012). Processing of Thermoplastic Composites. Polymer and Composites Processing, Polymer Composites Research Group, Iowa State University, 1-177.

22. Marshall Rouse, Dawn C. Jegley David M. McGowan, Harold G. Bush, W. Allen Waters. (2005) Utilization of the Building-Block Approach in Structural Mechanics Research; NASA, 105-116

23. M. Carello, N. Amirth, A. G. Airale, M. Monti & A. Romeo. (2017). Building Block Approach' for Structural Analysis of Thermoplastic Composite Components for Automotive Applications. Applied Composite Materials. DOI 10.1007/s10443-017-9592-x

24. Dr. Darrel R. Tenney, Dr. John G. Davis, Jr, Dr. R. Byron Pipes, Dr. Norman Johnston; (2009). NASA Composite Materials Development: Lessons Learned and Future Challenges. NATO Research and Technology Agency (RTA).

25. Orifici, A, Herszberg, I and Thomson, R (2008), 'Review of methodologies for composite material modelling incorporating failure', Composite Structures, vol. 86, no. 1-3, pp. 194-210.

26. Mast PW, Nash GE, Michopoulos JG, Thomas R, Badaliance R, Wolock I. Characterization of strain-induced damage in composites based on the dissipated energy density: part I to III. Theor Appl Fract Mech 1995;22:71–125.

27. Hashin Z. (1980) Failure criteria for unidirectional composites. J Appl Mech ;47:329–34.

28. Hashin Z, Rotem A. (1973) A fatigue failure criterion for fiber reinforced materials. J Compos Mater 1973; 7:448–64.

29. Chang F-K, Chang K-Y. (1987) A progressive damage model for laminated composites containing stress concentrations. J Compos Mater 1987; 21:834–55.

30. Puck A, Schürmann H. (1998) Failure analysis of FRP laminates by means of physically based phenomenological models. Compos Sci Technol; 58:1045–67

31. Tsai SW, Wu EM. (1971) A general theory of strength for anisotropic materials. J Compos Mater; 5:58–80.

32. Hinton MJ, Kaddour AS, Soden PD. (2004) Failure criteria in fibre reinforced polymer composites. Amsterdam, The Netherlands: Elsevier.

33. Pinho ST, Dávila CG, Camanho PP, Iannucci L, Robinson P. (2005) Failure models and criteria for FRP under in-plane or three-dimensional stress states including shear non-linearity. NASA/TM-2005-213530. VA, USA: NASA Langley Research Center.

34. Prof. W.G. Knauss, Luis Gonzalez. (2001). Global Failure Modes in Composite Structures NASA Grant NAG 1-1975. National Aeronautics and Space Administration., p1-61.

35. Whitcomb JD. (1984) Analysis of instability-related growth of a through-width delamination. NASA TM-86301.

36. White SR. Mixed-mode interlaminar fracture of graphite/epoxy. Washington University; 1987.

37. Hashemi S, Williams JG. (1991) Mixed-mode fracture in fiber-polymer composite laminates. In: O'Brien TK, editor. Composite materials: fatigue and fracture, vol. 3. ASTM STP 1110. W. Conshohocken (PA): ASTM Int.

38. Reeder JR. (1993) A bilinear failure criterion for mixed-mode delamination. In: Componeschi Jr ET, editor. Composite materials: testing and design (eleventh volume). ASTM STP 1206. W. Conshohocken (PA): ASTM Int.; p. 303–22.

39. Davidson BD, Zhao W. (2007) An accurate mixed-mode delamination failure criterion for laminated fibrous composites requiring limited experimental input. J Compos Mater; 41(6):679–702

40. Talreja R. (1994) Damage mechanics of composite materials. Composite materials series, vol. 9. Oxford, UK: Elsevier Science Ltd..

41. F. Pascon, M. Bruyneel, M. Schultz, C. Brauner, H. Hasselbruch, H. Krieger, T. Gries, K. Jalta, Dr. Ir. Michaël Bruyneel. (2013). Finite element analysis of the thermoforming process of thermoplastic composite parts. NAFEMS World Congress. 2262, 1–7.

42. P. de Luca, P. Lefébure, and A.K. Pickett. (1998) Numerical and experimental investigation of some press forming parameters of two fibre reinforced thermoplastics: APC2-AS4 and PEI-CETEX. Composites Part A: Applied Science and Manufacturing, 29(1-2):101–110.

43. S P Haanappel, R. Ten Thije, and R Akkerman. (2010) Forming Predictions of UD Reinforced Thermoplastic Laminates. 14th European Conference on Composite Materials, pages 1–10.

44. Sebastiaan P. Haanappel, Ulrich Sachs, Rene H.W. ten Thije, Bert Rietman, and Remko Akkerman. (2012) Forming of Thermoplastic Composites. Key Engineering Materials, 504-506:237–242.

45. Sebastiaan Haanappel. (2013) Forming of UD fibre reinforced thermoplastics. Phd thesis, University of Twente.

46. S. P. Haanappel, R. H. W. Ten Thije, U. Sachs, B. Rietman, and R. Akkerman. (2015) Formability analyses of uni-directional and

textile reinforced thermoplastics. Composites Part A: Applied Science and Manufacturing, 56:80–92.

47. Alessandro Ferraris. (2016) PhD thesis, Doctoral Dissertation Doctoral Program in Mechanical Engineering (29thcycle), Politecnico di Torino. Automotive composite components design and test: a vibration reduction-oriented approach, 1–106. 2016.

48. Andrea Giancarlo Airale. (2014) PhD thesis, Doctoral Dissertation Doctoral Program in Mechanical Engineering, Politecnico di Torino. Study and analysis of advanced composite materials for suspension automotive applications, p1-108.

49. Tri-mack. (2016) Hybrid Molding; Available: http://www.trimack.com/hybrid-molding.

50. Dr. - Ing. Joachim Starke. Carbon Composites in Automotive structural applications. Brussels: BMW Group. 2016

51. O. J. Zoellner and J. A. Evans. (2002) Plastic-metal hybrid: A new development in the injection molding technology. In Proceedings of SPE Annual Technical Conference (ANTEC), San Francisco, CA, USA.

52. C. A. J. R. Vermeeren. (2003) An historic overview of the development of fibre metal laminates. Applied Composite Materials; 10(4-5):189–205.

53. S. Minett and K. A. Fenwick. (1999) A steel-rubber laminate that can quieten cars & other machines. Noise & Vibration Worldwide; 30:12–13.

54. Ginger Gardiner. Hybrid Molding. 2015; Available: http://www.compositesworld.com/articles/overmolding-expands-peeks-range-in-composites

55. A. Baldan. (2004) Review: Adhesively-bonded joints in metallic alloys, polymers and composite materials: Mechanical and environmental durability performance. Journal of Materials Science; 39:4729–4797.

56. S.B. Sharma, M.P.F. Sutcliffe, S.H. Chang. (2003). Characterisation of material properties for draping of dry woven composite material. Composites: Part A. Applied science and manufacturing 34, Pages 1167–1175.

57. Peng Wang, Nahiène Hamila, Philippe Boisse, (2013). Thermoforming simulation of multilayer composites with continuous fibres and thermoplastic matrix. Composites Part B: Engineering. 52, 127–136.

58. B. Vieille, W. Albouy, L. Chevalier, L. Taleb. (2013). About the influence of stamping on thermoplastic-based composites for

aeronautical applications. Composites Part B: Engineering. 45, 821–834.

59. M. Komeili, A.S. Milani. (2016). On effect of shear-tension coupling in forming simulation of woven fabric reinforcements. Composites Part B: Engineering. 99, Pages 17–29.

60. J. Cao, R. Akkerman, P. Boisse, J. Gorczyca, P. Harrison, G. Hivet, J. Launay, W. Lee, L. Liu, S.V. Lomov, A. Longe,E. de Luycker. F. Morestin, J. Padvoiskis, X.Q. Peng, J. Sherwood, Tz. Stoilova, X.M. Tao, I. Verpoest, A. Willems, J. Wiggers, T.X. Yu, B. Zhu. (2008). A Cooperative Benchmark Effort on Testing of Woven Composites. Composites Part A: Applied Science and Manufacturing. 39, 1037–1053.

61. TEPEX® DYNALITE. Maximum strength at minimum weight 2015; Available: http://bond-laminates.com/en/materials/tepexR-product-families/tepexR-dynalite/

62. Fibermod™ GD301FE. Fibermod. (2015); Available: http://www.borealisgroup.com/en/polyolefins/products/Fibermod/Fibermod-GD301FE/

63. Cristex Composite Materials. (2016). WVR 600 T. Available: http://www.cristex.co.uk/uploads/certification/CCM%20WVR600%20T.pdf.

64. ISO/TC 61/SC 13 Composites and reinforcement fibres. (2012). Fibre-reinforced plastic composites -- Determination of the in-plane shear stress/shear strain response, including the in-plane shear modulus and strength, by the plus or minus 45 degree tension test. Available: https://www.iso.org/standard/23641.html.

65. ISO/TC 61/SC 13 Composites and reinforcement fibres. (2015). Fibre-reinforced plastic composites -- Determination of compressive properties in the in-plane direction. Available: https://www.iso.org/standard/23638.html.

66. ISO/TC 61/SC 13 Composites and reinforcement fibres. (2013). Fibre-reinforced plastic composites--Determination of flexural properties. Available: https://www.iso.org/standard/23637.

67. ASTM D3039 / D3039M-17, Standard Test Method for Tensile Properties of Polymer Matrix Composite Materials, ASTM International, West Conshohocken, PA, 2017, www.astm.org

68. Rajbhandari SP, Scott ML, Thomson RS, Hachenberg D. An approach to modelling and predicting impact damage in composite

structures. In: Proceedings of the 23rd congress of the international council of the

69. Tsai S W and Wu E M (1971). A general A general theory of strength for anisotropic materials. Journal of Composite Materials vol 5 pp Journal of Composite Materials. vol. 5, pp. 58-80.

70. Michele, Rabito Crescimanno. (2013). 2013 European Altair Technology Conference. Optimisation Based Composites Materials Characterization. pp 1-31.

71. Altair University: Academic Program. (2015). Crash Analysis with RADIOSS A Study Guide. Hyperworks. 1-294.

72. Altair Hyperworks: RADIOSS User Guide. (2017). Crash Analysis with RADIOSS A Study Guide. Hyperworks. Pp. 1-390.

73. Pedro Ponces Camanho. (2002). Departamento de Engenharia Mecânica e Gestão Industrial Faculdade de Engenharia da Universidade do Porto.Failure Criteria for Fibre-Reinforced Polymer Composites, pp. 1-13.

74. Hashin Z. (1980) Failure Criteria for Unidirectional Fiber Composites. Journal of Applied Mechanics; 47:329-34.

75. Helga Kuhlmann, Pieter Volgers, Zhenyu Zhang. (2014). Application and CAE simulation of overmolded short and continous fiber Thermoplastic composite. 13th International LS-DYNA Users Conference.

76. Sebastiaan Haanappel. (2013). Forming of UD fibre reinforced thermoplastics. PhD Thesis, University of Twente, Enschede, the Netherlands. 1-178.

77. Tzvetelina Stoilova, Stepan Lomov. (2004). Characterisation of glass/polypropylene fabrics. KU Leuven: Round- Robin Formability Study., 1-23.

78. R. Akkerman, R. Ten Thije, U. Sachs and M. De Rooij. (2010). Friction in Textile Thermoplastic Composites Forming. Recent Advances in Textile Composites, 271-279.

79. Ulrich Sachs. (2014). Friction and bending in thermoplastic composites forming processes. PhD Thesis, University of Twente, Enschede, The Netherlands. Enschede, 1-115.

80. Boisse P., Aimène Y., Dogui A., Dridi S., Gatouillat S., et al. (2010) Hypoelastic, hyperelastic, discrete and semi-discrete approaches for textile composite reinforcement forming. International Journal of Material Forming. 3: S1229-S40.

81. Flores F.G., Oñate E. (2005) Application of a rotation-free triangle element for finite strain analysis of thin shells and membranes. In: Kröplin B, editor. Textile Composites and Inflatable Structures. Berlin: Springer; pp. 69-88.

82. U. Sachs, R. Akkerman, K. Fetfatsidis, E. Vidal-Sallé, J. Schumacher, G. Ziegmann, S. Allaoui, G. Hivet, B. Maron, K. Vanclooster, S.V. Lomov. (2014). Characterization of the dynamic friction of woven fabrics: Experimental methods and benchmark results. Composites: Part A. (67), 289-298.

83. Sachs U. (2014) Friction and bending in thermoplastic composites forming processes. Enschede: University of Twente. ISBN: 946259483X.

84. Benedikt Eck and Guillaume Chambon. (2016). Automotive view on forming of continuous fiber reinforced composites and its simulation. AIP Conference Proceedings. 1769 (10.1063), 1.4963587.

85. Tom James, Director of Innovation, FORMAX. (2015). Characterization and simulation of structural fabrics – Part 1: A crossindustry review of approaches to composites engineering. Reinforced Plastics: Feature. 59, 1-6.

86. Philippe Boisse (2010). Simulations of Composite Reinforcement Forming, Woven Fabric Engineering, Polona Dobnik Dubrovski (Ed.), InTech, DOI: 10.5772/10460.

87. Dr. Stefan Hartmann, Dr. André Haufe, Dr. Thomas Klöppel, Christian Liebold. (2014). Simulation of the Manufacturing and Serviceability of Continuous Fiberreinforced Plastics. Webinar: Composite Analysis (DYNA MORE). DYNAmore GmbH, Stuttgart , 1-91.

88. Gazzo-Hanna, E. et al. Inter-ply fiber wrinkling (2009) in JNC 16, AMAC

89. Per Hallander. (2016). Doctoral Thesis, KTH School of Engineering Sciences. Towards defect free forming of multi-stacked composite aerospace components using tailored interlayer properties. Stockholm (ISSN 1651-7660), ISBN 978-91-7595-950-4.

90. Livermore Software Technology Corporation (LSTC). LS-DYNA® Keyword User's Manual. 2 ((r:8345)), 288-340.

91. Hart-Smith, L. J.: (1989) A New Approach to Fibrous Composite Laminate Strength Prediction. Eighth DOD/NASA/ FAA Conference on Fibrous Composites in Structural Design, NASA CP-3087, Part 2, pp. 663-693.

92. Melo JDD, Radford DW. (2005) Time and temperature dependence of the viscoelastic properties of CFRP by dynamic mechanical analysis. Compos Struct; 70:240–53.

93. Mallach, Annegret, et al. (2015) "Material characterization and draping simulation of thermoplastic prepregs: the influence of temperature." Society of Plastics Engineers-Automotive Composites Conference & Exhibition Proceedings.

94. D. Dörr, F. J. Schirmaier, F. Henning, L. Kärger, (2017) A viscoelastic approach for modeling bending behavior in Finite

Element forming simulation of continuously fiber reinforced composites, Composites: Part A 94 113–123, doi: 10.1016/j.compositesa.2016.11.027.

95. Altair Hyperworks: RADIOSS User Guide. (2017). Crash Analysis with RADIOSS A Study Guide. Hyperworks. Pp.1-390.

96. S. P. Haanappel, R. ten Thije, U. Sachs, B. Rietman, R. Akkerman, (2014) Formability analyses of uni-directional and textile reinforced thermoplastics, Composites Part A: Applied Science and Manufacturing pp.80–92

97. P. de Luca, P. Lefébure, A. K. Pickett, (1998) Numerical and experimental investigation of some press forming parameters of two fibre reinforced thermo- 390 plastics: Apc2-as4 and pei-cetex, Composites Part A: Applied Science and Manufacturing 29 (1-2) pp.101–110

98. D. Dörra, W. Brymerski, S. Ropers, D. Leutz, T. Joppich, L. Kärger, F. Henning. (2017). A Benchmark Study of Finite Element Codes for Forming Simulation of Thermoplastic UD-Tapes. 1st Cirp Conference on Composite Materials Parts Manufacturing, cirp-ccmpm2017. 66, 101-106.

99. Pierre-Christophe MASSON. (2014). Innov'Day Composites. Simuler les composites et leur mise en forme avec HyperWorks, pp 1-44.

100. ASTM D5035-11 (2015), Standard Test Method for Breaking Force and Elongation of Textile Fabrics (Strip Method), ASTM International, West Conshohocken, PA, 2015, www.astm.org

101. Zouari, B., J. L. Daniel, and P. Boisse, (2006) A woven reinforcement forming simulation method. Influence of the shear stiffness. Computers & Structures. 84(5-6): p.351-363.

102. Skelton, J. and W.D. Freeston, Mechanics of Elastic Performance of Textile Materials . Shear Behavior of Fabrics Under Biaxial Loads.Textile Research Journal. 41(11): p. 871-880.

103. Gabriele Barbagallo, Angela Madeo, Ismael Azehaf, Ivan Giorgio, Fabrice Morestin, Philippe Boisse. (2016). Bias extension test on an unbalanced woven composite reinforcement: Experiments and modeling via a second-gradient continuum approach. Sage Journals. 51, 153-170.

104. Frank Härtel, Philip Harrison. (2014). Evaluation of normalisation methods for uniaxial bias extension tests on engineering fabrics. Composites: Part A. 67 (A), 61-69.

105. R.S. Pierce, B.G. Falzon, M.C. Thompson, R. Boman. Contributions to the process modelling of resin infusion under flexible tooling (RIFT) manufacturing for composite

aerostructures. ICCM19 - 19th International Conference on Composite Materials.

106.   Harrison P., Clifford M.J., Long A.C., (2004) Shear Characterisation of Viscous Woven Textile Composites: A Comparison Between Picture Frame and Bias Extension Experiments. Composites Science and Technology, vol. 64, pp 1453-1465.

107.   I. Taha, Y. Abdin, and S. Ebeid. (2013). Comparison of Picture Frame and Bias-extension Tests for the Characterization of Shear Behaviour in Natural Fibre Woven Fabrics. Fibers and Polymers. 14 (2), 338-344.

108.   P. Harrison, J. Wiggers and A. C. Long. (2008). Normalization of Shear Test Data for Rate-independent Compressible Fabrics. Sage Journals. 42 (22), 2315-2344.

109.   Long A.C. (Editor), Design and Manufacture of Textile Composites. (2005), Woodhead Publishing and CRC Press LLC, ISBN 9781855737440.

110.   Thije, R.H.W. ten. (2007). Forming simulation of laminated composite forming processes. PhD thesis, University of Twente. URL http://doc.utwente.nl/57908/.

111.   Liang B, Hamila N, Peillon M, Boisse P. (2014) Analysis of thermoplastic prepreg bending stiffness during manufacturing and of its influence on wrinkling simulations. Compos Part A: Appl Sci Manuf; 67:111–22.

112.   J. L. Gorczyca-Cole, J. A. Sherwood, J. Chen, (2007) A friction model for thermostamping commingled glass-polypropylene woven fabrics, Composites Part A: Applied Science and Manufacturingpp. 393–406.

113.   Steffen Ropers, Marton Kardos, Tim A. Osswald. (2016). A thermo-viscoelastic approach for the characterization and modeling of the bending behavior of thermoplastic composites. Composites: Part A. 90, 22-32.

114.   Qi Zhang, Qiang Gao, Jin Cai. (2014). Experimental and simulation research on thermal stamping of carbon fiber composite sheet. Trans. Nonferrous Met. Soc. China. 24, 217-223.

115.   Masato Nishi, Tei Hirashima, Sean Wang. (2016). Constitutive Modeling for Composite Forming Simulation and Development of a Tool for Composite Material Design. 14th International LS-DYNA Users Conference. (Constitutive Modeling), 1-11.

116.   Rozant O, Bourban PE, Manson JAE. (2000). Drapability of dry textile fabrics for stampable thermoplastic preforms. Compos Part A; 31:1167–77.

117.   Prodromou AG, Chen J. (1997). On the relationship between shear angle and wrinkling of textile composite preforms. Compos Part A;28A:491–503.

118.   Patricia P. Parlevliet, Harald E.N. Bersee, Adriaan Beukers. (2006). Residual stresses in thermoplastic composites—A study of the literature—Part I: Formation of residual stresses. Composites: Part A. 37 (1), 1847–1857.

119.   Trende A, Astrom BT, Nilsson G. (2000).Modelling of residual stresses in compression moulded glass-mat reinforced thermoplastics. ComposPart A—Appl Sci Manufact ;31:1241–54.

120.   Barnes JA, Byerly GE. (1994). The formation of residual-stresses in laminated thermoplastic composites. Compos Sci Technol; 51(4):479–94.

121.   Christian Liebold, Andrea Erhart. (2015). 10th European LS-DYNA Conference, Würzburg, Germany. Recent Enhancements on Short-Fiber Reinforced Plastics Modeling in LS-DYNA. pp 1-9.

122.   Ls-Dyna Envyo User's Manual. (August 2017). DYNA more GmbH Industriestr. 2 D- 70565 Stuttgart Germany, pp 1-35.

123.   Willems, A., et al., (2007) Optical strain fields in shear and tensile testing of textile reinforcements Composites Science and Technology. 68(3-4): p.807-819.

Appendix 1

Specimen dimensions and features

The appendix shows the results of the mechanical characterization carried out by for the continuous fibre composite fibre (TEPEX® Dynalite 104-RG600(2)/47%)) and short fibre composite (Xmod™ GD301FE) tensile, shear, compression and bending tests. For each specimen the force-travel and tension-strain curves were obtained, elastic modulus, maximum tension, breaking deformation and maximum load were calculated; from the elaboration of the data the average mechanical characteristics of the material have been obtained.

All the experimental traction, compression and bending tests were performed using the Instron Model 8801 hydraulic-type testing machine and with a maximum load of 100 kN present in the Laboratory of the Mechanical and Aerospace Engineering Department of the Politecnico of Turin. The machine is equipped with automatic hydraulic grippers that allow you to quickly grasp the specimens and ensure they are gripped without causing sliding between the specimen bases and the test machine crossmember.

Table 1a Specimen categorisation for TEPEX® Dynalite 104-RG600(2)/47%)

Material	Catalogue	Test	Dimension	Quantity
E-glass+ Polipropiline	TG 1-5	Tensile test 0°	200x25x2 mm	5
	TG 6-10	Shear test	200x25x2 mm	5
	TG 11-15	Compression	120x25x4 mm	5
	TG 15-20	Bending	100x15x4 mm	5
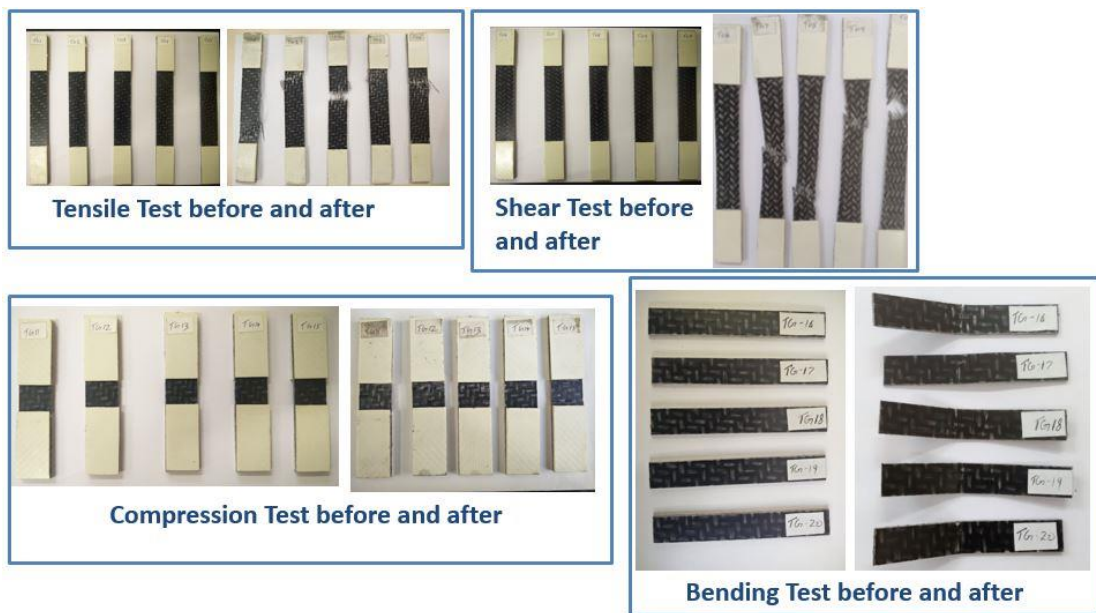
Figure 1a Specimen categorisation for TEPEX® Dynalite 104-RG600(2)/47%)

Table 1b Specimen categorisation for short fibre Xmod™ GD301FE

Material	Catalogue	Test	Dimension	Quantity
E-glass (short fiber) + Polipropiline Xmod TM GD301FE	GG 1-5	Tensile test 0°	90x20x2 mm	5
	GG 6-10	Shear test	90x20x2 mm	5
	GG 11-15	Compression 0°	90x20x2 mm	5
	GG 15-20	Tensile test 90°	90x20x2 mm	5
	GG 20-25	Compression 90°	90x20x2 mm	5
	GG 25-30	Compression	60x20x2 mm	5
	GG 30-35	Bending	60x20x2 mm	5
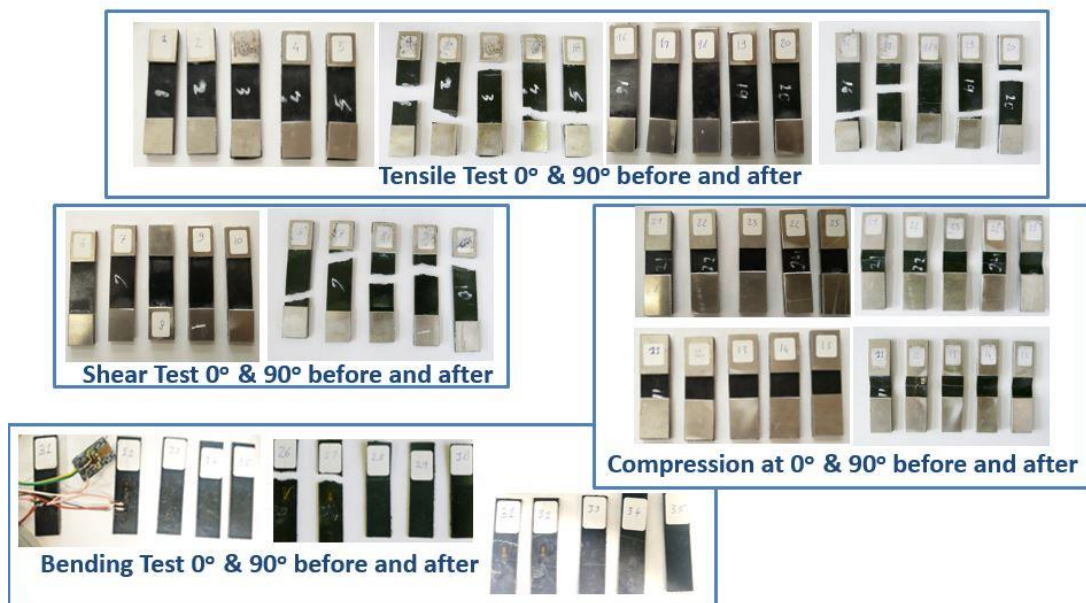
Figure 1b Specimen for short fibre Xmod™ GD301FE

Appendix 2

Short fibre card fitting done

For short fibre thermoplastic overmold (Xmod™ GD301FE), a specific law for short fiber composite in LS-DYNA is used which is material Law 157. The material model combines the properties of the anisotropic elastic model and anisotropic plastic model with a Tsai-Hill/ Tsai-Wu failure criterion for defining brittle orthotropic failure. An anisotropic constitutive matrix is used for determining the material model. FE specimens were made as per the dimensions used in the experimental characterisation, with a mesh size of 2.5 mm solid element and a fully integrated QBAT formulation as property for both Radioss and LSDYNA.

(a) Compression 0° test
(b) Compression 90° test
(c) Shear test
(d) Tensile 0° test
(e) Tensile 90° test
(f) Flexion test validation
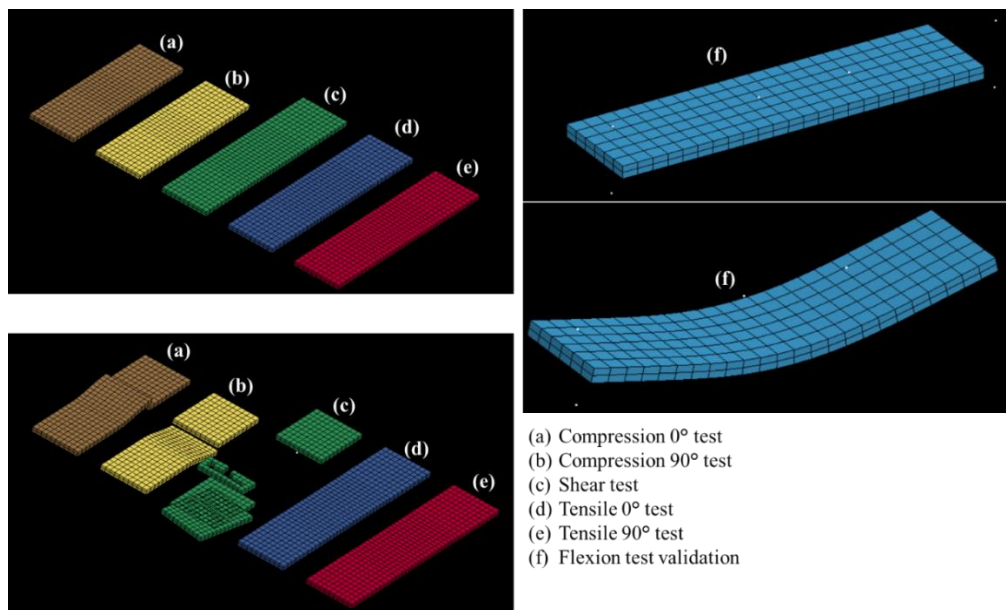
Figure 2a FE Specimen for short fibre Xmod™ GD301FE
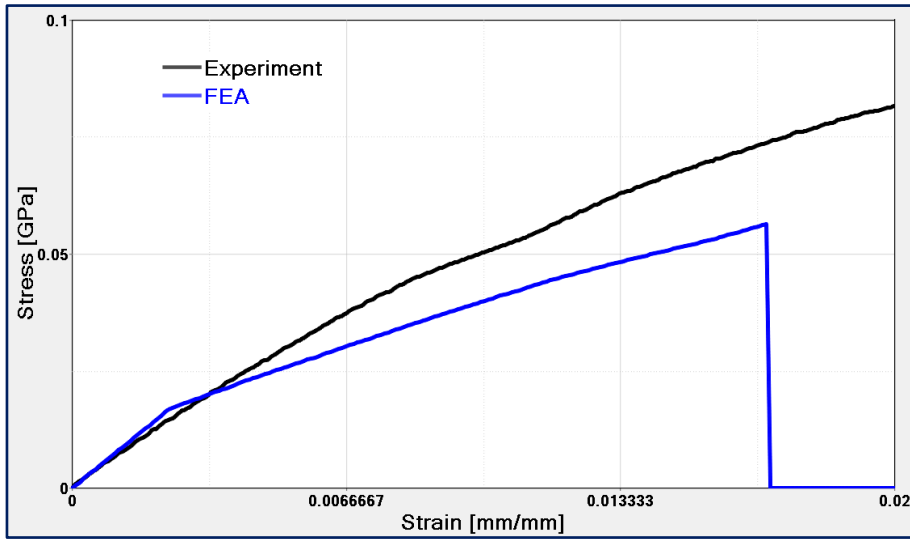
Figure 2b.a Card fitting done on the short fibre Xmod™ GD301FE:Tensile 0•
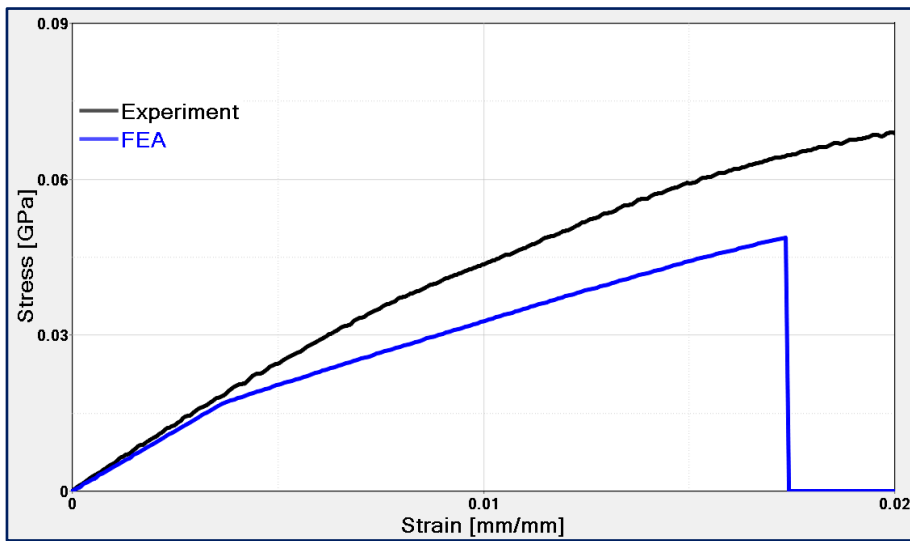
Figure 2b.b Card fitting done on the short fibre Xmod™ GD301FE:Tensile 90•
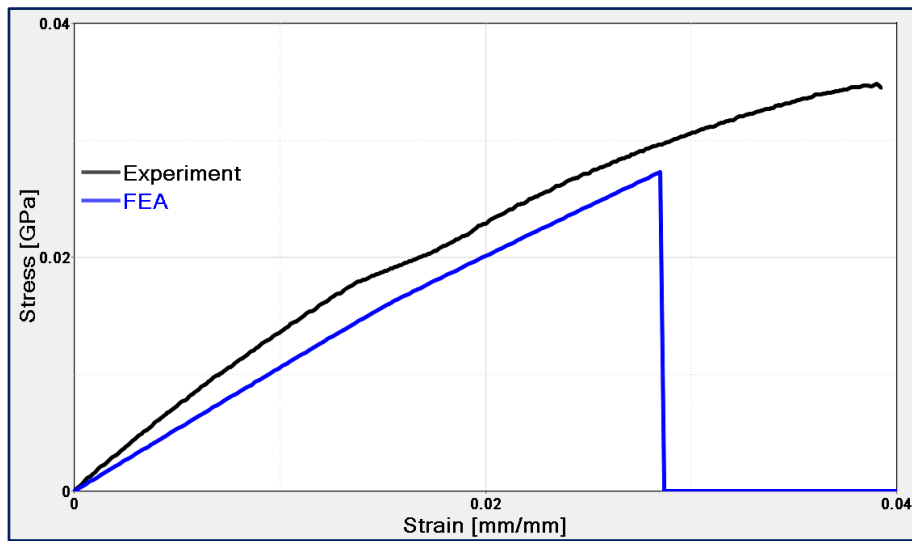
Figure 2b.c Card fitting done on the short fibre Xmod™ GD301FE: Shear test
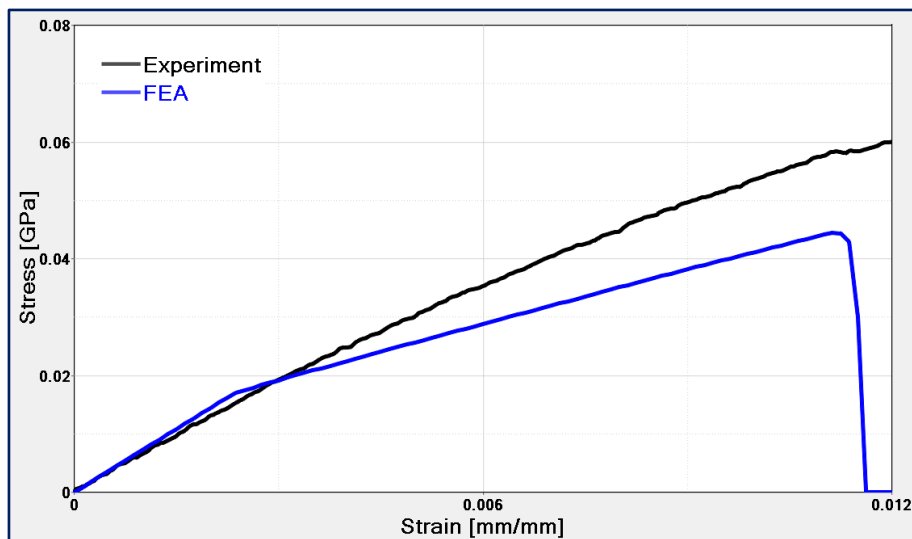
Figure 2b.d Card fitting done on the short fibre Xmod™ GD301FE: compression 0•
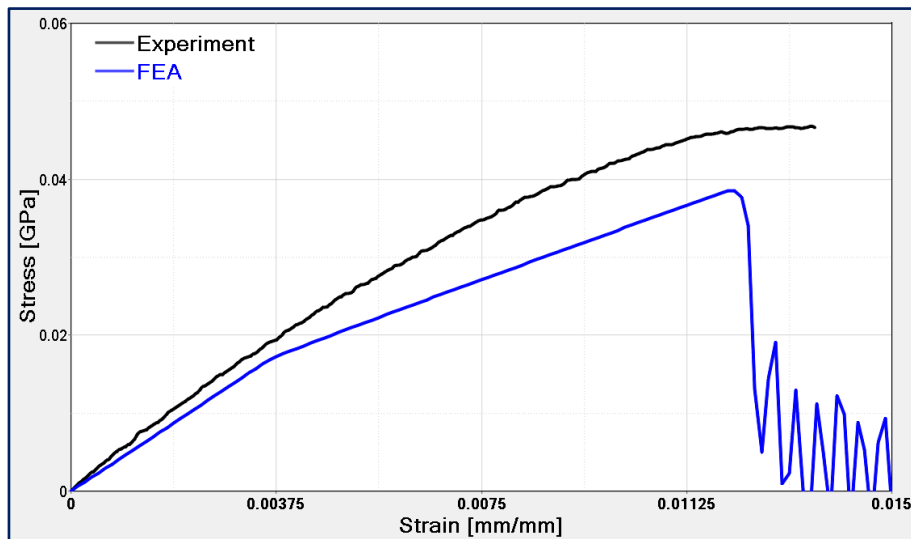
Figure 2b.e Card fitting done on the short fibre Xmod™ GD301FE: compression 90°
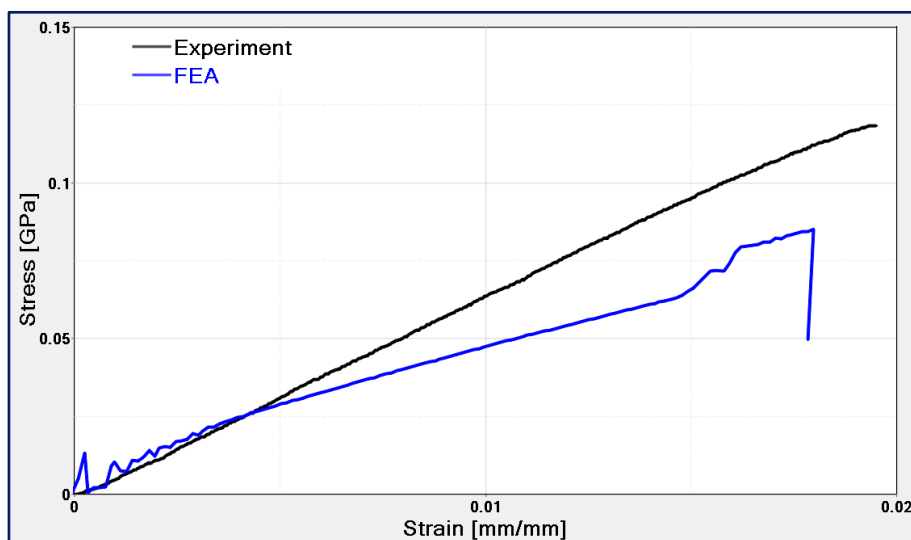
Figure 2b.f Card fitting done on the short fibre Xmod™ GD301FE: Bending test

As detailed in Fig 2b.a to Fig 2b.f the initial results from the card fitting gives a moderately good result, with a lot of scope for improvement. Although both the materials were initially characterised, further research on the injection overmold was kept on hold as the techniques for accurate predictions demanded high

computational power and was time-consuming. The focus was on studying the implications of the laminate reinforcement, and the study on the short fiber injection overmold has been kept as a vital issue for future research.

Appendix 3

Four-point bending machine accuracy study

All the FEA simulations done have been scrutinised and reviewed. Regarding the four-point bending tests, for all the specimen/ coupons tests done in the first level of the building block and a strain gauge for sampling the results. But for the actual component, the physical strain gauges have been proved ineffective, as there was a considerable variance between the results. This is because of the geometry of the component used, and currently, a reliable digital image correlation methodology is established in our lab.

However, to try validating the experimental results, a series of tests by taking HD sequential images (every 5 seconds) as illustrated in Figure 3a. For the machine we use for testing, the displacement recorded corresponds to the moving crosshead at the bottom and not the displacement of the reactive crosshead at the top. So, to check for errors, the displacement of the base crosshead was manually measured as shown in Figure 3a which will correspond to the displacement transferred to the component. Extreme care was taken while measuring the displacement to avoid any possible errors.
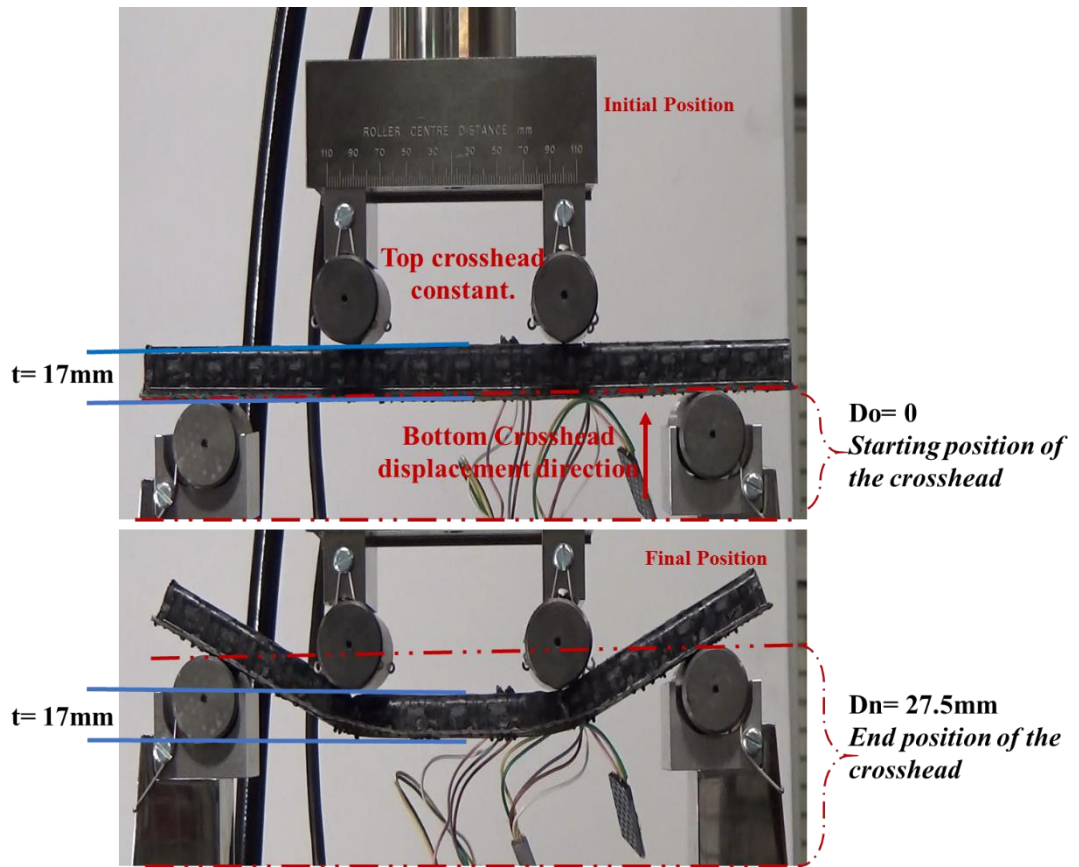
Figure 3a Sequential HD images taken for validating the displacement of the testing machine

Figure 3b shows the comparison of the Force-Displacement curves between the values from the testing machine and by manual measurement. Although the results are not extremely accurate, the difference is not high enough to make it unreliable.
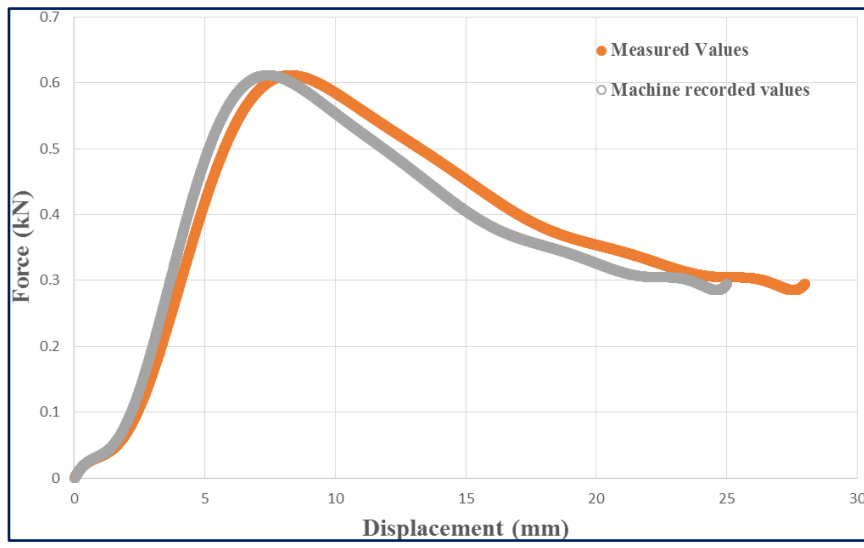
Figure 3b Force vs. Displacement comparison for Laminate Component

Appendix 4

LAW_ 25 Radioss

The law can be used to define an Orthotropic Shell, and Solid Material is utilising the Crasurv Formulation. This material law considers an orthotropic-elastic till the Tsai-Wu criterion and develops into nonlinear afterwards. For solid elements, the material is assumed to be linearly elastic in the transverse direction. The Tsai-Wu criterion can be set dependent on the plastic work and strain rate in each of the orthotropic directions and in shear to model material hardening. Strain and plastic energy criterion for brittle damage and failure are available. A clear delamination criterion based on an out-of-plane shear angle can be used.

```
##
##-------------------------------------------------------------------------------
## Material Law No 25. COMPOSITE SHELL
##-------------------------------------------------------------------------------
#---1----|----2----|----3----|----4----|----5----|----6----|----7----|----8----|----9----|---10----|
#-  2. MATERIALS:
#---1----|----2----|----3----|----4----|----5----|----6----|----7----|----8----|----9----|---10----|
#            E11              E22              NU12    Iform                          E33
#            G12              G23              G31              EPS_f1            EPS_f2
#          EPS_t1           EPS_m1           EPS_t2            EPS_m2              dmax
#          Wpmax            Wpref    Ioff    IFLAWP             ratio
#              c          EPS_rate_0           alpha                          ICC_global
#          sig_1yt            b_1t             n_1t            sig_1maxt           c_1t
#          EPS_1t1          EPS_2t1         SIGMA_rst1         Wpmax_t1
#          sig_2yt            b_2t             n_2t            sig_2maxt           c_2t
#          EPS_1t2          EPS_2t2          sig_rst2          Wpmax_t2
#          sig_1yc            b_1c             n_1c            sig_1maxc           c_1c
#          EPS_1c1          EPS_2c1          sig_rsc1          Wpmax_c1
#          sig_2yc            b_2c             n_2c            sig_2maxc           c_2c
#          EPS_1c2          EPS_2c2          sig_rsc2          Wpmax_c2
#          sig_12yt          b_12t            n_12t           sig_12maxt          c_12t
#          EPS_1t12         EPS_2t12         sig_rst12         Wpmax_t12
#          GAMMA_ini        GAMMA_max          d3max
#  Fsmooth            Fcut
```

Figure 4a LAW_25 parameters

Table 4a LAW_25 input parameters for the model

Law 25 Values	Actual Values
Rho_initial	1.61e-006
Nu_12	0.09
E11	20
SIG1_yt	0.064
b1_t	800
n1_t	0.8
E22	20
SIG2_yt	0.064
b2_t	800
n2_t	0.8
SIG1_yc	0.04
b1_c	400
n1_c	0.5
SIG2_yc	0.04
b2_c	400
n2_c	0.5
G12	1.3
SIG12_yt	0.008
b12_t	25
n12_t	0.35

Appendix 5

LAW_ 58 Ls-Dyna

Material law_58 can be used to model composite materials with unidirectional layers, complete laminates, and woven fabrics. This model can be realized for shell and thick shell elements using the ELFORM flag; 1 and 2.

```
*MAT_LAMINATED_COMPOSITE_FABRIC_TITLE
tepex
$#      mid          ro          ea          eb        (ec)        prba        tau1      gamma1
         21.61000E-6          15.0        15.0         0.0        0.09        0.01        0.01
$#      gab         gbc         gca      slimt1      slimc1      slimt2      slimc2       slims
        1.53        1.53        1.53         0.8        0.25         0.8        0.25         0.9
$#     aopt       tsize       erods        soft          fs        epsf        epsr        tsmd
         3.0         0.0         1.0         1.0        -1.0         0.3         0.5         0.9
$#       xp          yp          zp          a1          a2          a3        prca        prcb
         0.0         0.0         0.0         1.0         0.0         0.0         0.0         0.0
$#       v1          v2          v3          d1          d2          d3        beta
         0.0         1.0         0.0         0.0         0.0         0.0         0.0
$#     e11c        e11t        e22c        e22t         gms
       0.011       0.028       0.011       0.028        0.54
$#       xc          xt          yc          yt          sc
        0.17        0.46        0.18        0.46       0.063
$#     lcxc        lcxt        lcyc        lcyt        lcsc       lctau       lcgam          dt
           0           0           0           0           0           0           0         0.0
$#    lce11c      lce11t      lce22c      lce22t       lcgms
           0           0           0           0           0
```

Figure 5a: LAW_58 input parameters

Table 5a LAW 58 input parameter definition for the model

Field Variable	Contents Definition
EA	Ea, Young's modulus - longitudinal direction
EB	Ea, Young's modulus – Transverse direction
PRBA	vba, Poisson's ratio ba
PRCA	vca, Poisson's ratio ca
PRCB	vcb, Poisson's ratio ca
TAU1	$\tau 1$, stress limit of the first slightly nonlinear part of the shear
GAMMA1	$\gamma 1$, strain limit of the first slightly nonlinear part of the shear
GAB	Gab, shear modulus ab direction
GBC	Gbc, shear modulus bc
GCA	Gca, shear modulus ca
SLIMT1	Factor to determine the minimum stress limit after stress maximum (fiber tension).
SLIMC1	Factor to determine the minimum stress limit after stress maximum (fiber compression).
SLIMT2	Factor to determine the minimum stress limit after stress maximum (matrix tension).
SLIMC2	Factor to determine the minimum stress limit after stress maximum (matrix compression).
SLIMS	Factor to determine the minimum stress limit after stress maximum (shear).
AOPT	Material axes options
TSIZE	Time step for automatic element deletion
ERODS	Maximum effective strain for element layer failure. A value of unity would equal 100% strain.
SOFT	Softening reduction factor for strength in the crashfront.
FS	Failure surface type:
EPSF	Damage initiation transverse shear strain.
EPSR	Final rupture transverse shear strain.
TSMD	Transverse shear maximum damage, default = 0.90.
BETA	Material angle in degrees
E11C	Strain at longitudinal compressive strength, a-axis (positive).
E11T	Strain at longitudinal tensile strength, a-axis.
E22C	Strain at transverse compressive strength, b-axis.
E22T	Strain at transverse tensile strength, b-axis.
GMS	Engineering shear strain at shear strength, ab plane.
XC	Longitudinal compressive strength
XT	Longitudinal tensile strength
YC	Transverse compressive strength
YT	Transverse tensile strength
SC	Shear strength

APPENDIX 6

LAW_249 Ls-Dyna

This recently developed material law is specifically designed for thermoplastic composite part forming. The figure 6a shows the required input parameters for the material law.

		1	2	3	4	5	6	7	8
matrix	Card 1	MID	RO	EM	LCEM	PRM	LCPRM	LCSIGY	BETA
material coordinate definition	Card 2	NFIB	AOPT	XP	YP	ZP	A1	A2	A3
	Card 3	V1	V2	V3	D1	D2	D3	MANGLE	THICK
	Card 4	IDF1	ALPH1	EF1	LCF1	G23_1	G31_1		
	Card 5	G12	LCG12	ALOCK12	GLOCK12	METH12			
Fiber contribution	Card 6	IDF2	ALPH2	EF2	LCF2	G23_2	G31_2		
	Card 7	G23	LCG23	ALOCK23	GLOCK23	METH23			
	Card 8	IDF3	ALPH3	EF3	LCF3	G23_3	G31_3		

Figure 6a LAW_249 input parameters

Table 6a LAW_249 input parameters

Variable	Component Definition
RO	Density.
Matrix Parameters	
EM	Young's modulus
LCEM	Load Curve id: Young's modulus Vs Temperature
PRM	Poisson's ratio
LCPRM	Load curve id: Poisson's ratio Vs Temperature
LCSIGY	Load Curve or table id: Yield stress vs Plastic Strain (Vs T)
BETA	Hardening Parameter
General Fiber Parameters	
NFIB	Number of fibers per IPT
Single Fiber Parameters	
IDFx	ID of fiber x
AIPHx	Orientation angle of fiber x (WRT to material direction)
G23_x, G31_x	Modulus for transverse shear in direction of fiber x
Efx	Young's modulus of fiber x
LCFx	Load curve id: Fiber x response to length changes
Fiber interaction parameters	
Gxy	Shear coefficient for interaction between fiber x and y
ALOCKxy	Locking angle between fiber x and y
LCGxy	Load curve id for interaction between fiber x and y
GLOCKxy	Shear coefficient after locking
METHxy	Option for shear between fiber i and j

This material model describes a reinforced thermoplastic composite material. The reinforcement is defined as an anisotropic hyper-elastic material with up to three distinguished fiber directions. The matrix is modelled with a simple thermal elasto-plastic material formulation. For a composite, an additive composition of fiber and matrix stresses is used. In other words, it is the material model of blank at forming temperature: additive split between isotropic, elasto-plastic matrix (von-Mises yield criterion) and anisotropic hyper-elastic fibers. i.e. the combined stress response of the matrix and the composite fabric will be equal to the stress response of the whole laminate.

The principle values required for completing this material card is the fibre density, matrix density, tensile modulus, shear modulus (as a function of shear angle) and the static and dynamic frictional coefficients. The tensile and the shear load curves are considered directly for accuracy.

The fiber elastic limits (undergoing tension or compression) and the shear behaviour are denoted based on the standard textbook mechanics of anisotropic and hyper-elastic materials.

Elastic stresses within the fibers are denoted by:

$$\sigma_T^f = \sum_{i=1}^{n} \frac{1}{J} f_i\,(\lambda_i)(m_i \otimes m_i)$$

Where the function fi of the fiber stretch λi, corresponds to the input tensile curve of the fabric.

Shear behaviour of the reinforcement is denoted by:

$$\sigma_S^f = \sum_{i=1}^{2} \frac{1}{J} g_{i,i+1}\,(K_{i,i+1})(m_i \otimes m_{i+1})$$

Where, $\kappa i,+1$ denotes the shear angle in rad (or scalar shear product). The shear locking angle along with pre and post locking shear modulus is input.